FINAL REPORT

CONTAMINATION STUDY

NAS8-36955 D.O. 36
UAH Account No. 5-32180

Submitted to:

NASA/MSFC
Marshall Space Flight Center, AL 35812

Submitted by:

Kenneth A. Herren for R. Barry Johnson
University Of Alabama in Huntsville
Center for Applied Optics
Huntsville, Alabama 35899

September 1990

Preface

The work reported herein was performed by personnel at the University of Alabama in Huntsville's Center For Applied Optics, Huntsville, Alabama, under contract titled "Contamination Study". The measurements portion of the task was accomplished at the Materials and Processess Laboratory at NASA's Marshall Space Flight Center. The author would like to express appreciation to Mr. Roger Linton for the many helpful suggestions and discussions during this period.

ABSTRACT

NASA's In Situ Contamination Effects Facility, Marshall Space Flight Center has been used to measure the time dependence of the angular reflectance from molecularly contaminated optical surfaces in the Vacuum Ultraviolet (VUV). The light scattering measurements are accomplished in situ on optical surfaces in real time during deposition of molecular contaminants. The measurements are taken using non-coherent vacuum ultraviolet (VUV) sources with the predominant wavelengths being the Krypton resonance lines at 1236 and 1600 Angstroms. Detection of the scattered light is accomplished using a set of three solar blind VUV photomultipliers. An in-plane VUV BRDF experiment is described and details of the on-going program to characterize optical materials exposed to the space environment is reported.

1.0 INTRODUCTION

The purpose of this work is to analyze the forms of molecular contamination present in the space environment by measuring the loss of specular reflectance and increased scatter on good optical surfaces while the contamination is underway. The various potential contaminants are space candidate polyurethanes, silicones and fluorinated silicones. Since we are interested in the optical effects of the contamination a short introduction to light scattering is required to understand any data gathered in this effort.

Light incident on any real surface will scatter some portion of the incident energy into all allowed angles relative to the surface normal. In the scalar scattering theory, the intensity of the scattered light will be a function of both the incident angles and scattered angles as well as the surface material and its condition. The accepted parameter for describing this bidirectional reflectance, or angular scattering, is the Bidirectional Reflectance Distribution Function (BRDF)[1]. Figure 1.1 shows the geometry considered in this work.

However, to adequately describe the scattering, the vector nature of the light must be included. That is, the functional form of the scattered light should be written in the following way;

$$\underline{S}'(\theta_o, \phi_o, \pi_o, \lambda_o) = [M] * \underline{S}(\theta_s, \phi_s, \pi_s, \lambda_s) \qquad (1)$$

where $\underline{S}$ is the Stokes vector of the incident light, M is the Mueller matrix of the surface under consideration and $\underline{S}'$ is the Stokes vector of the scattered light. Note that we can also carry the angular dependence of the incident and scattered light in the Stokes vector. (See, for example Bickel, et. al.[2]).
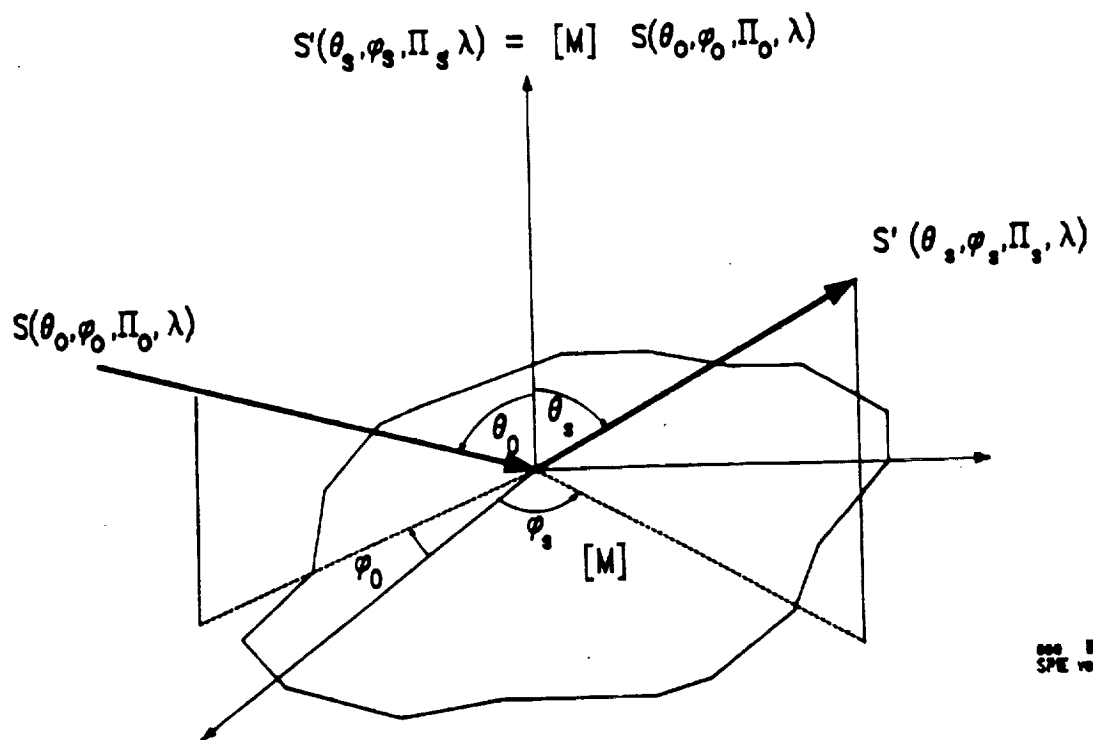
At short wavelengths the scattering process is strongly wavelength dependent due to the relative scale sizes between surface irregularities and the incident wavelength. And since we are measuring M as a function of surface contamination, the total description of the scattering matrix must also include this time dependence.

The surface Mueller matrix is well behaved when the wavelength is much larger than the characteristic surface irregularity but becomes increasingly more complicated as the wavelength to characteristic irregularity dimension ratio approaches zero (i.e. small wavelengths/rough surface).

Figure 1.2.a. shows a typical uncontaminated mirror used in this work. The mirrors are quartz substrates with a 1000 angstrom coating of aluminum and a 250 angstrom overcoat of magnesium fluoride. Figure 1.2.b. shows a mirror that has been contaminated

with a molecular contaminant (Chemglaze Z-306) used in this program. As can be seen, the contamination due to this contaminant proceeds in a discrete fashion, i.e. islands of contaminant appear rather than a uniform layer or film. During a typical contamination run, a mirror will develop surface irregularities whose diameters approach that of the incident wavelength and, according to Mie theory, there may occur peaks in the scattered intensity when the surface scatterers are approximately equal to the wavelength. We want to take advantage of this to determine the growth rate and optical properties of the contamination.

Therefore, the thrust of this work is to describe the measurements of scattered light in the region where the long wavelength approximations no longer hold and to compare these data with measurements of the scattering functions in the long wavelength approximation.

$$S'(\theta_s, \varphi_s, \Pi_s, \lambda) = [M] \ S(\theta_o, \varphi_o, \Pi_o, \lambda)$$

$S'(\theta_s, \varphi_s, \Pi_s, \lambda)$

$S(\theta_o, \varphi_o, \Pi_o, \lambda)$

θ_o

θ_s

φ_s

$[M]$

φ_o

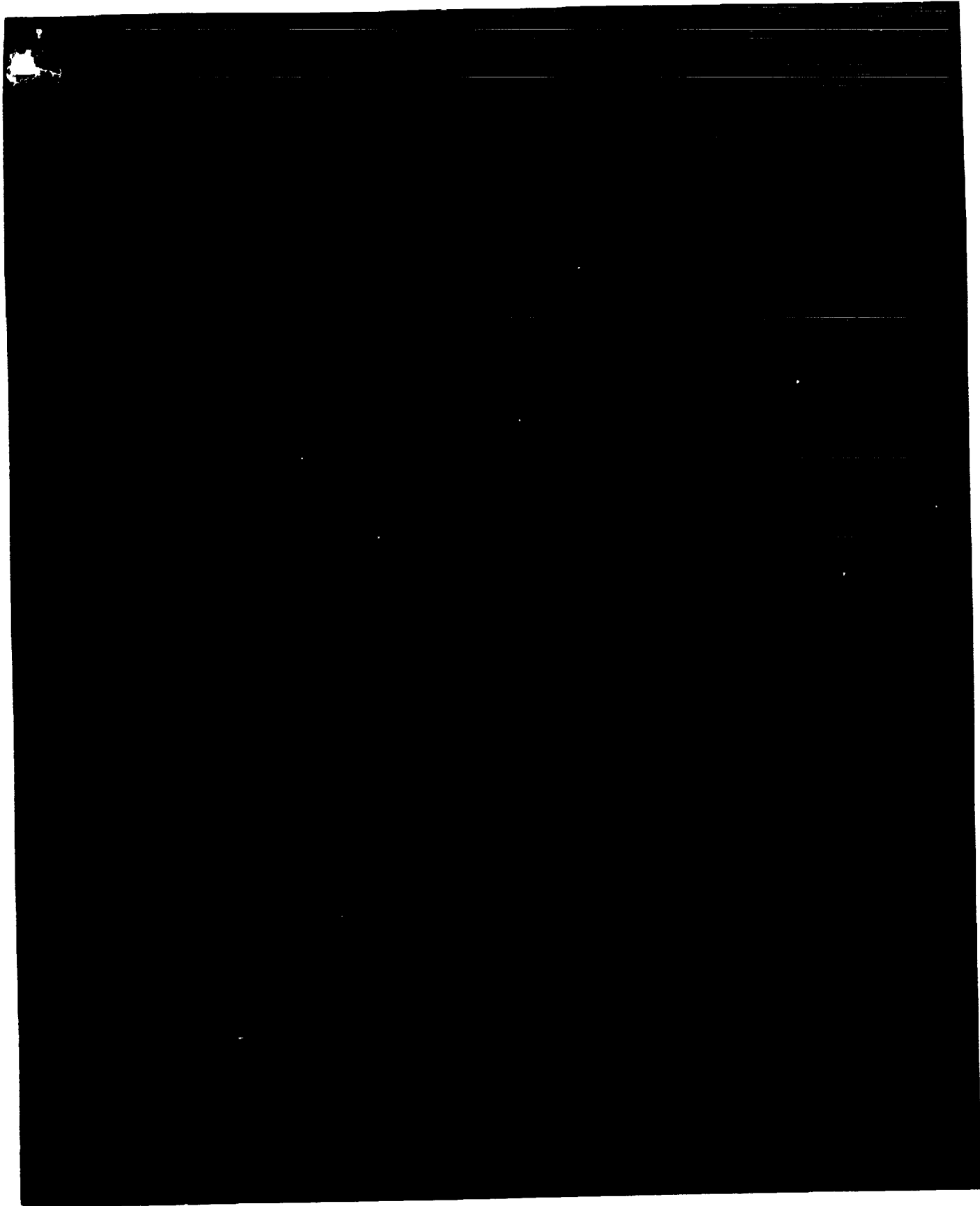Figure 1.1   BRDF Geometry
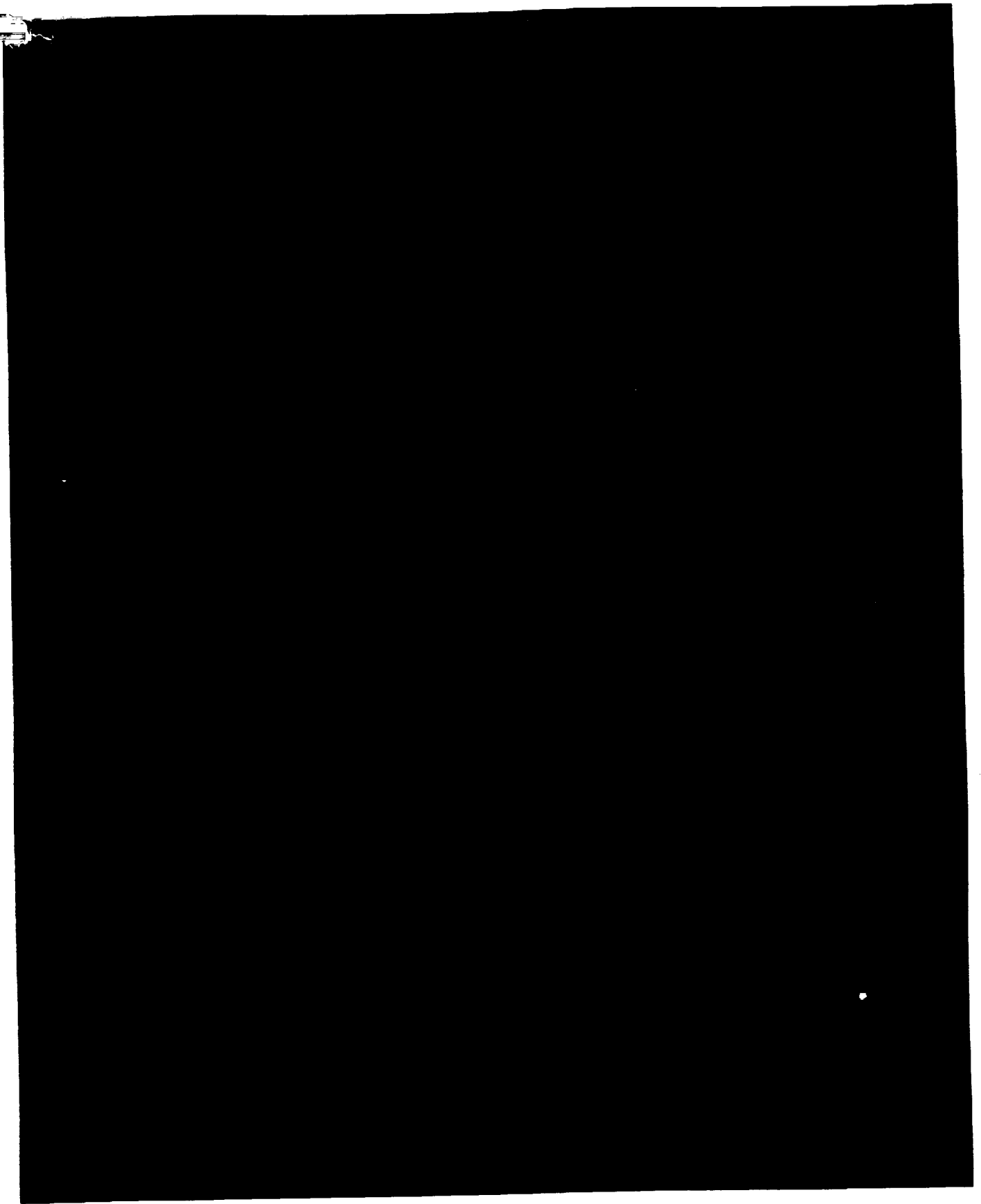
Figure 1.2a.   Clean mirror.

Figure 1.2b. Mirror highly contaminated with Z-306.

2.0 THEORY

Light incident on an optical surface will be scattered due to the irregular structure of the surface at the microscopic level. These irregularities will cause some of the incident light to be reflected, or scattered, at an angle not predicted by Snell's law applied to the mean surface value. The phenomenon of surface scattering is commonly divided into broad categories based on the size of the surface irregularities causing the scattering[3]. There are two important regions dealt with in this work. First is the long wavelength region where scattering arises from small imperfections on the surface. Secondly is the intermediate wavelength region where the scattering is caused by imperfections comparable to the wavelength in size. A detailed description of the theory of scalar and vector scattering theory is presented in the Appendices and won't be repeated here.

The main point of the present work is to produce baseline data in the long wavelength region, and while contamination is underway, to observe the transition of the scattering from the long wavelength to the intermediate wavelength region.

3.0 EQUIPMENT

These measurements have been carried out at the In Situ Contamination Effects and the VUV BRDF Facilities at NASA's Marshall Space Flight Center, Huntsville, Alabama and at the Visible BRDF Facility and the Center for Applied Optics, UAH.

3.1 In Situ Contamination Effects Facility

The In Situ Optical Surface Measurement Facility shown schematically in figure 3.1. is an equipment package designed to measure the real time deposition of outgassed molecular constituents from candidate space materials. These measurements are made using VUV light and observing the deleterious effects of the material deposition on the surface reflectivities of optical materials while the depositions are in process. This arrangement is used to simulate the on-orbit effects of contamination and degradation of optical surfaces such as Space Telescope.

VUV light is generated using a low pressure RF excited discharge Krypton lamp. The krypton resonance line at 123.6 nm is coupled into the vacuum chamber through a window or filter port. Typical VUV filters have a spectral width of 10 nm and any continuum output in the longer wavelengths are down by five or more orders of magnitude. The physical mount for the source tube and filter housing serve as a limiting aperture of approximately 6 mm, used in collimating the incident light.

After the filter we place the reflection type polarizer followed by the second aperture in the collimating scheme. This work employs three mirror metal front surface polarizers of the type reported by Hamm et.al.[4] Typical diattenuation values of 0.996 have been reported for these polarizers. These polarizers allow minimum deflection of the optical axis and introduce little problem in alignment of the system.

The collimated light is incident on the sample mirror and specular light and scattered light will be collected by the three fixed solar blind photomultiplier tubes (PMT). Placed in front of the PMT's is another polarizer used as an analyzer. These PMT's are arranged so that the specular channel is at 30 degrees angle of reflection, the forward and back scatter channels are at +30 and - 45 degrees, respectively, relative to the specular.

In addition to the signal PMT's there is a reference channel PMT at the output of the source. Part of the signal is picked off by the beamsplitter and directed to the reference. This setup allows us to monitor the condition of the source output.

Figure 3.1. Schematic Diagram of the In Situ Optical Surface Measurement Facility

The contamination source is a simple resistance heater in contact with the outgassing material and is housed in front of and beside the back scatter PMT. The temperature of the sample is held to within one degree either side of the desired temperature. Mass loss and therefore contamination level is determined by using a temperature controlled quartz crystal microbalance (TQCM). For our 15 Mhz TQCM the mass loading, m, is given by $m = 1.56 \times 10^{-9}$ g/cm^3 hz. In this application the TQCM is located coplaner above the sample mirror and the housing is temperature controlled and monitored to less than one degree.

This set-up approximates a planer BRDF measurement at three positions, i.e. the incident light, surface normal and scattered light are in the same plane. Measurements can then be taken using incident linearly polarized light at any orientation and analyzed at any orientation while contaminant is being deposited.

3.2. VUV BRDF Facility

In addition to the In Situ Facility there is available a 0.5 meter MacPherson VUV spectrometer, shown schematically in figure 3.2. This equipment is used for measuring angular scattering in the UV and the VUV. This device uses a mercury vapor lamp as the source and an acrylic light pipe coated with sodium salicylate (a florescent material) as the detector. The output of the 1/8" florescent spot is directed through the light pipe to a visible photomultiplier. The light pipe is free to rotate about the sample at a distance of 1.5 inches giving a solid angle of roughly 0.007 steradians.

3.3. Visible BRDF Facility

The BRDF Facility at UAH is capable of measuring the entire full angle scattering function for a given surface. The facility consists of the three meter motor driven detector arm, gimballed sample pedestal, source and detection electronics as well as the computer software and hardware required to control the measurements.

The facility is capable of handling most visible and infrared laser sources with little extra effort. Due to ease of use, the wavelength most often employed is 632.8 nm from a HeNe laser. The long wavelength approximation for scattering occurs when the characteristic height of the surface irregularities is much smaller than the wavelength so that the small angle approximation holds. For typical "good" optical surfaces with roughnesses less than 100 angstroms the HeNe red line is in the long wavelength approximation and thus provides a control measurement of the surface quality for comparison with the VUV measurements.
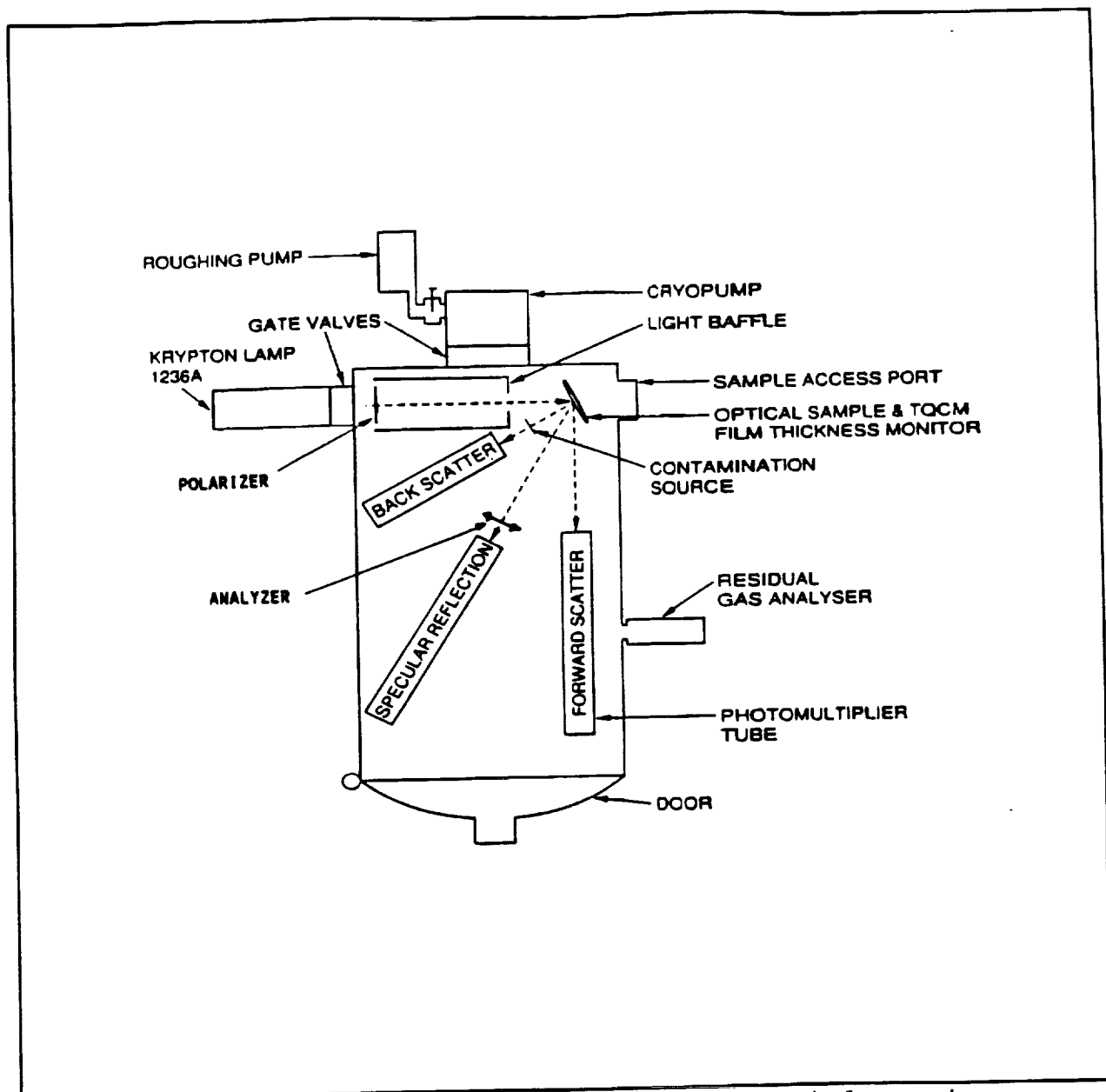
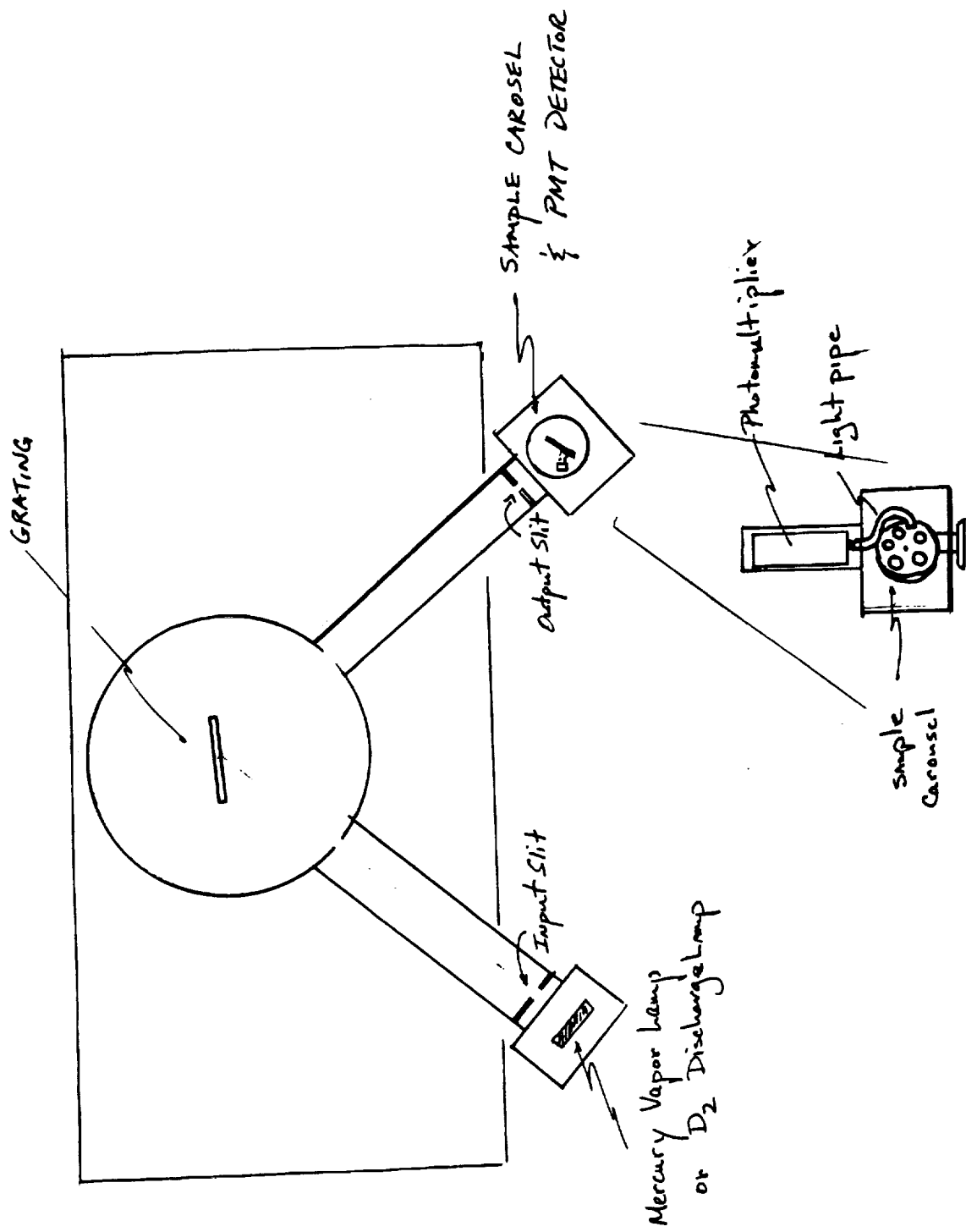Figure 3.1.   In-situ Optical Surface Measurement Apparatus

GRATING

SAMPLE CAROSEL & PMT DETECTOR

Output Slit

Input Slit

Mercury Vapor Lamp or D₂ Discharge Lamp

Sample Carousel

Photomultiplier

Light Pipe

Figure 3.2.

VUV BRDF MEASUREMENT EQUIPMENT — 0.5 METER SCANNING VUV MONOCHROMETER

4.0 EXPERIMENTAL METHOD

Molecular contamination of optical surfaces from outgassed material has been shown to proceed from acclimation centers (see figure 1.2). The origin of these centers at the surface is not well understood but each grows faster than the surrounding surface area. This implies that the contaminant has a higher sticking ratio for itself than the surface has for it and as a result the surface will appear on the microscopic level to be composed of many small "islands" of accumulated material with plains of relatively clean surface in between. This situation provides the experimenter with many roughly hemispherical scattering centers that are growing with time. This is analogous to the common static situation for scattering of near infrared light from surfaces by dust particles (see Bennett[3]). By using a fixed wavelength and observing the scattered light as the islands grow, we will observe the typical resonance peak in scattered light predicted by the Mie theory.

This sort of scattering situation suggests using the Mie Theory to explain the angular scattering; and the form of the scattering can be used to shed some light on the growth rates of the islands and therefore the activation energies of the outgassing phenomena.

Appendix A presents the mathematical model developed during this contract perion for predicting the scattering versus island size and angle. Figure 4.1 shows a typical scattered output versus time (or island size) for contamination in the intermediate wavelength region. In the results section of this report we will see that the scatter, in some cases, does match that shown in figure 4.1.

Figure 5.6. shows the relevant data on the mirror shown in figure 1.2.b. Notice that there is the resonance peak in the scattered light as predicted by the Mie theory. We calculate from this curve that the index of refraction of the surface contaminant is approximately given by m = (1.1 -0.04 i). It should be pointed out that the numbers that are derived from this model are relatively soft. The model can accommodate a plus or minus ten percent change in the real part and factors of two to three in the imaginary part of the index of refraction and still give good fit to the experimental data. This derives from the complexity of the model and the lack of knowledge of the size distribution of scatterers on the surface. We also see that the specular reflectivity drops fairly quickly after contamination starts but reaches a steady state value with no further significant change.
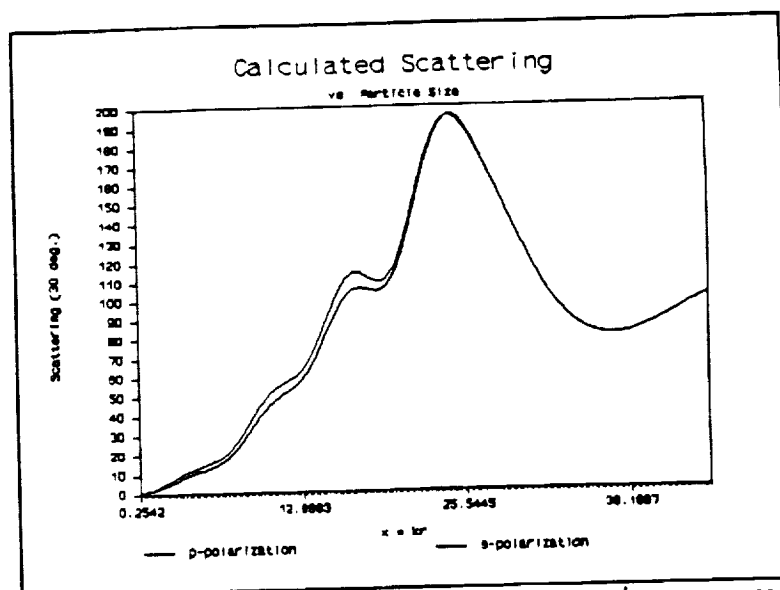
Calculated Scattering

vs Particle Size

Figure 4.1. Theoretical scattering curve
vs. time.

5.0   RESULTS

The experimentally obtained data in this work will be presented in this section. Section 5.1 will show the data from the In Situ Contamination Effects Facility, section 5.2 will present the data acquired in the VUV BRDF Facility and Section 5.3 will show the data from the Visible BRDF Facility.

5.1   In situ contamination

Figure 1.2.a shows a typical optical surface before contamination. These mirrors are one inch quartz flats with a 1000 angstrom coating of aluminum and a final 250 angstrom overcoat of magnesium fluoride which provides a high reflection coating at 1200 angstroms. Close inspection shows some imperfections in the MgF coating as well as the Al reflective coat. These imperfections provide a baseline scatter which is always there and this baseline is directly related to the size and number of the imperfections on the surface.

Figure 1.2.b shows a typical mirror contaminated by Chemglaze Polyurethane Z-306. This mirror was exposed to the contaminant at elevated temperatures up to 160 degrees centigrade for approximately four hours. The Z-306 paint had previously been baked at 60 degrees for two days.

Figures 5.1 thru 5.13 show the raw data for the important measurement runs taken during this reporting period. All runs shown are for Z-306 except for Series 10 and 11 which are DC 93-500. Table 5.1.a and 5.1.b shows a summary of the important runs during this contract.

5.2   VUV BRDF Runs

The data shown in figures 5.14 through 5.17 show the results of measurements of the angularly scattered VUV light from some of the important mirrors in this task.

Figure 1.2c shows a mirror contaminated with Silastic E. The material was cured at 100 degrees centigrade for four hours before this 90 minute run at 125 degrees. Note how the form of the contamination is in roughly circular islands similar to those formed by Z-306 but are much more sharply peaked than the hemispherical islands of the Z-306. However, the scattered light is very different in that the scatter channels don't show the resonance scattering that occurs with the Z-306 contamination. Figure 5.14 shows the results of the BRDF measurements done on the 0.5 meter VUV spectrometer at about 2300 angstroms. The mirror K-1 is heavily contaminated with Z-306 and mirror 47-89 is the Silastic E. The data shows the increased scatter at large angles from Z-306 over that from the Silastic E. Also notice that since our detector has such a large solid angle we are measuring the beam shape at small angles relative to specular. For comparison figure 6.b shows the measured BRDF at a wavelength of 6328 angstroms for mirror K-1.

This mirror was highly contaminated with Z-306

Figures 5.15, 5.16 and 5.17 show typical results of angularly scattered light on contaminated mirrors versus a clean mirror (mirror #43-85). Note that at large angles the clean mirror has less scattered light but at intermediate angles the scattering of the contaminated mirrors is less.

5.3 Visible BRDF Runs

The BRDF measurements from mirrors contaminated in the In Situ Facility are shown in figures 5.18 thru 5.25. In addition to these mirrors, the BRDF of other optical surfaces were measured during this contract. Figures 5.26 and 5.27 show the BRDF from two paint samples flown on the LDEF spacecraft. In addition soft and hard anodized aluminum samples were measured before and after exposure to atomic oxygen. The results of these measurements are shown in figures 5.28 thru 5.35.

Figure 5.18 shows the BRDF for our calibration sample. We use a nearly Lambertian surface for calibration. For a perfect Lambertian surface the BRDF would be unity for all angles. Figure 5.19 shows the BRDF of a Z-93 paint sample used in this work. Notice that this sample is very close to Lambertian. Figure 5.20 shows the BRDF for a clean mirror. The next three figures (5.21, 5.22 and 5.23) show the measured BRDF for mirror K-1, a highly contaminated mirror in the normal, back and forward scatter directions. For comparison, figure 5.24 shows the BRDF for a clean mirror in the forward scatter direction. Finally, figure 5.25 shows the BRDF for a lightly contaminated mirror at near normal incidence.

Figure 5.26 and 5.27 show the BRDF for two S13GL paint samples flown on the LDEF spacecraft. Figure 5.26 is for an unexposed paint sample whereas figure 5.27 is for a sample exposed to the space environment.

Figures 5.28 through 5.35 show a series of measurements taken on black anodized aluminum samples. Figures 5.28 and 5.29 show type II anodized aluminum and figures 5.30 and 5.31 show type III anodized aluminum before exposure to atomic oxygen. Figures 5.32 through 5.35 are the corresponding figures for the samples after exposure to atomic oxygen. Each sample is measured at two positions corresponding to when the machining grooves on the aluminum surface are vertical and horizontal.
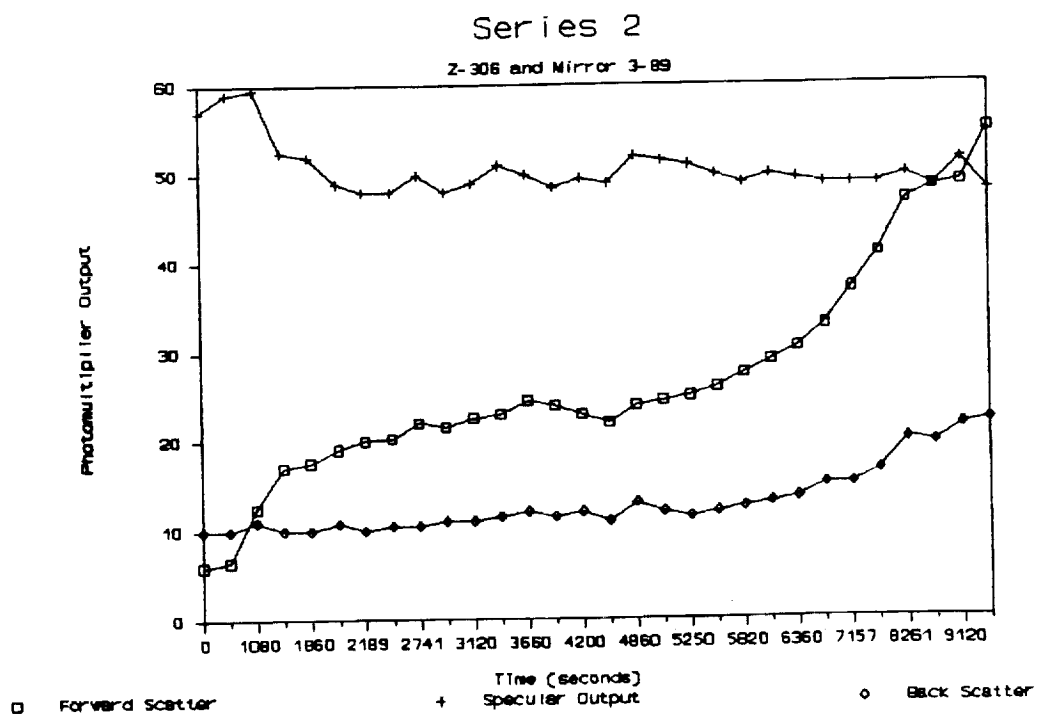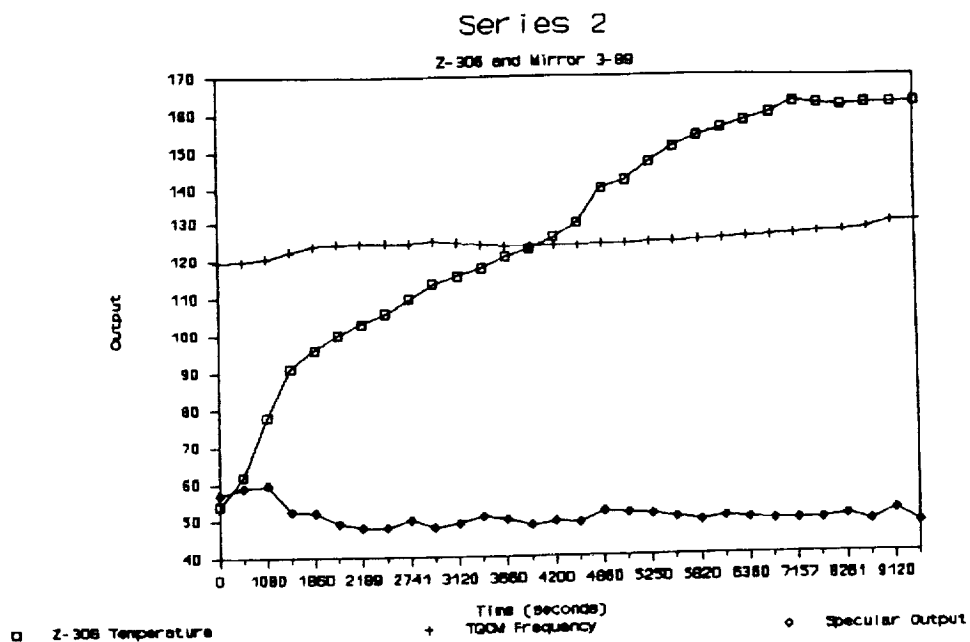
Series 2

Z-306 and Mirror 3-89

Legend:
□ Z-306 Temperature
+ TQCM Frequency
◇ Specular Output

Series 2

Z-306 and Mirror 3-89

Legend:
□ Forward Scatter
+ Specular Output
◇ Back Scatter

Figure 5.1. Relevant Data for Mirror 3-89

CONTAMINATION SUMMARY

Series #	Mirror #	Contaminant	Total TQCM Change (hertz)	Specular Change (%)	"Island" Diameter (micron)	Comment
1	35-88	Z-306	220	31	1.5/2.0	Baked 4 hrs
2	3-89	Z-306	< 100	<5	0.7/0.9	Baked 4 hrs
3	85-88	Z-306	103	-	NA	Uncured Z-306, baked
4	6-88	Z-306	179	43	0.57/0.8	1st ref. run
5	44-89	Z-306	90	22.5	0.46/0.92	Cured Z-306
6	45-89	Z-306	52	12	0.3/0.45	Cont'd with same Z-306
7	47-89	Silastic E	408	-	-	Chaotic Surface
8	48-89	Z-306	303	40	0.23/0.5	Run resumed next day
-	-	Kapton	26	-	-	No Degradation

Table 5.1a.

CONTAMINATION SUMMARY

Series #	Mirror #	Contaminant	Total TQCM Change (hertz)	Specular Change (%)	"Island" Diameter (micron)	Comment
9	49-89	Z-306	110	25	0.5/0.9	Same Paint as previous run
10	5-90	DC 93-500	820	57	0.7/0.9	Uncured sample
11	40-89	DC 93-500	303	–	NA	Cured sample
12	14-90	Z-306	215	15	0.35/0.8	reference run
13	11-90	Z-306	395	72	0.45/0.9	s-polarization
14	K-1	Z-306	2747	74	0.4/1.25	p-polarization
15	114-84	Z-306	1116	18	0.5/0.75	same paint as previous

Table 5.1b.

Series 3

Z-306 and Mirror 85-88

Time (seconds)

□ Z-306 Temperature   + TQDM Frequency   ◇ Specular Output

Series 3

Z-306 and Mirror 85-88

Time (seconds)

□ Forward Scatter   + Specular Output   ◇ Back Scatter

Figure 5.2.   Relevant Data for Mirror 85-88

Series 4

Z-306 and Mirror 6_88

Output

160
150
140
130
120
110
100
90
80
70
60
50
40
30
20

0   911   1901   2381   2760   3131   3491   3761   4001   4211   4721

Time (seconds)

+   TQCM Frequency   ◇   Reference PMT   △   Spe

Photomultiplier Output vs. Time

Z-306 and Mirror 6-88

Voltage Output

70

60

50

40

30

20

10

0

0   911   1901   2381   2760   3131   3491   3761   4001   4211   4721

Time (seconds)

▢   Forward Scatter   +   Specular Channel   ◇   Back Scatter

Figure 5.3.   Relevant Data for Mirror 6-88

Series 5

Z-306 and Mirror 44-89

Output

Time (seconds)

+   TQCM Frequency   ◊   Specular Output   Δ

Series 5

Z-306 and Mirror 44-89

Photomultiplier Output

Time (seconds)

□   Forward Scatter   +   Specular Output   ◊   Back Scatter

Figure 5.4.   Relevant Data for Mirror 44-89

Series 6

Z-306 and Mirror 45-89

+   TQCM Frequency   ◊   Specular Output   Δ

Series 6

Z-306 and Mirror 45-89

□   Forward Scatter   +   Specular Output   ◊   Back Scatter

Figure 5.5.   Relevant Data for Mirror 45-89

Series 8

Z-306 and Mirror 48-89

Output

Time (seconds)

□ Z-306 Temperature   +   TQCM Frequency   ◇   Specular Output

Series 8

Z-306 and Mirror 48-89

Photomultiplier Output

Time (seconds)

□ Forward Scatter   +   Specular Output   ◇   Back Scatter

Figure 5.6.   Relevant Data for Mirror 48-89.

Series 9

Z-306 and Mirror 49-89

+ TQCM Frequency   ◇ Specular Output   △

Series 9

Z-306 and Mirror 49-89

□ Forward Scatter   + Specular Output   ◇ Back Scatter
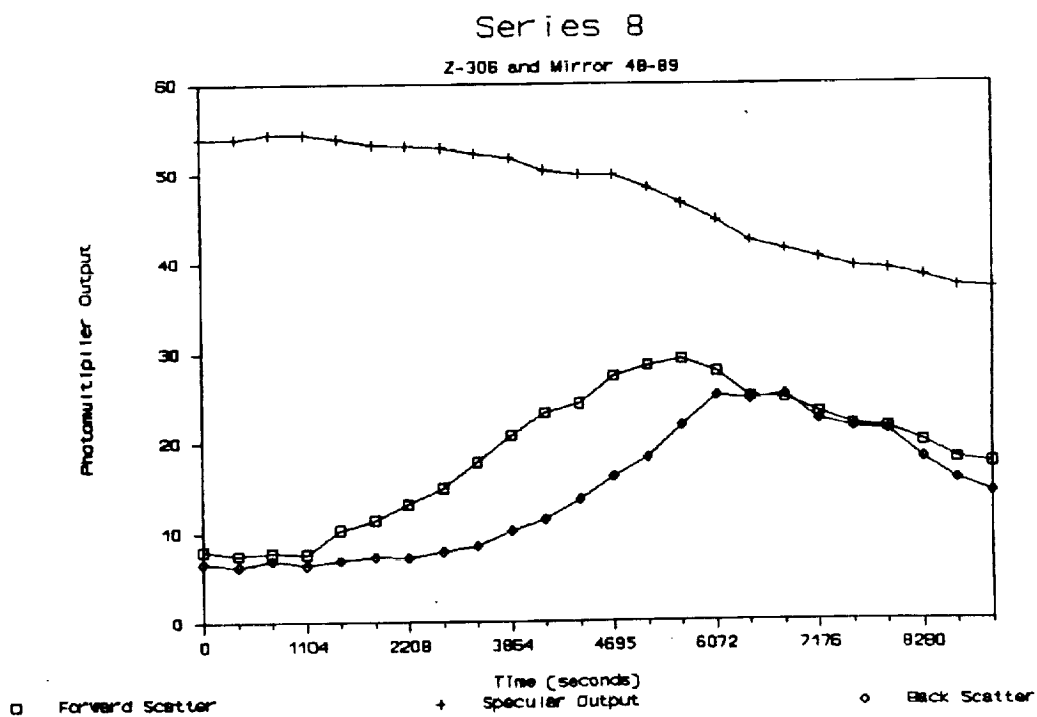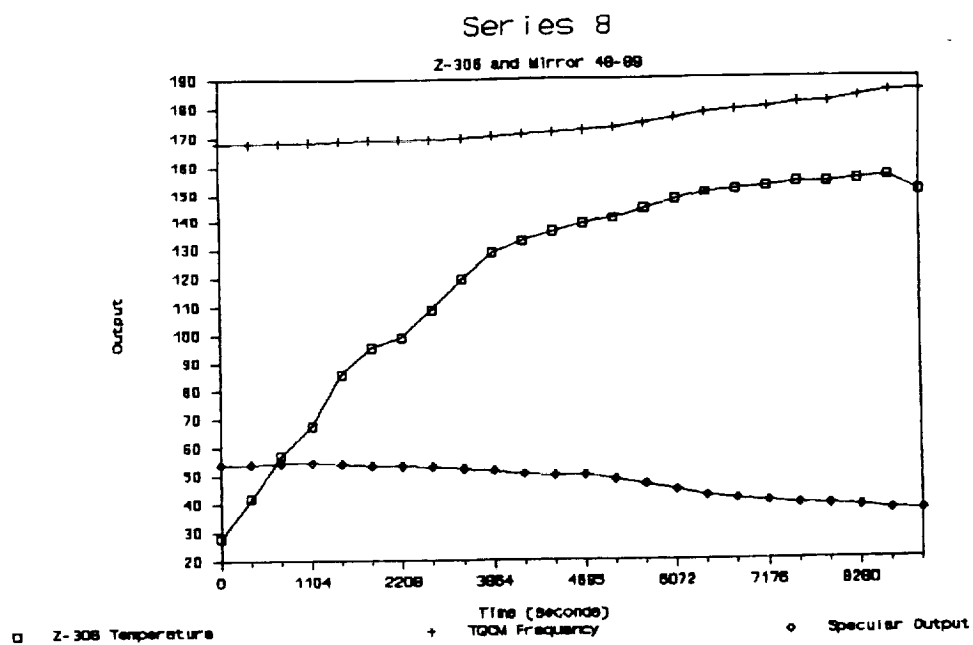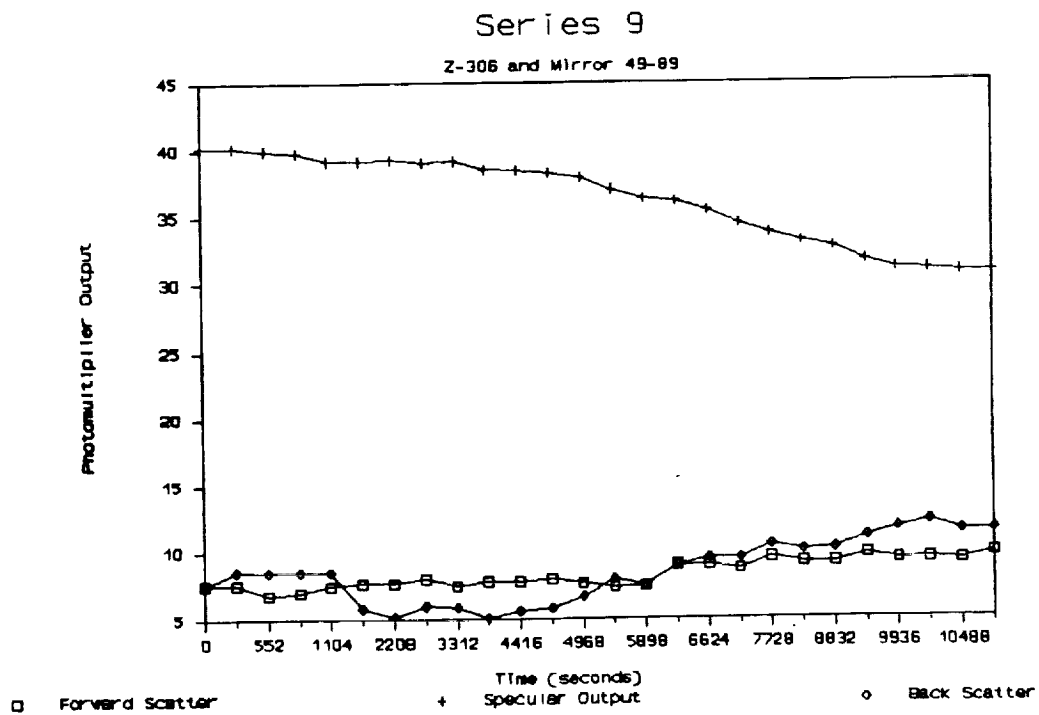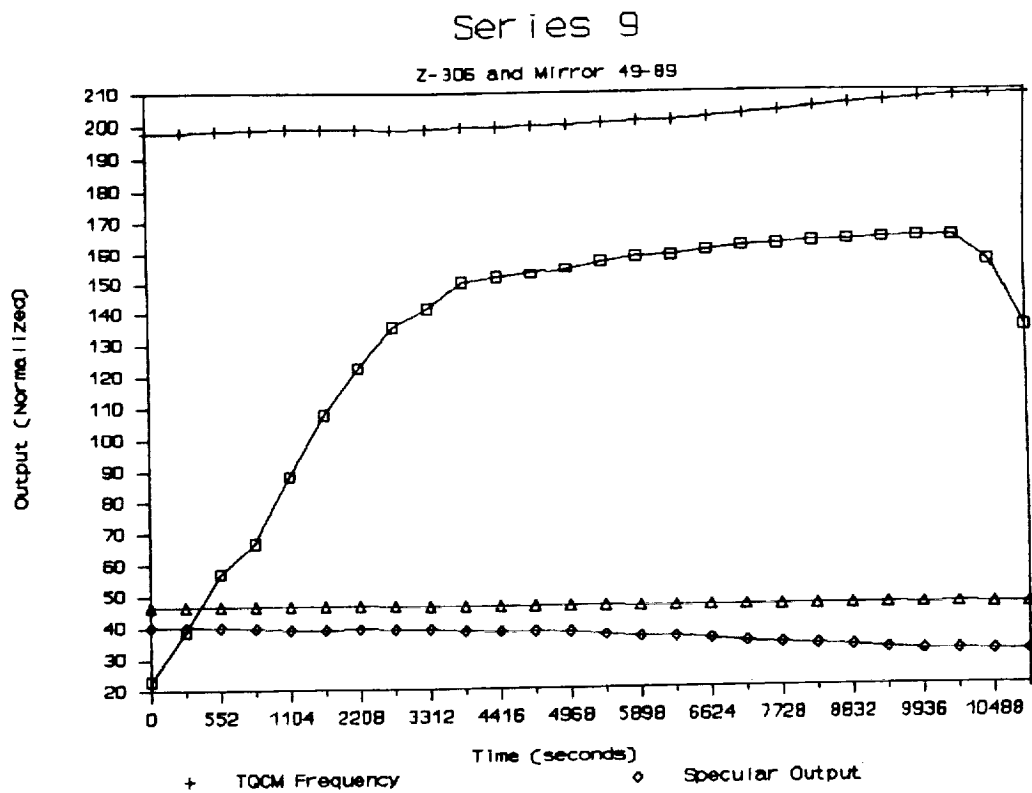
Figure 5.7.   Relevant Data for Mirror 48-89

Series 10

DC 93-500 and Mirror 5-90

Output (Normalized) vs Time (seconds)

| 00 Temp. | + TQCM Frequency | ◊ Specular Output | Δ Reference PMT |

Series 10

DC 93-500 and Mirror 5-90

Photomultiplier Outputs vs Time (seconds)

| ▢ Forward Scatter | + Specular Output | ◊ Back Scatter |
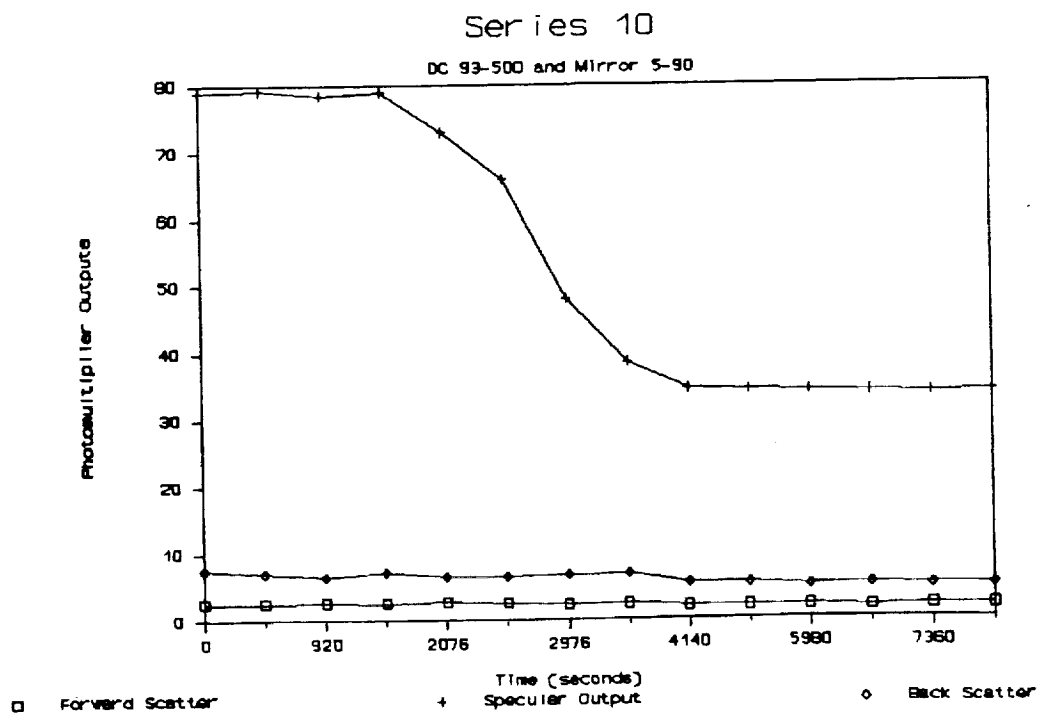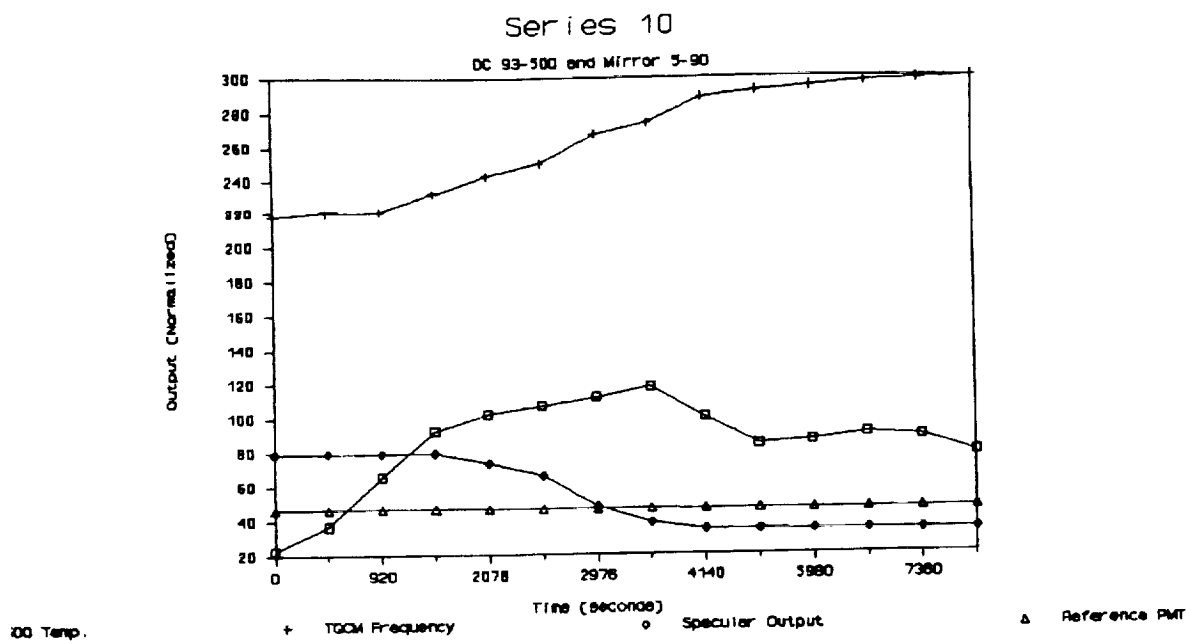
Figure 5.8.   Relevant Data for Mirror 5-90.

Series 11

Cured DC 93-500 and Mirror 40-89

Z-306 Temperature   + TQCM Frequency   ◇ Specular Output

Series 11

Cured DC 93-500 and Mirror 40-89

□ Forward Scatter   + Specular Output   ◇ Back Scatter
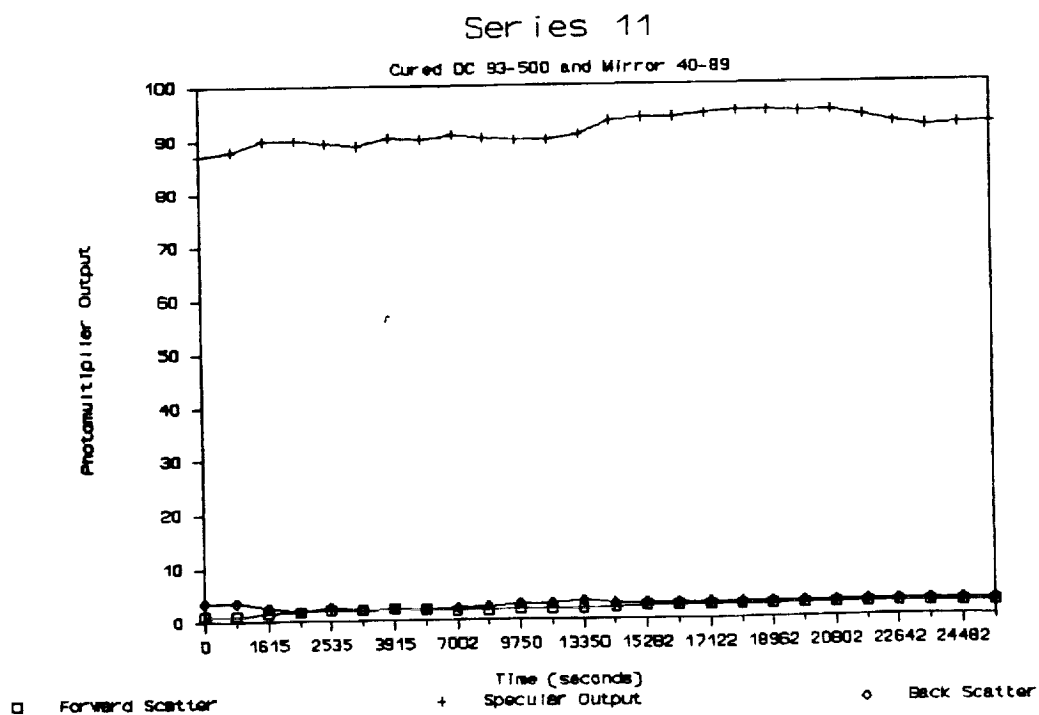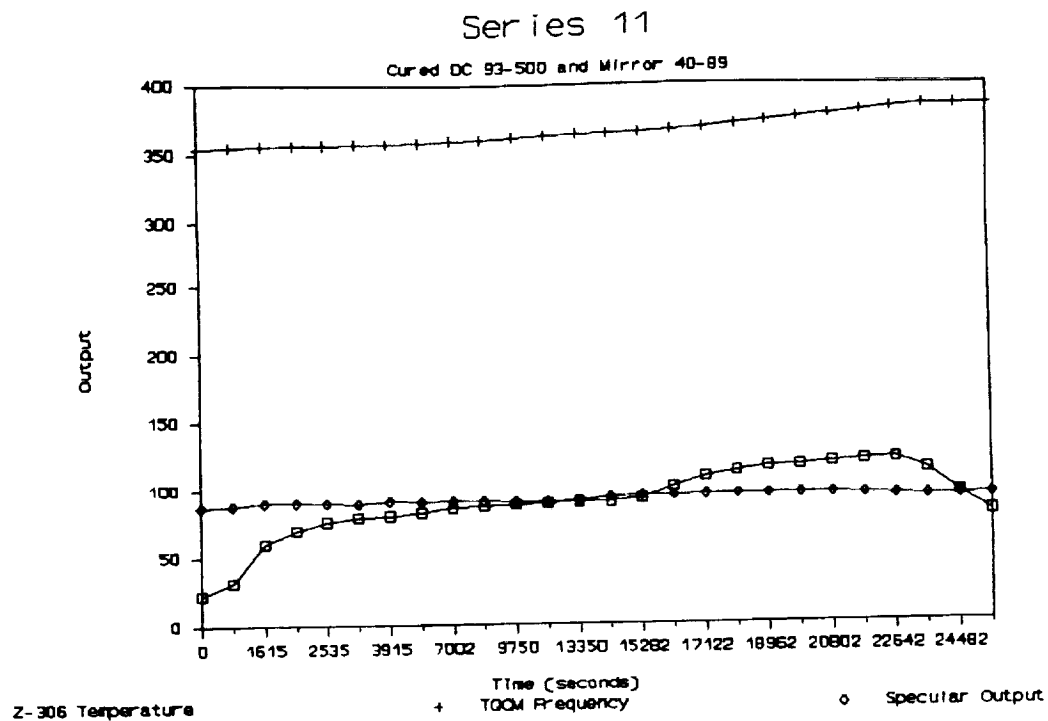
Figure 5.9.   Relevant Data for Mirror 40-89

Series 12

Z-306 and Mirror 14-90

+ TQCM Frequency   ◇ Specular Output   Δ

Series 12

Z-306 and Mirror 14-90

□ Forward Scatter   + Specular Output   ◇ Back Scatter
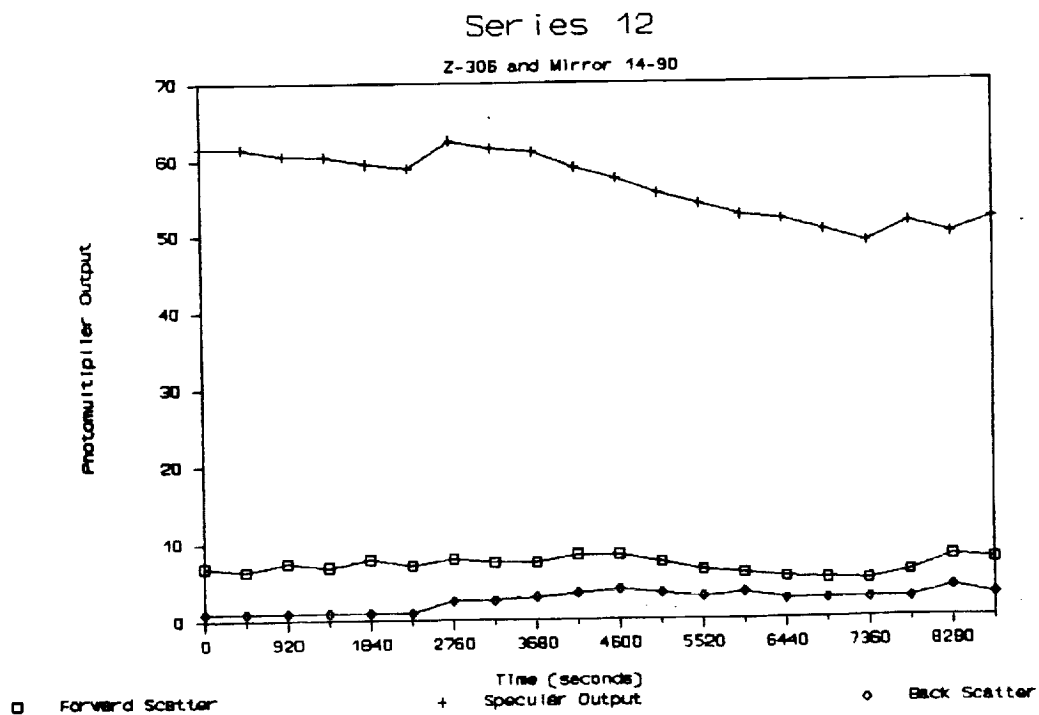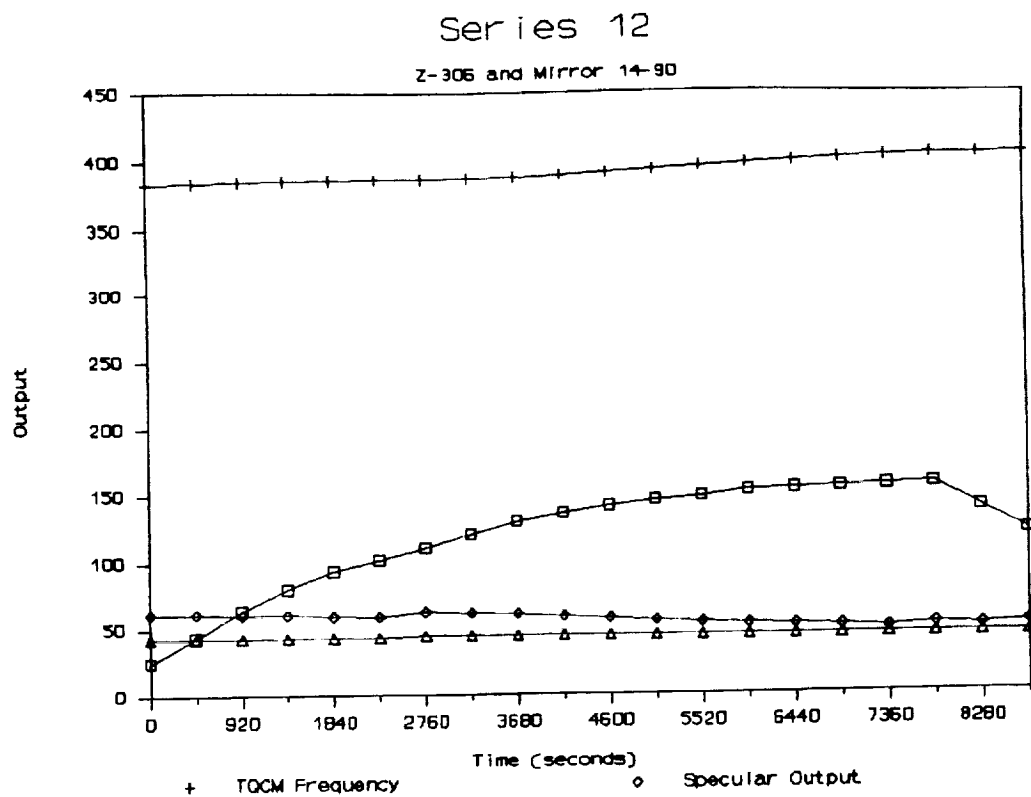
Figure 5.10. Relevant Data for Mirror 14-90.

Series 13

Z-306 w/s-polarization & Mirror 11-90

Z-306 Temperature   + TQCM Frequency   ◇ Specular Output

Series 13

Z-306 w/s-polarization and Mirror 11-90

□ Forward Scatter   + Specular Output   ◇ Back Scatter
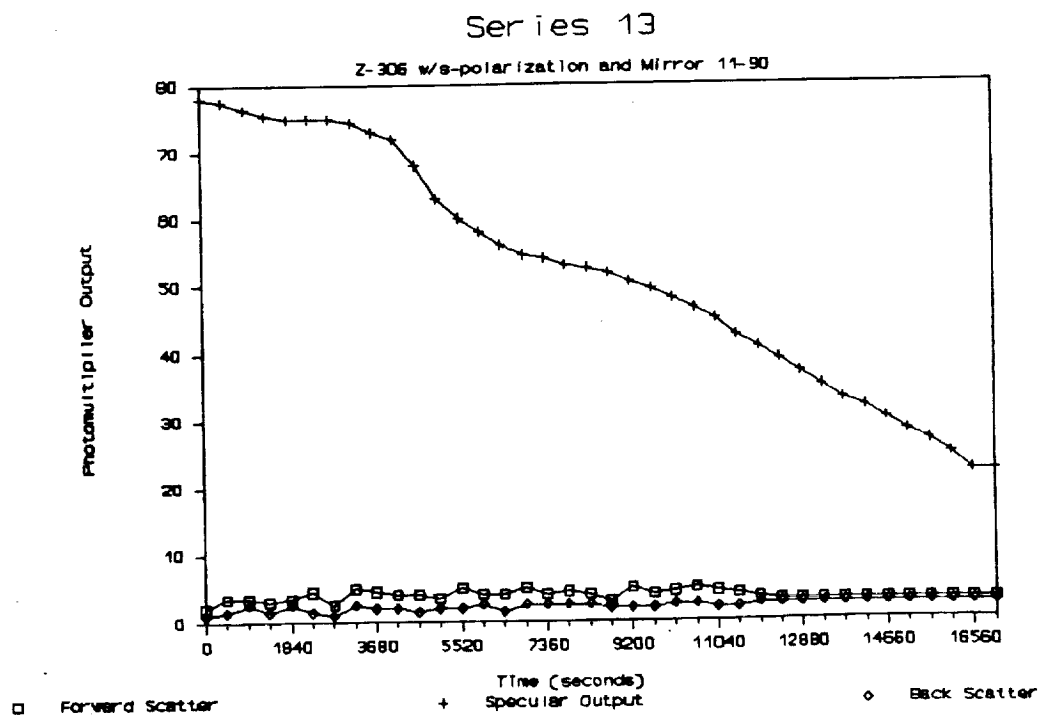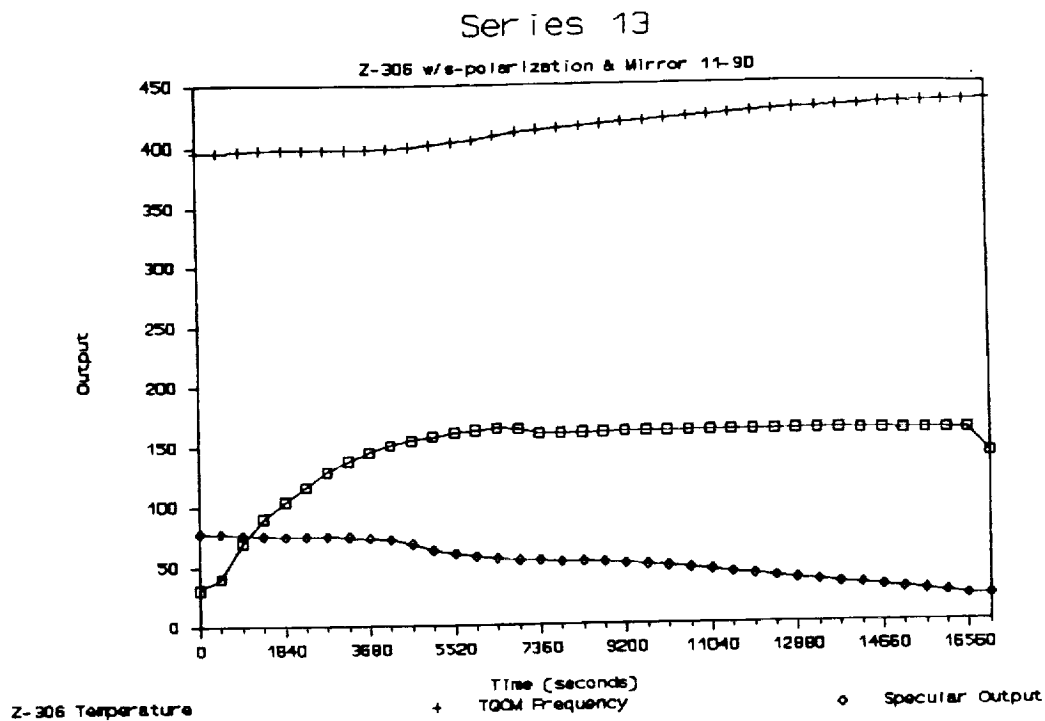
Figure 5.11. Relevant Data for Mirror 11-90.

Series 14

Z-306 w/p-polarization and Mirror K-90

Output (y-axis: 0 to 600)
Time (seconds) (x-axis: 0, 1111, 2951, 4791, 6631, 8100, 9780, 11400)

· 306 Temperature   + TQQM Frequency   ◇ Specular Output

Series 14

Z-306 w/p-polarization & Mirror K-90

Photomultiplier Output (y-axis: 0 to 60)
Time (seconds) (x-axis: 0, 1111, 2951, 4791, 6631, 8100, 9780, 11400)

□ Forward Scatter   + Specular Output   ◇ Back Scatter
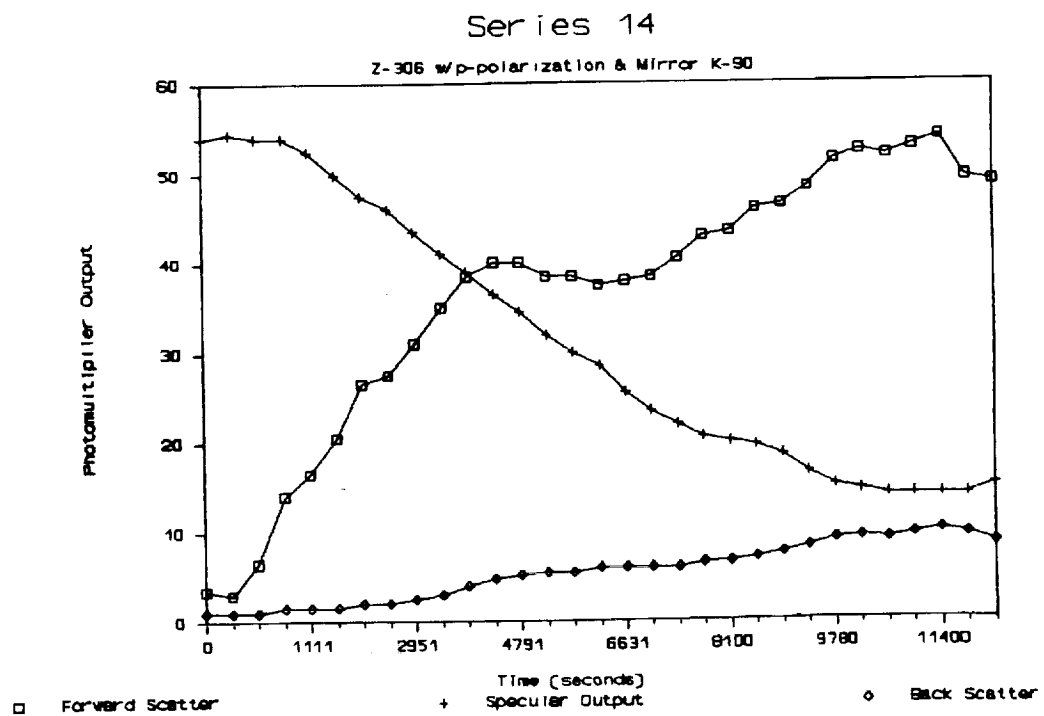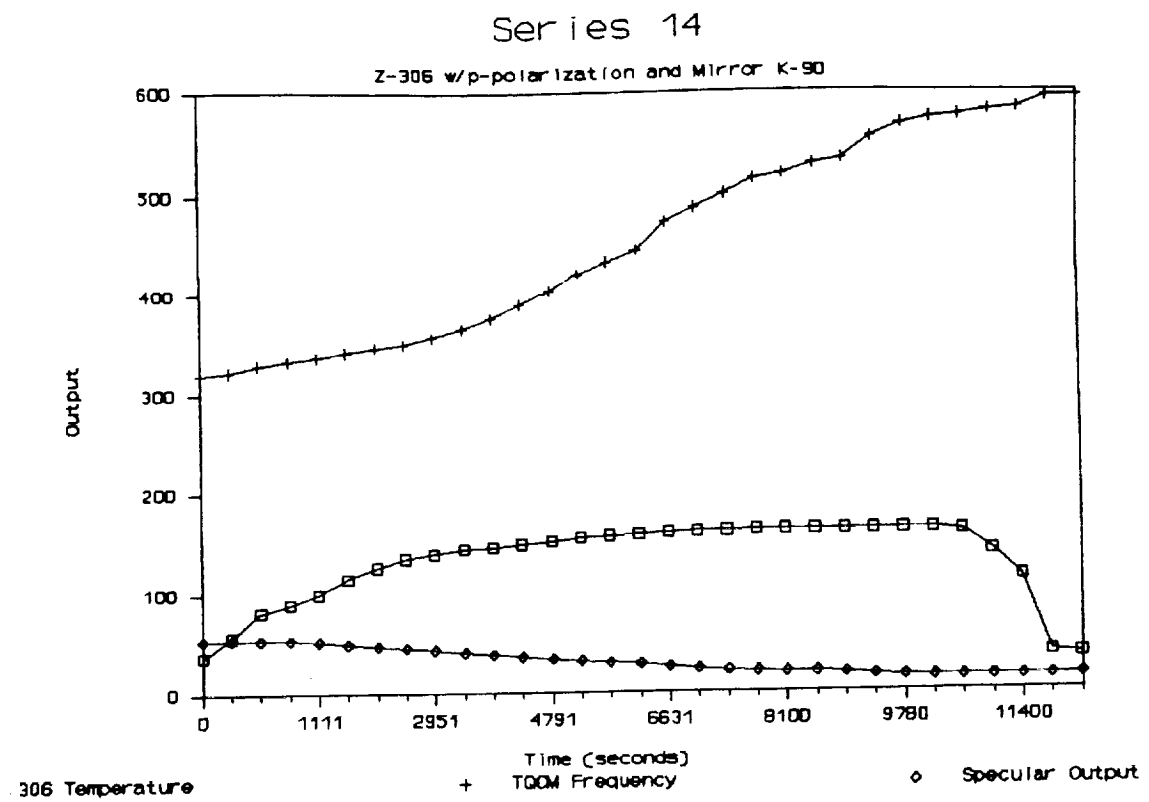
Figure 5.12.   Relevant Data for Mirror K-90.

Series 15

Z-306 w/p-polarization & Mirror 114-84

Z-306 Temperature   + TQCM Frequency   ◇ Specular Output

Series 15

Z-306 w/p-polarization & Mirror 114-84

□ Forward Scatter   + Specular Output   ◇ Back Scatter
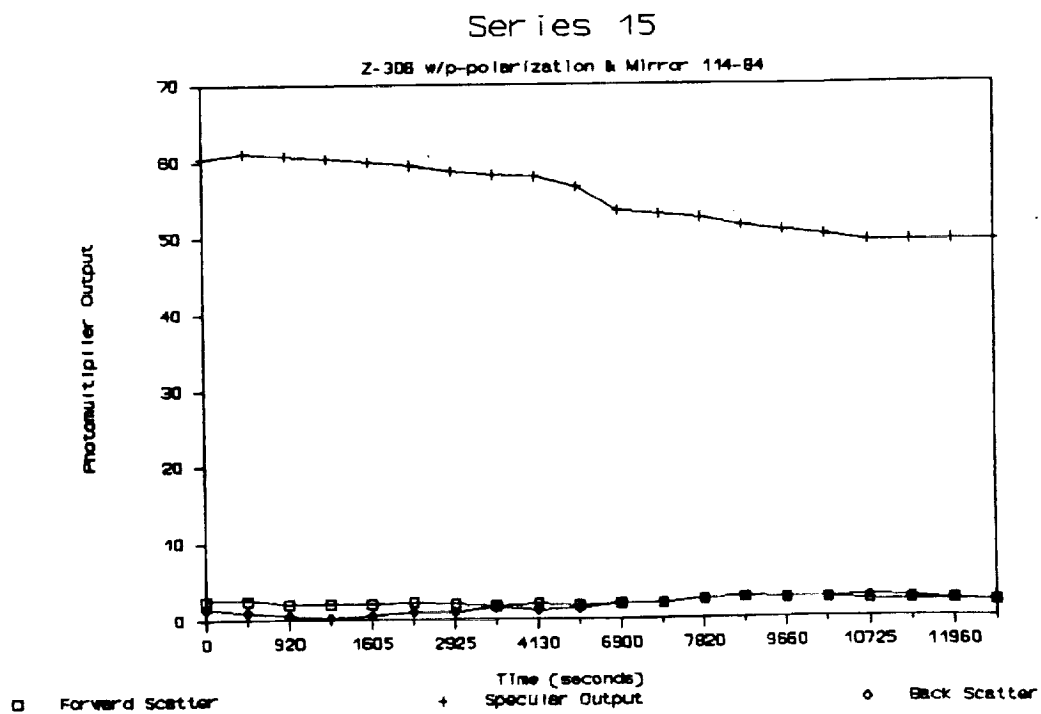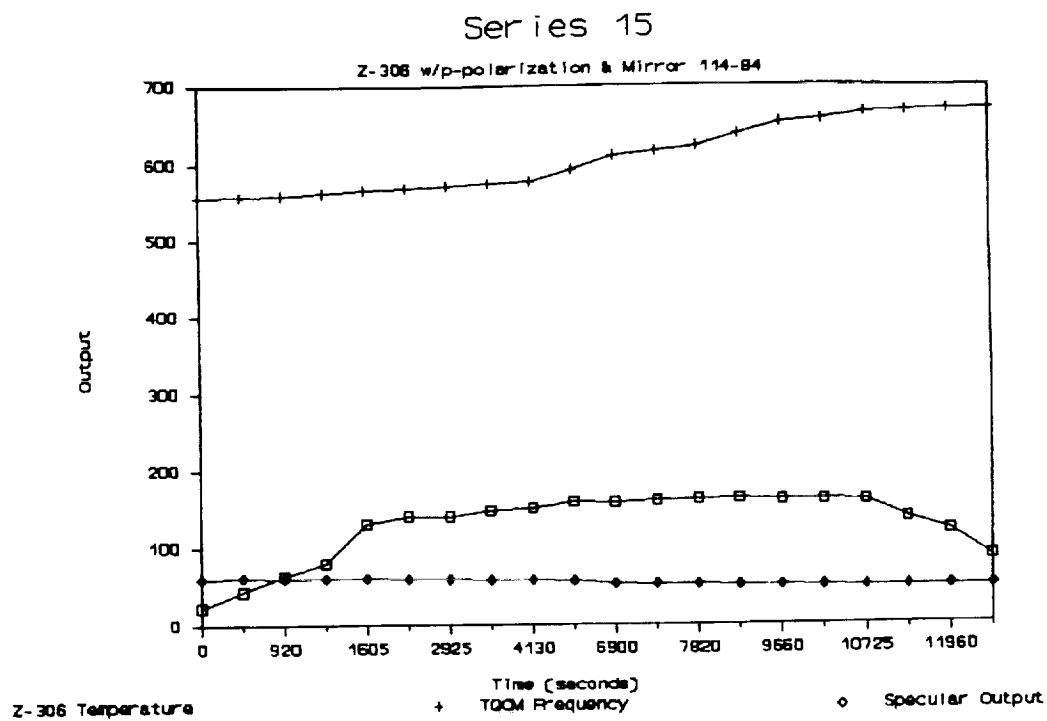
Figure 5.13.   Relevant Data for Mirror 114-84.

BRDF Values at 1606 Angstroms
(10 deg. angle of incidence)

Beta - Beta0

BRDF (1/sr)

□   3-89   +   43-85

Figure 5.15

BRDF Values at 2300 Angstroms
(10 deg. angle of incidence)

Beta - Beta0

BRDF (1/sr)

□   1-90   +   K-1   ◆   48-89

Figure 5.14

BRDF Values at 1606 Angstroms

(10 deg. angle of incidence)

Beta – Beta0

□ K-90   + 43-85

Figure 5.17

BRDF Values at 1606 Angstroms

(10 deg. angle of incidence)

Beta – Beta0

□ 49-89   + 43-85
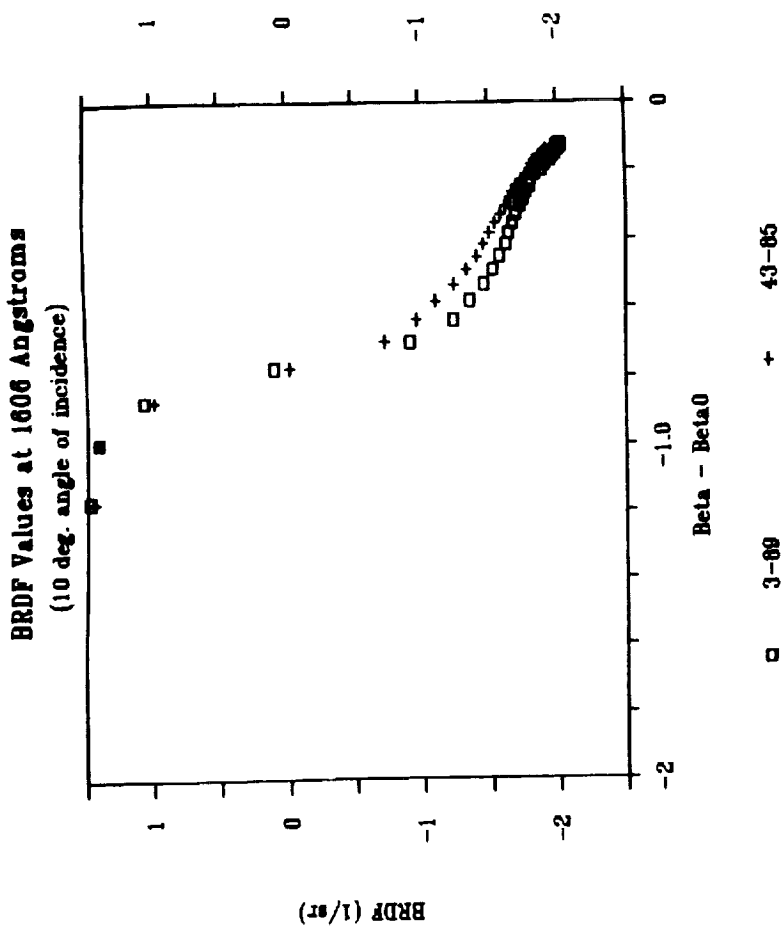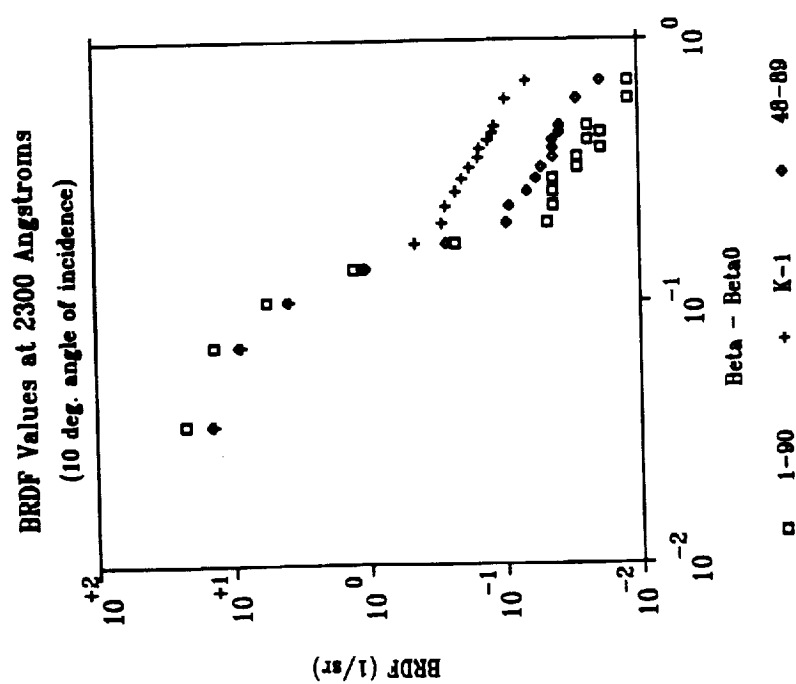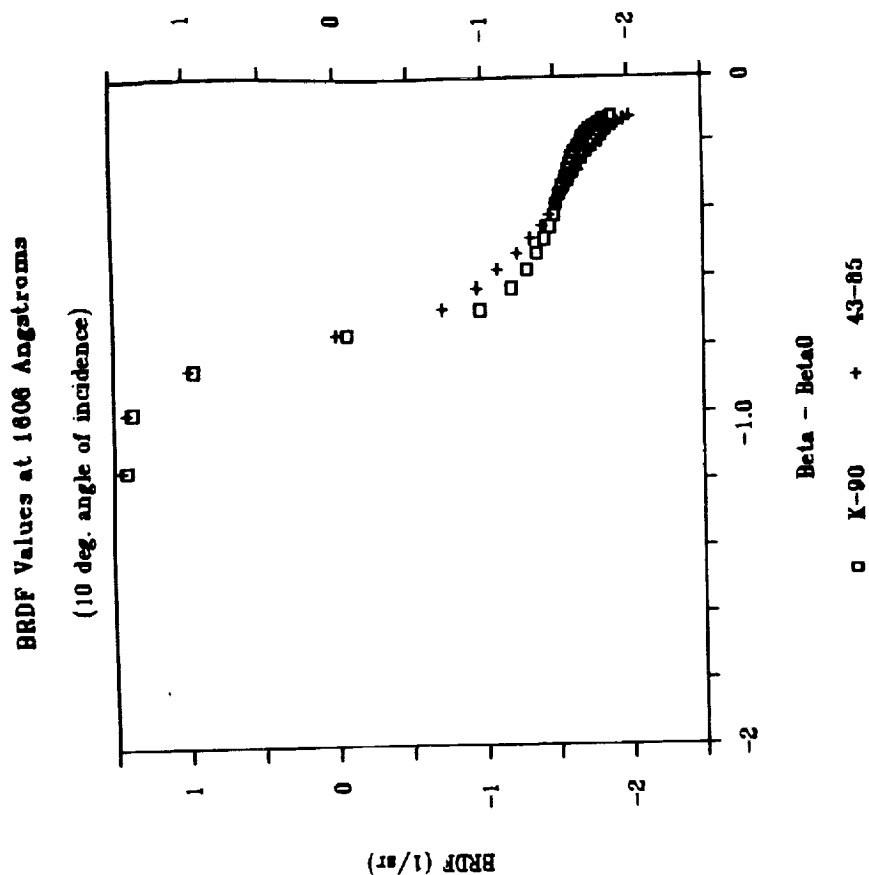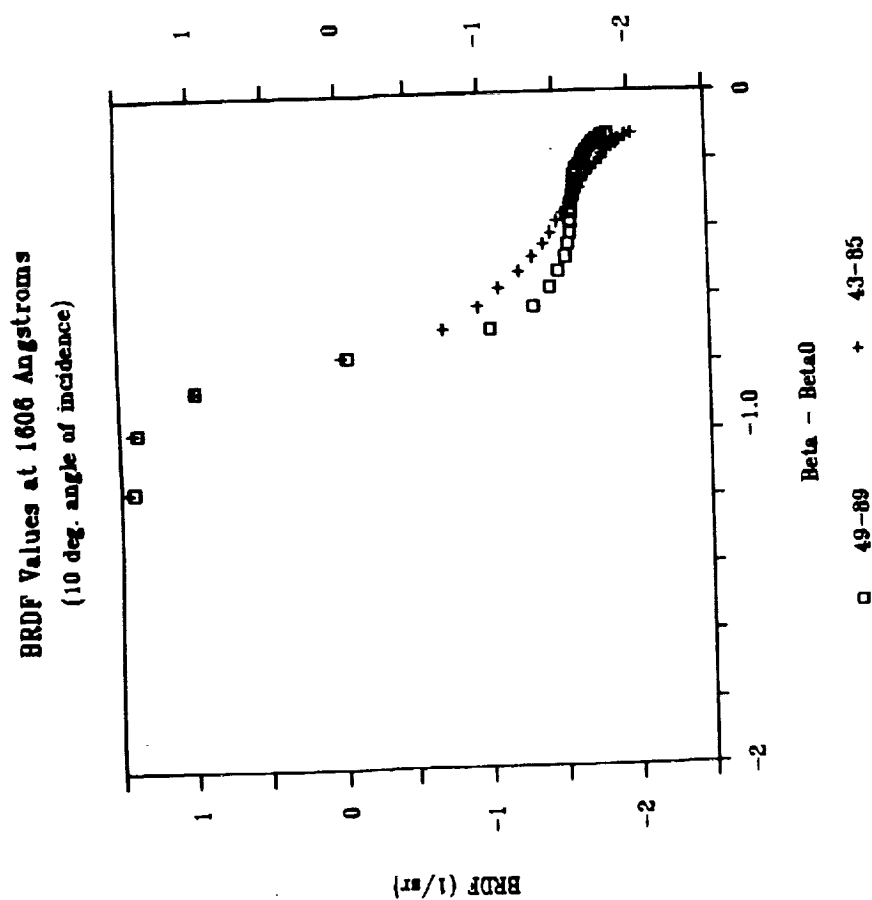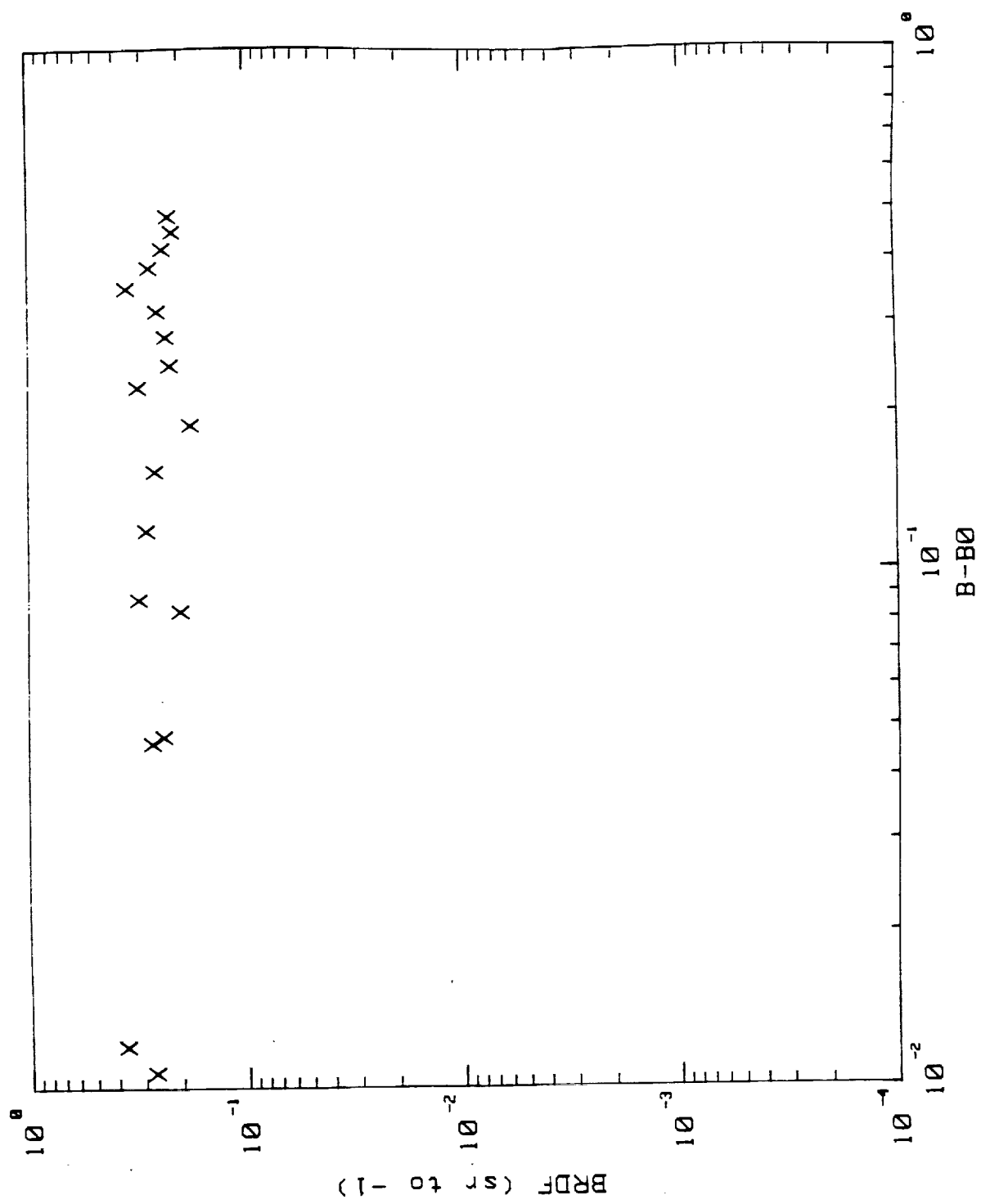
Figure 5.16

Figure 5.18.   Lambertian standard.
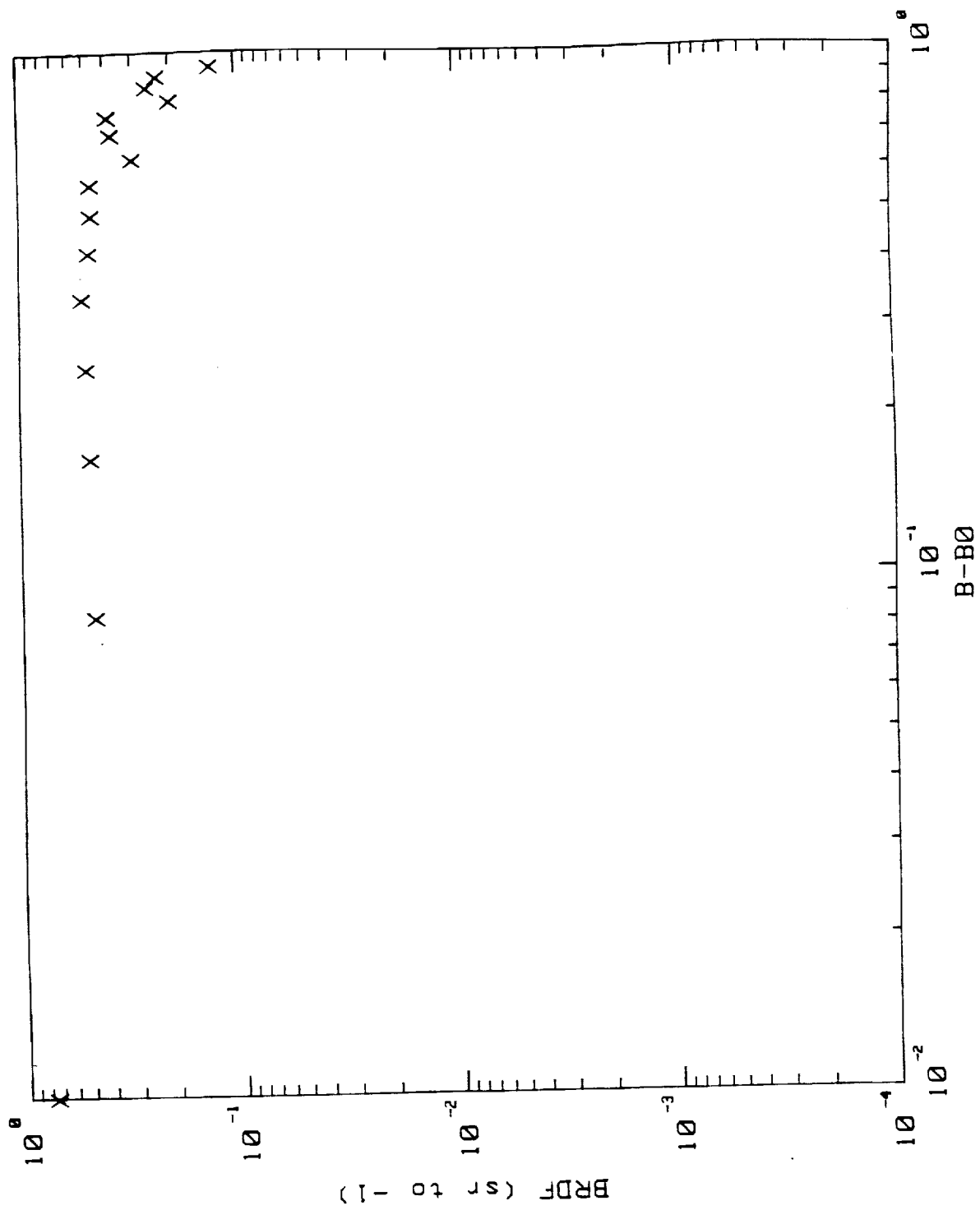
Figure 5.19.   BRDF of Z-93, white paint.
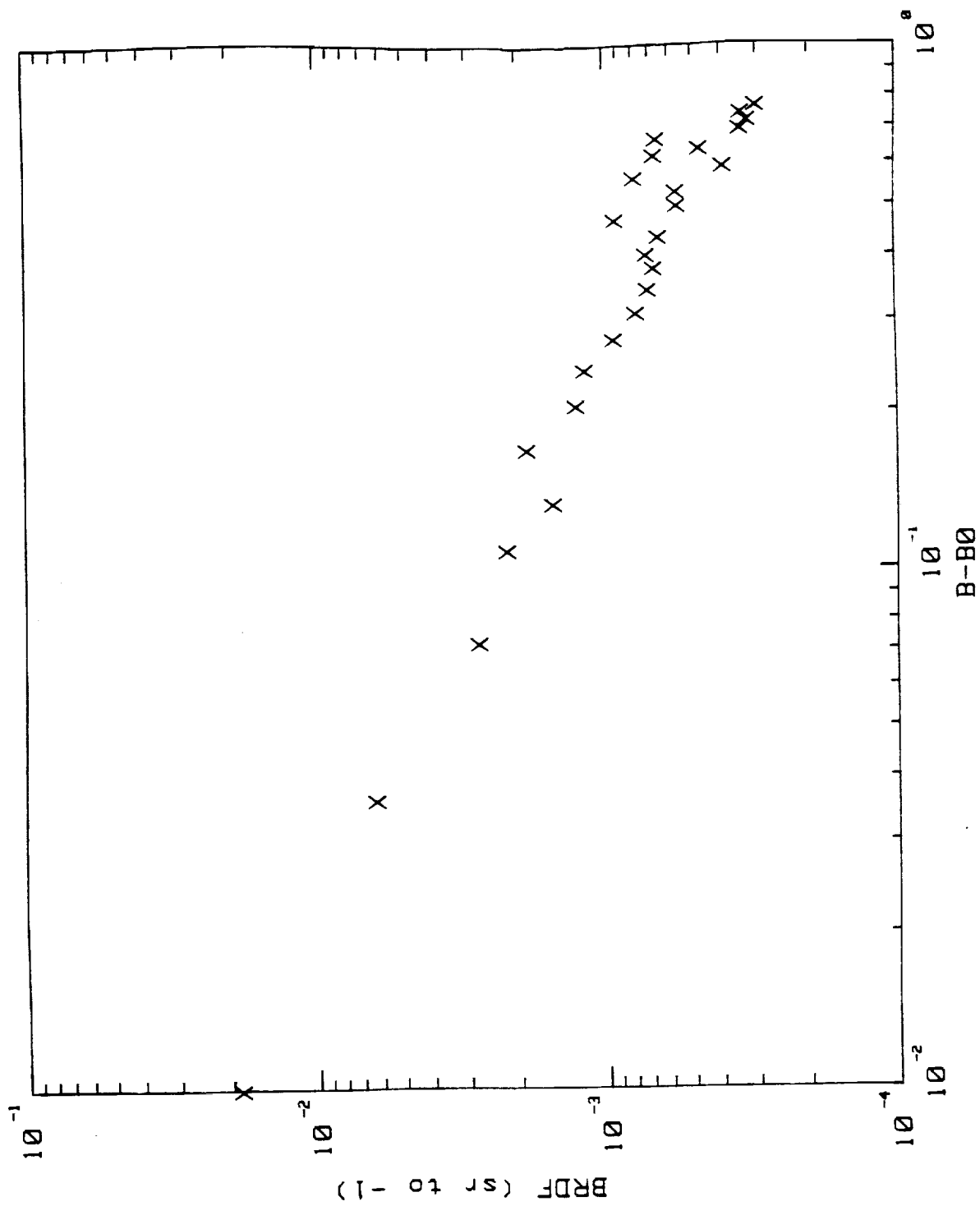
Figure 5.20. BRDF of a clean mirror.
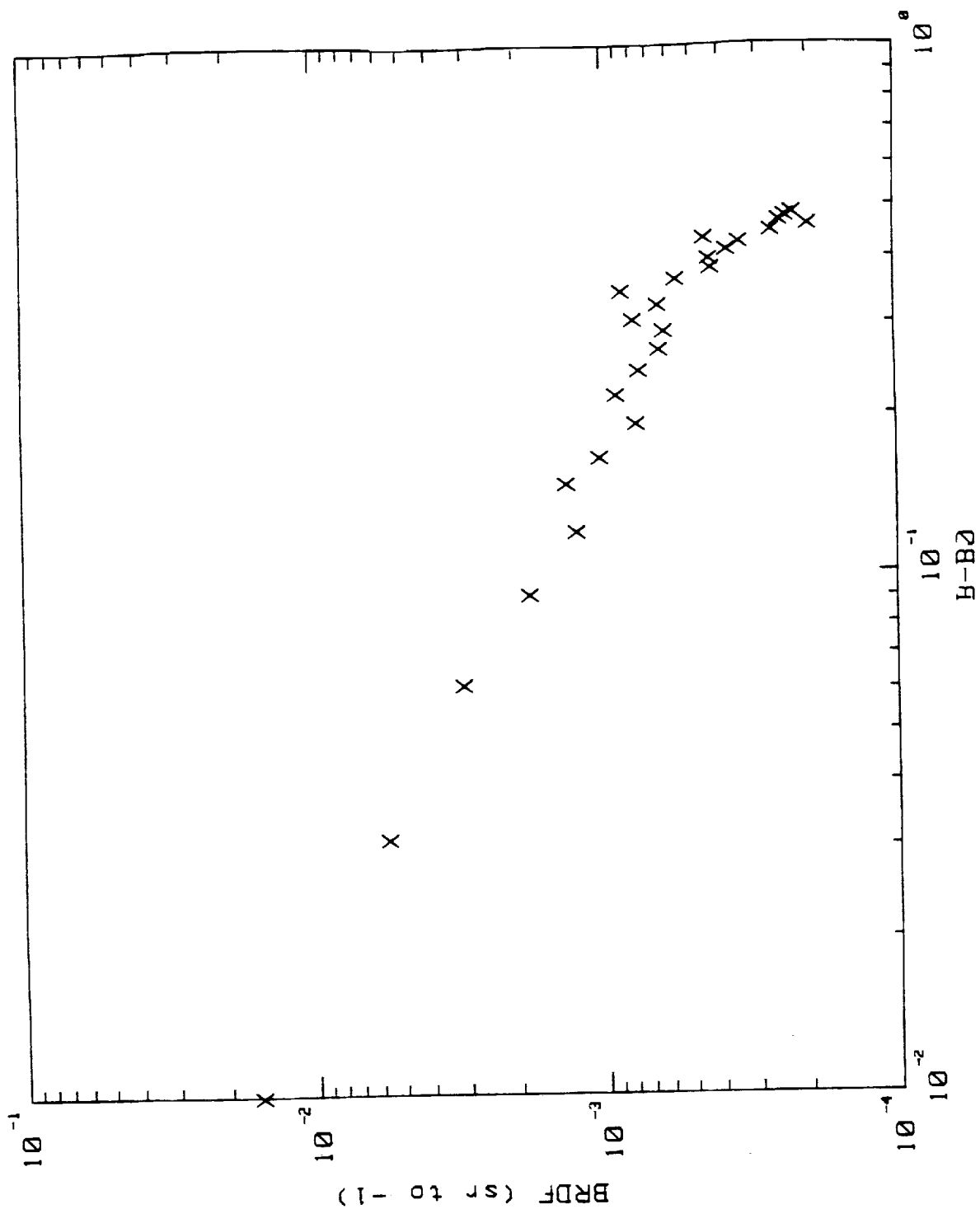
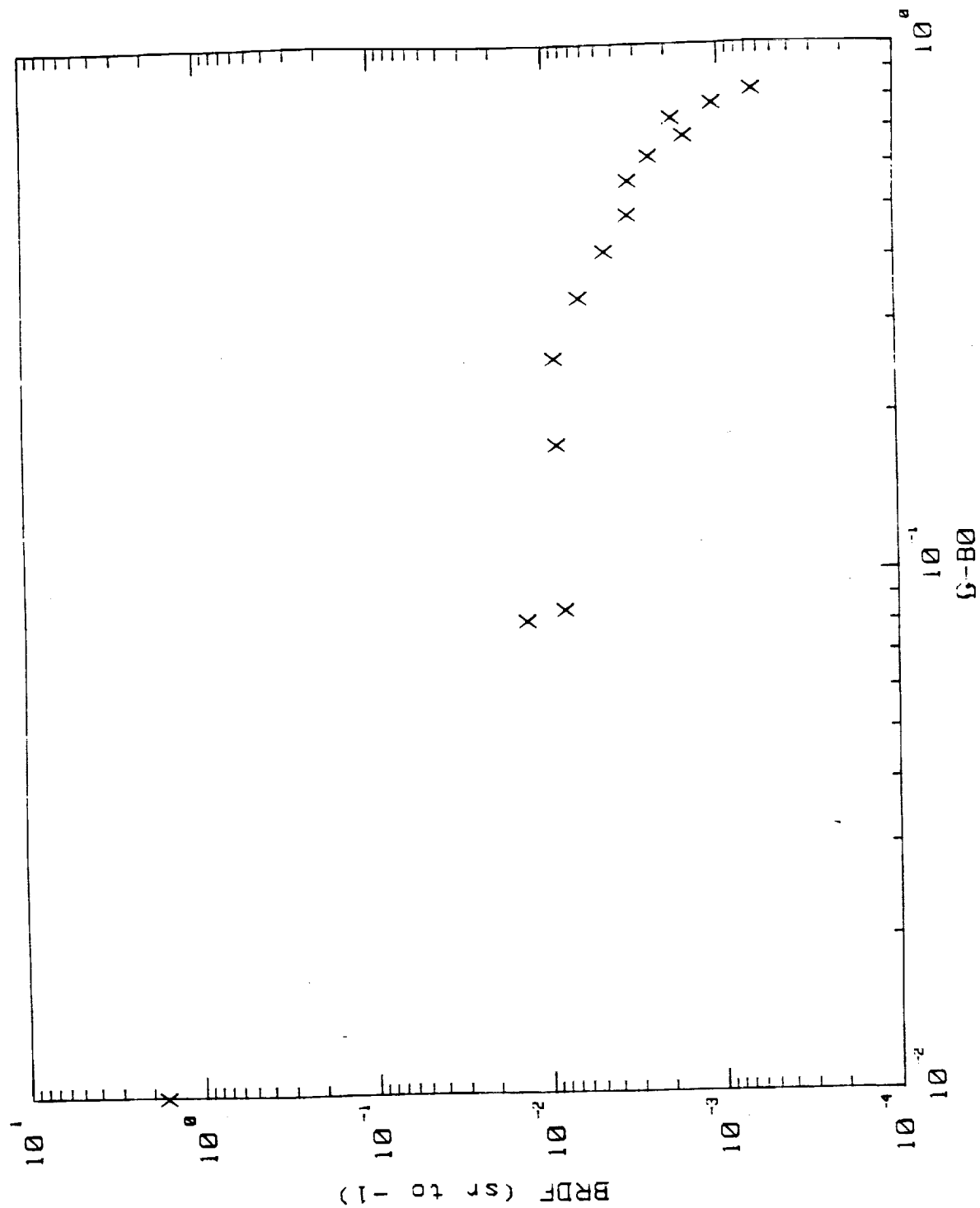Figure 5.24. Forward scatter for clean mirror at 30° incidence.

Figure 5.25. BRDF for lightly contaminated mirror (6-88) at near normal incidence.
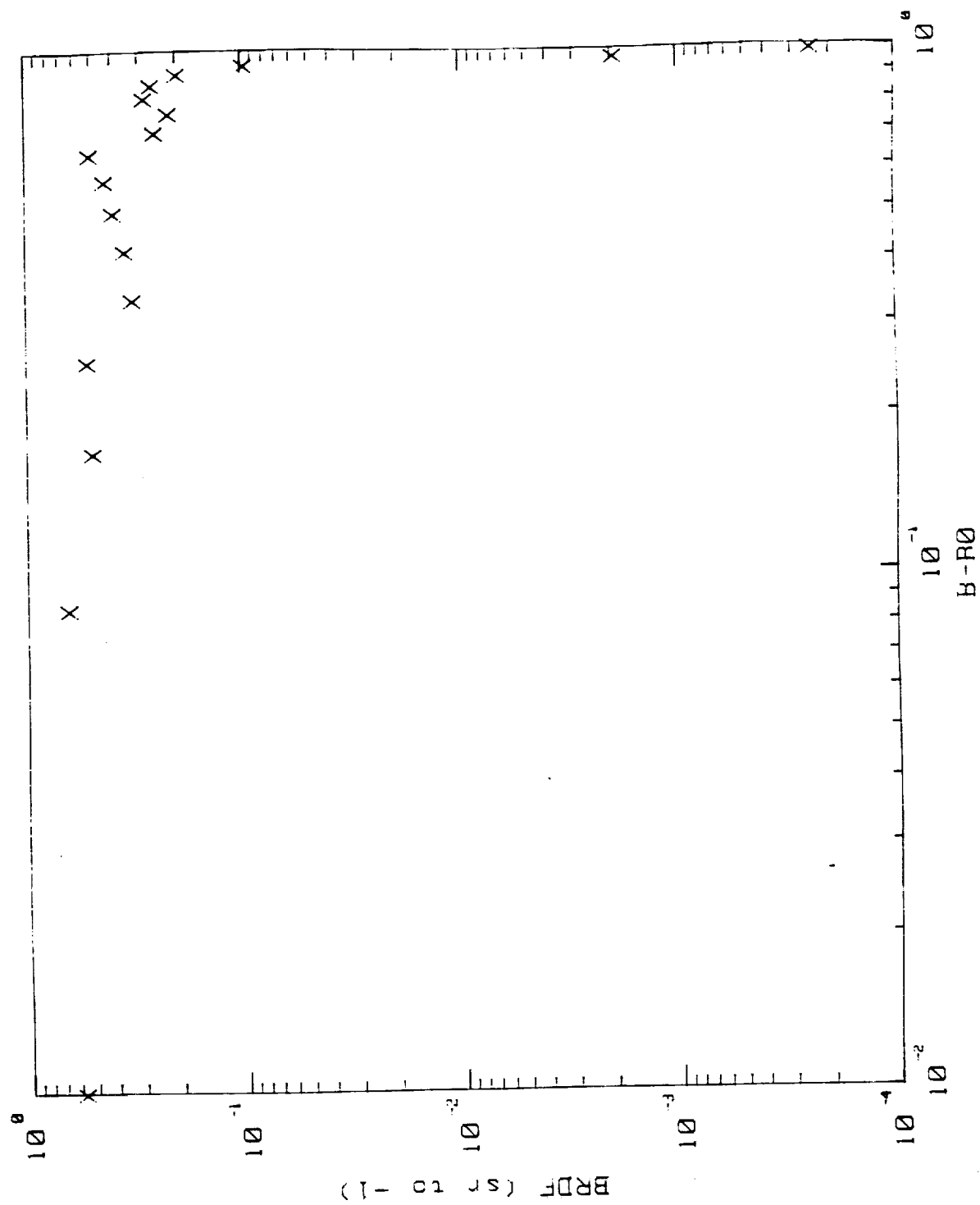
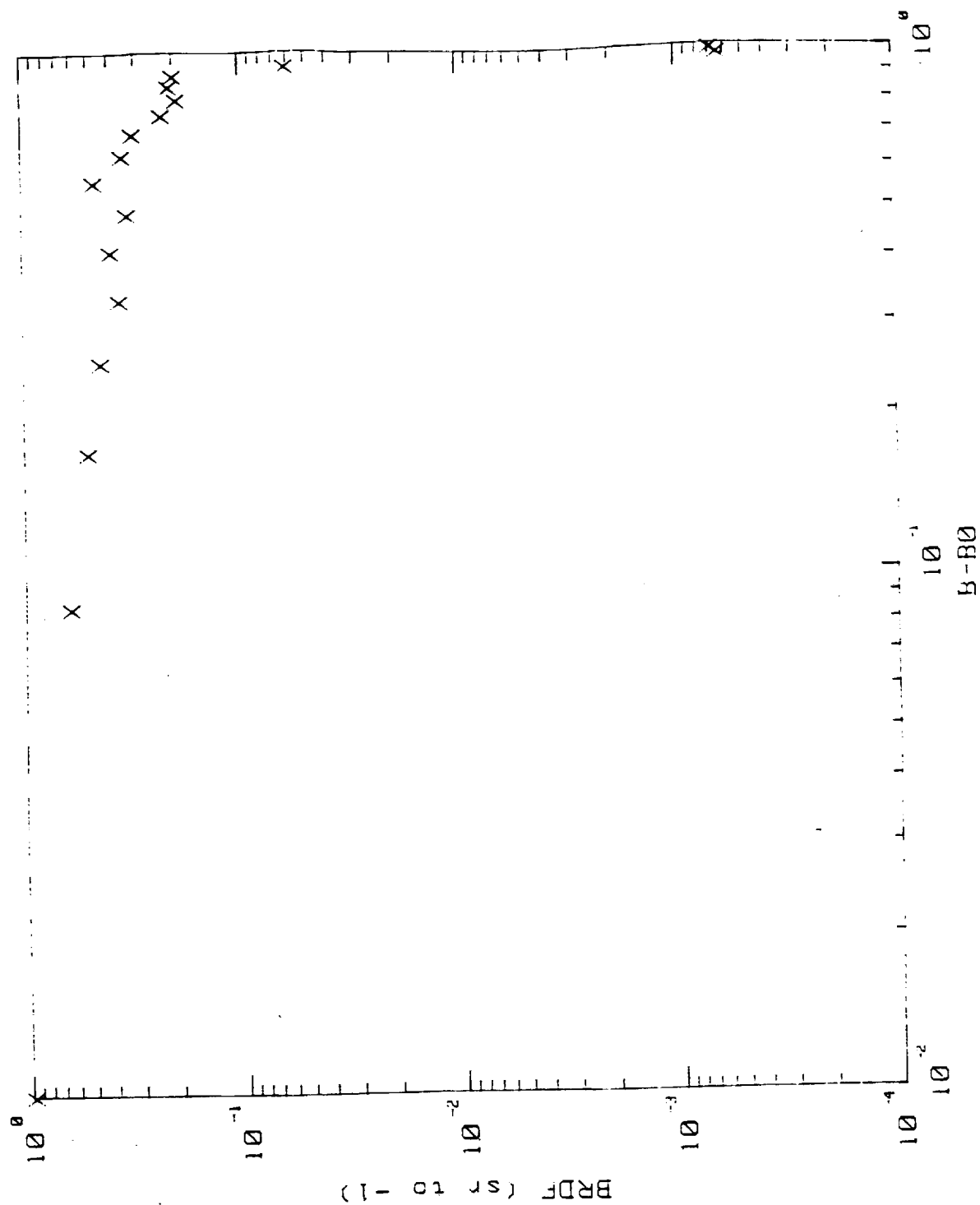Figure 5.26. BRDF of unexposed paint sample S136L flown on LDEF.

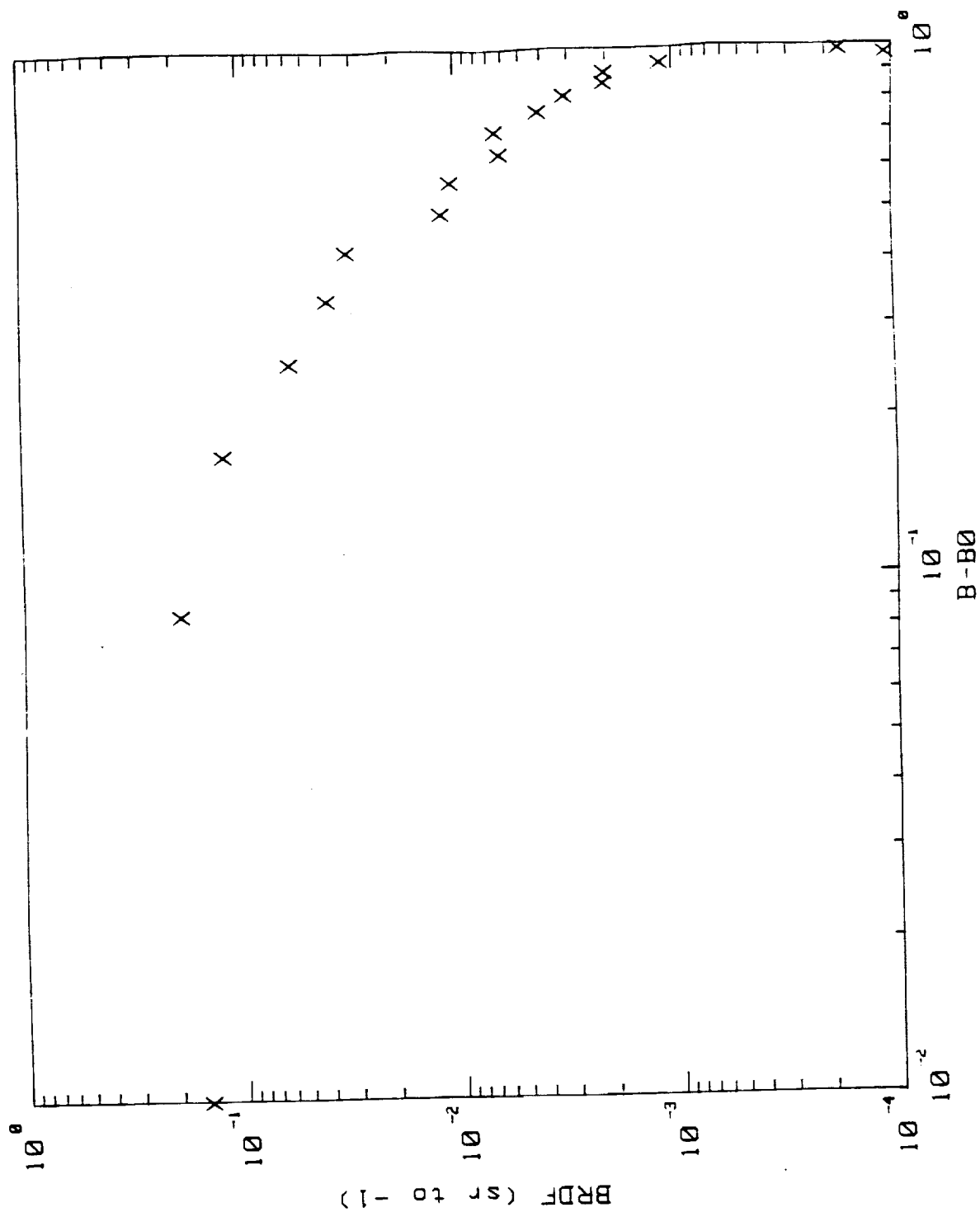Figure 5.27. BRDF of exposed samples of paint S136L flown on LDEF.

Figure 5.28. Type II anodized aluminum before exposure to atomic oxygen (grooves vertical).
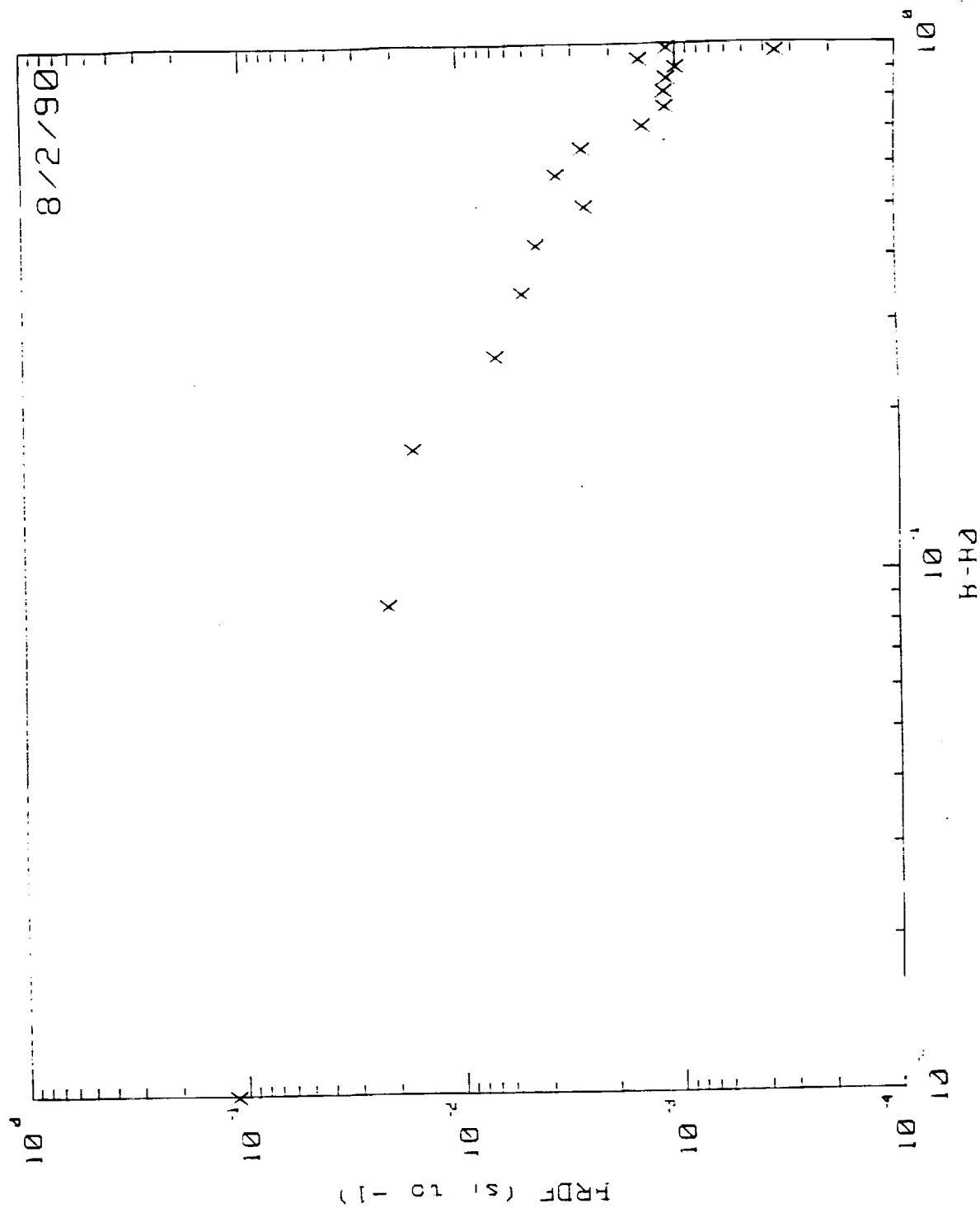
Figure 5.29. Type II anodized aluminum before exposure to atomic oxygen (Grooves horizontal).
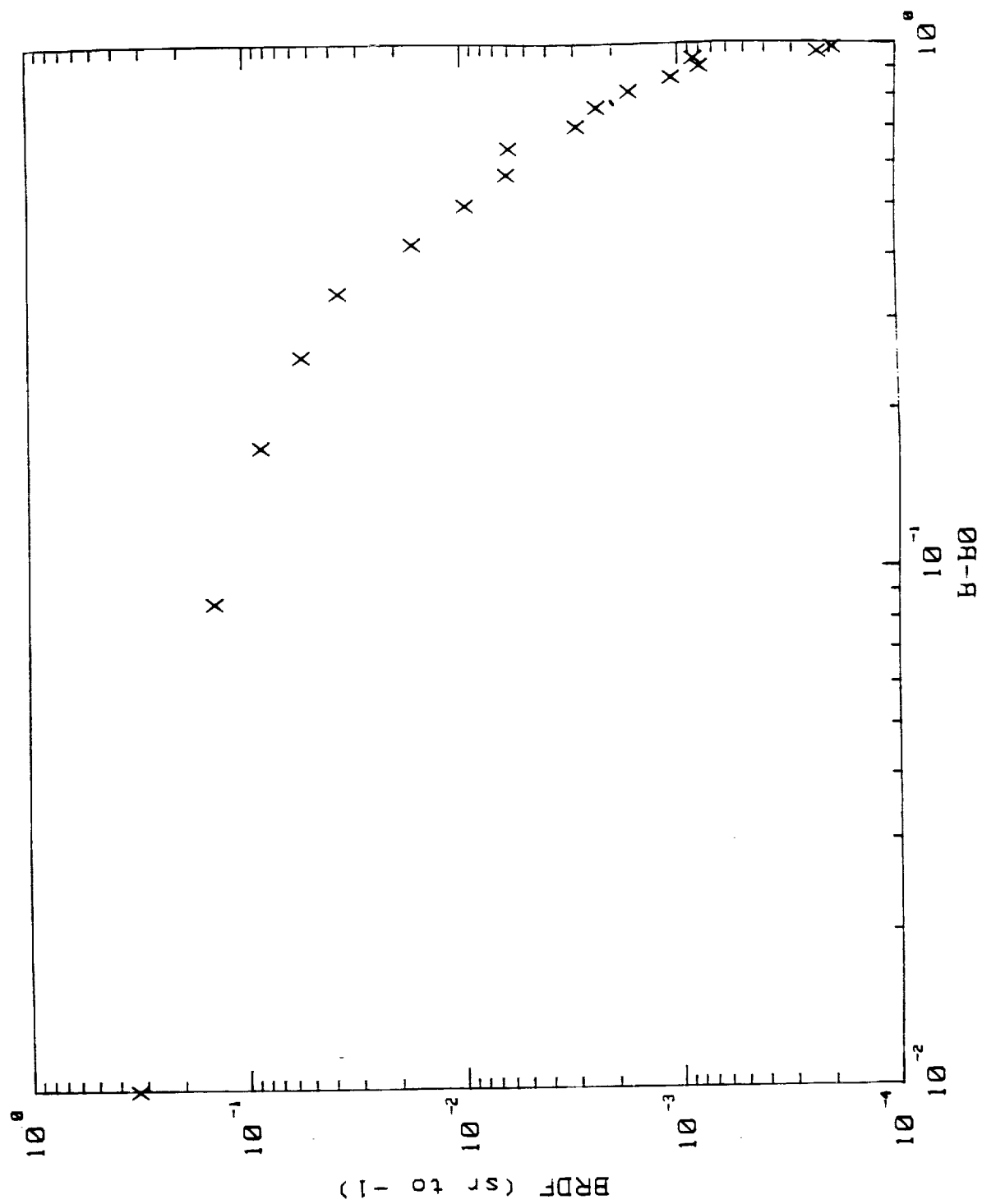
Figure 5.30. Type III anodized aluminum before exposure to atomic oxygen (grooves vertical).
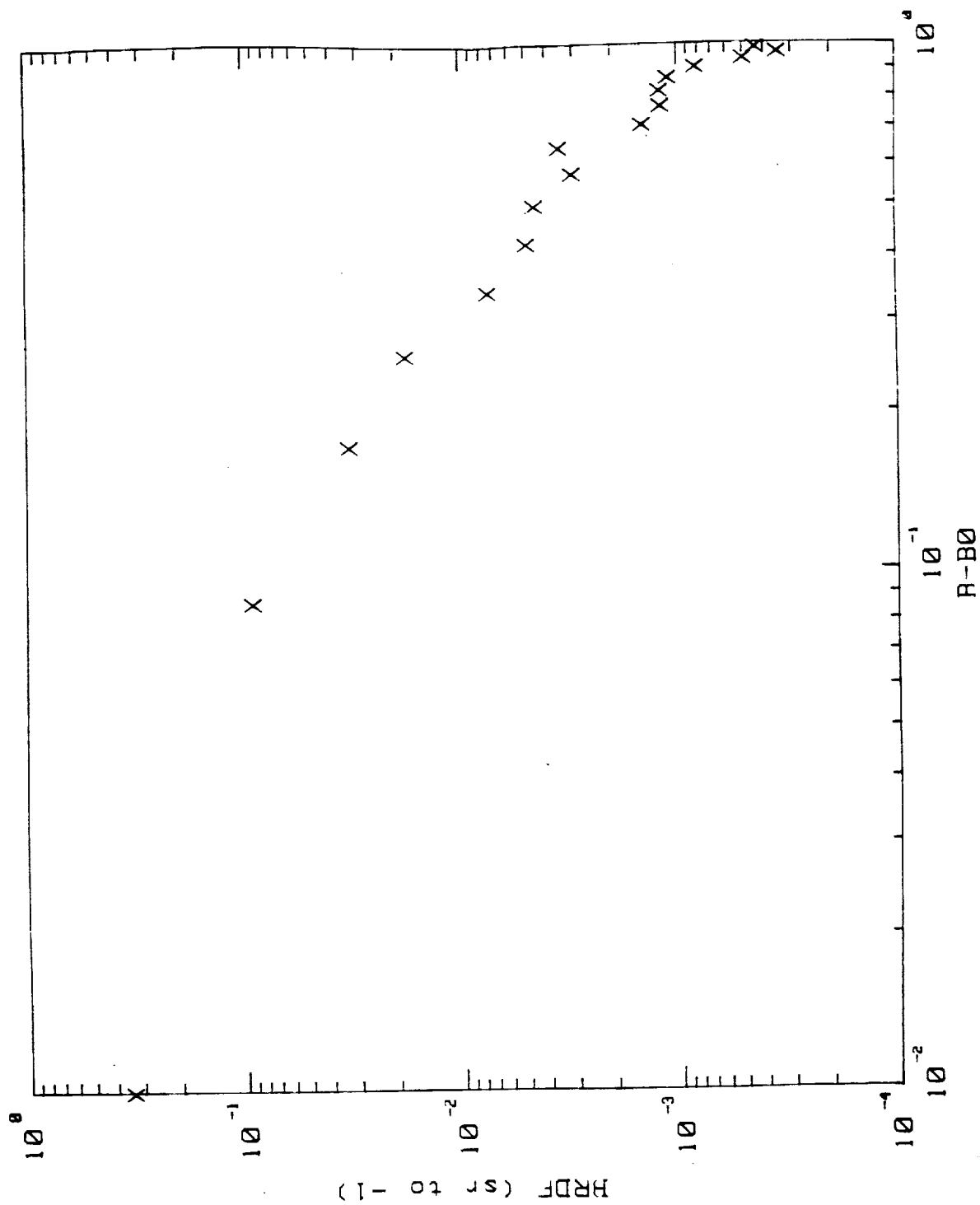
Figure 5.31. Type III anodized aluminum before exposure to atomic oxygen (grooves horizontal).

Figure 5.32. Type II anodized aluminum after exposure to atomic oxygen (grooves vertical).

Figure 5.33. Type II anodized aluminum after exposure to atomic oxygen (grooves horizontal).

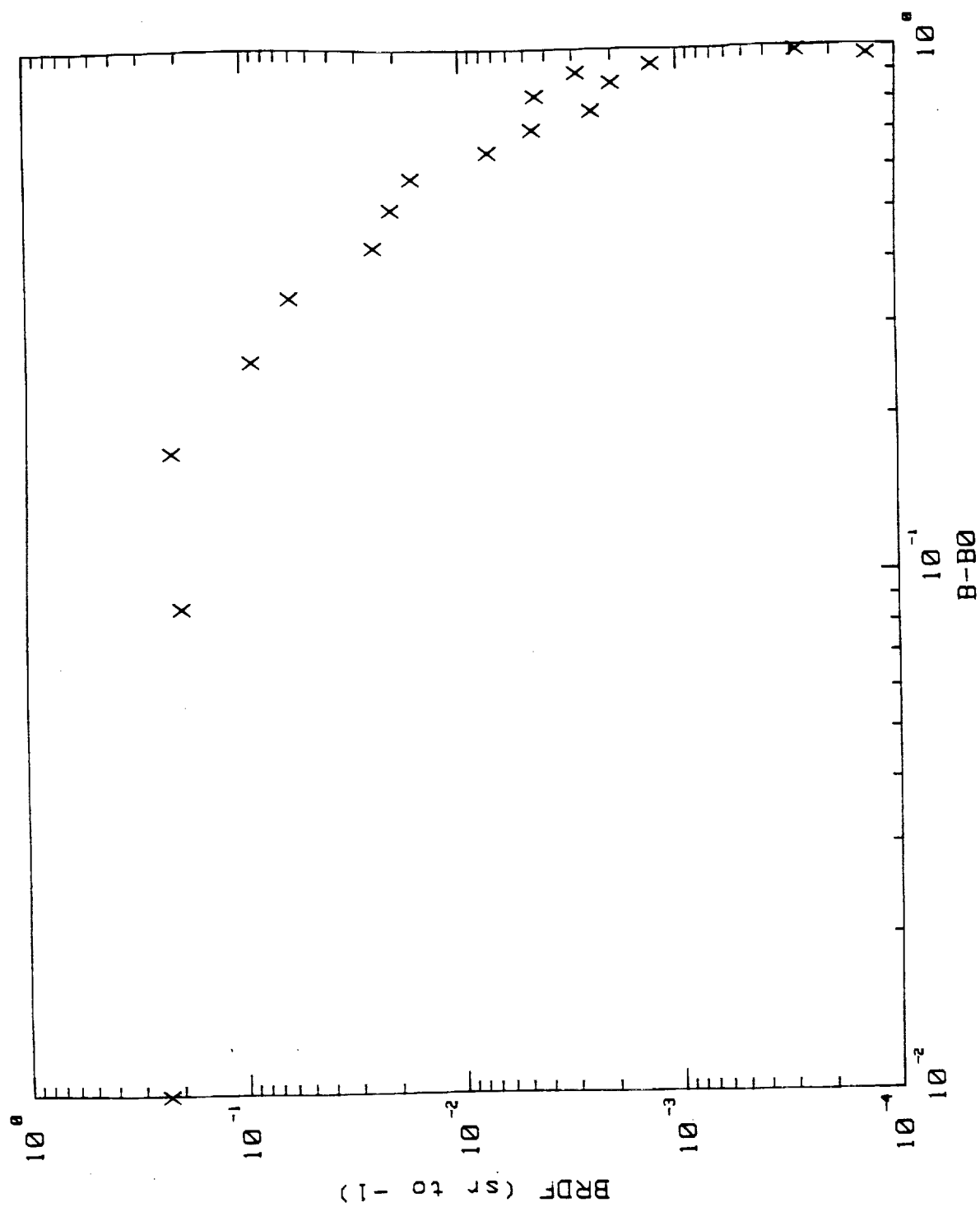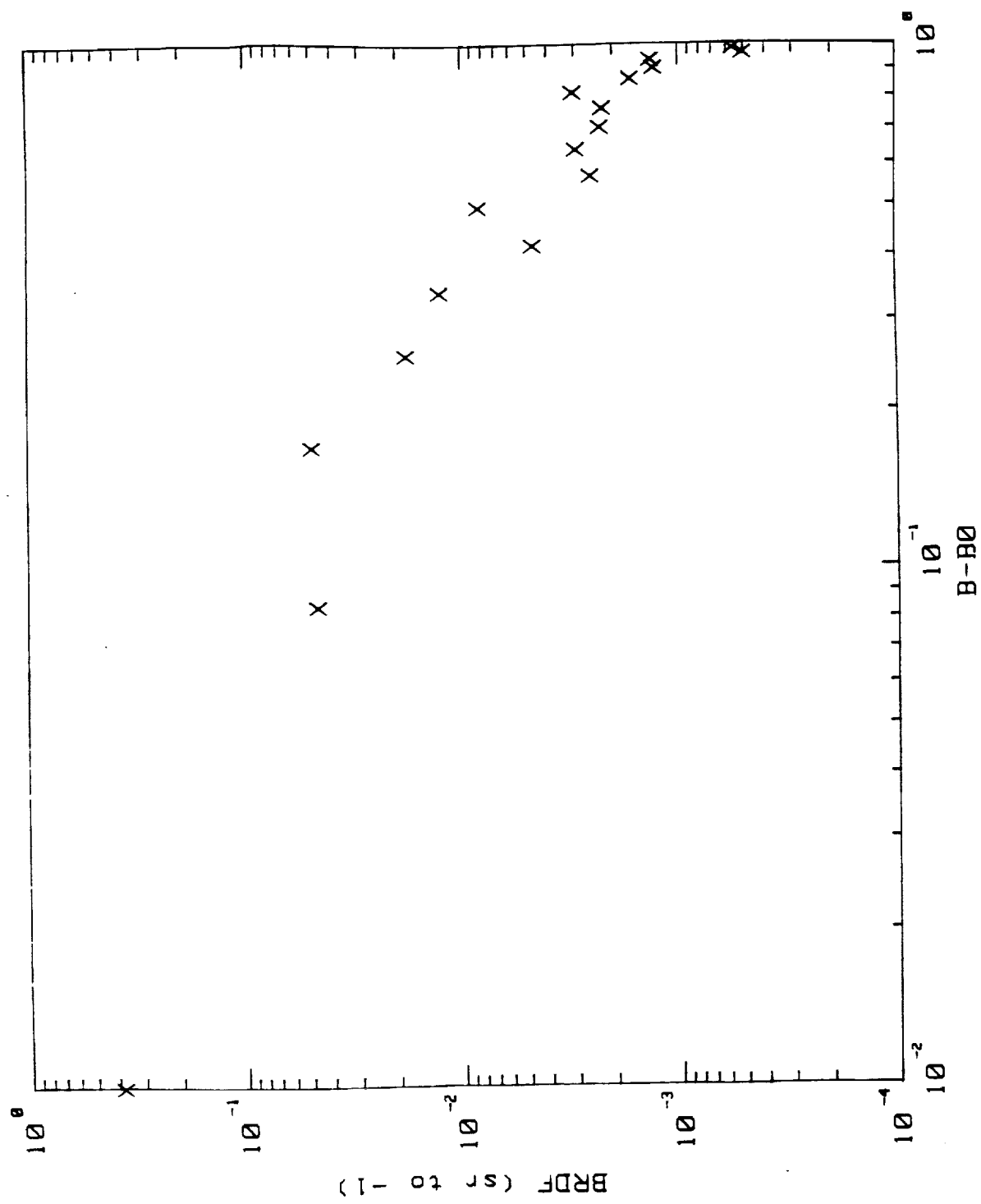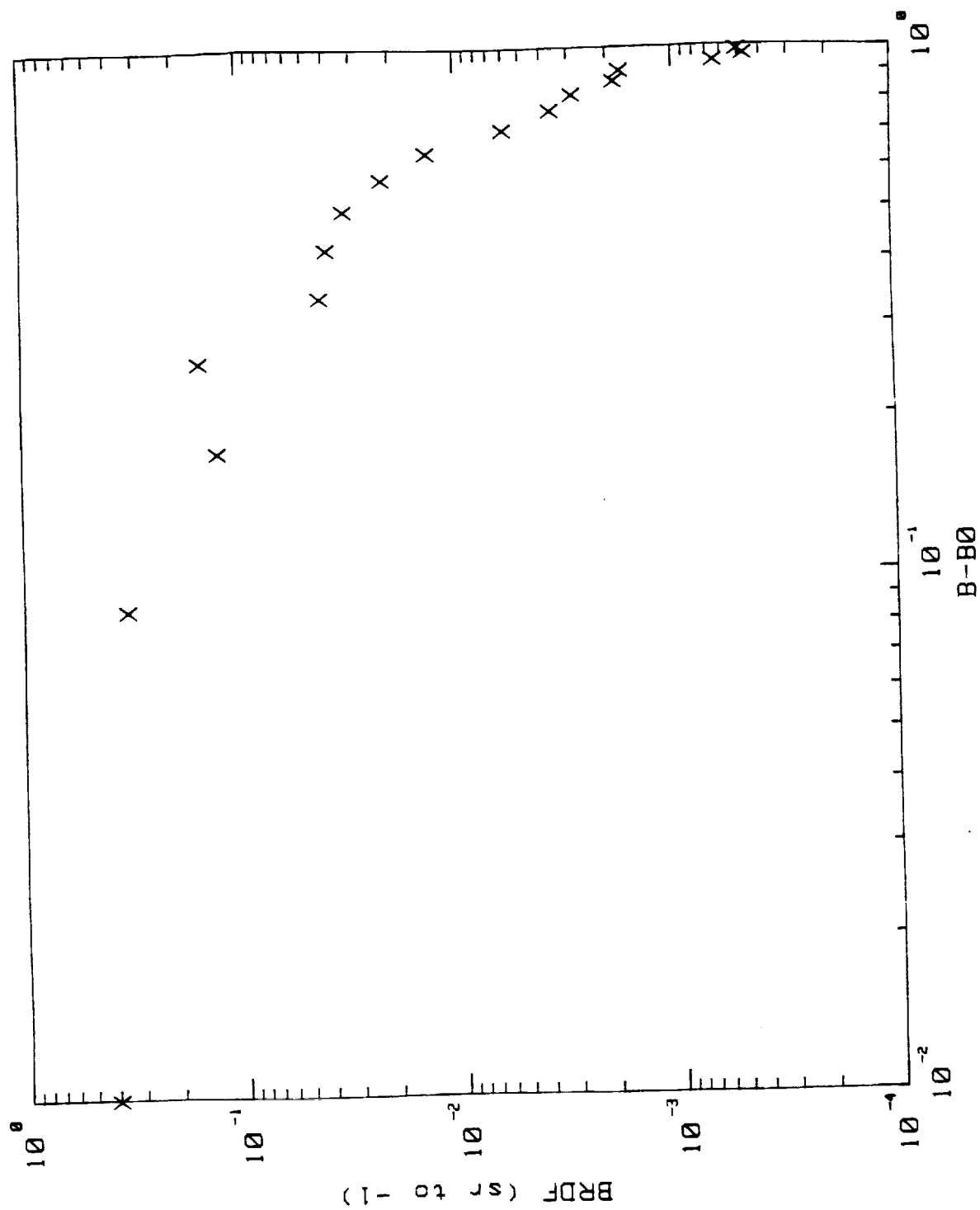Figure 5.34. Type III anodized aluminum after exposure to atomic oxygen (grooves vertical).
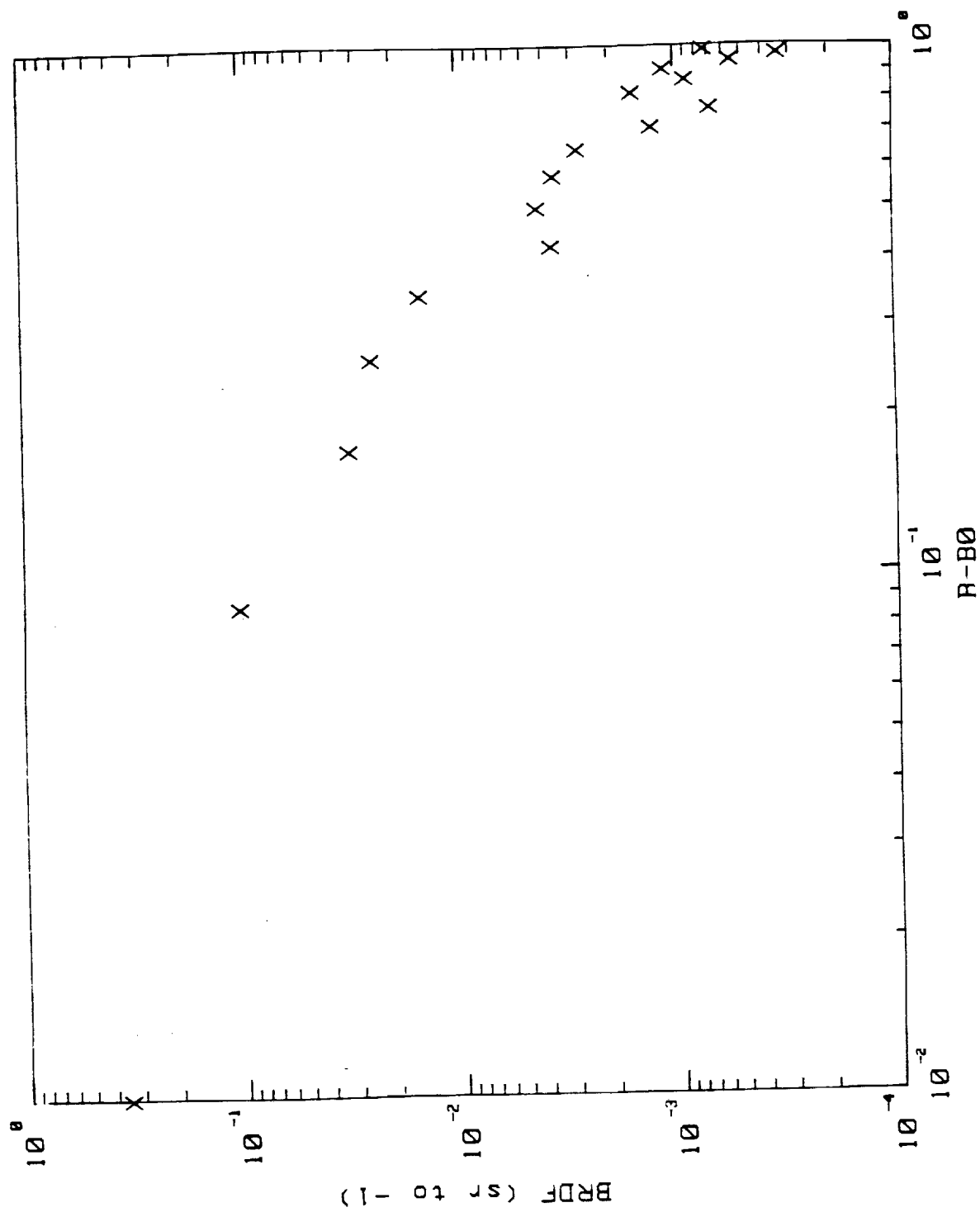
Figure 5.35. Type III anodized aluminum after exposure to atomic oxygen (grooves horizontal).

6.0 CONCLUSIONS

Measurements of the contamination of optical surfaces show that in some cases the material grows in separate distinct islands of contamination rather than in a uniform thin film. This can produce an increase in scattered light due to Mie type resonance scattering which can, because of the angular distribution of the scattering, impact the design of optical systems. We see that the current tests for acceptable levels of optical contamination must include not only loss of surface reflectance but also the distribution of any scattered light. In addition we have seen that by measuring the scattering in situ we can determine the effectiveness of a potential contaminant in a short time.

7.0 REFERENCES

1. Nicodemus, F.E., "Reflectance Nomenclature and Directional Reflectance and Emissivity," Appl. Opt. 9, 1474 (1970).

2. Bickel, W.S., Hsu, J., Chiao, S., Abromson, D. and Iafelice, V., "The Mueller Matrix-Stokes Vector Representation of Surface Scattering," Polarization Considerations for Optical Systems, SPIE Vol. 891, 32-39 (1988).

3. Bennett, H.E., "Scattering Characteristics of Optical Materials," Opt. Eng., 17, 480-488 (1978).

4. Elson, J.M. and Bennett, J.M., "Vector Scattering Theory," Opt. Eng., 18, No. 2, p. 116 (1979).

5. Elson, J.M., "Light Scattering from Semi-infinite Media for Non-normal Incidence," Phys Rev B, 12, No. 6, p. 2541 (1975).

6. Wang, Y. and Wolfe, W.L., "Scattering from Microrough Surfaces: Comparison of Theory and Experiment," J. Opt. Soc. Am., Vol. 73, No. 11, p. 1596, (Nov. 1983).

7. Church, E.L., Jenkinson, H.A. and Zavada, J.M., "Relationship between Surface Scattering and Microtopographic Features," Opt. Eng. 18, No. 2, p. 125 (1979).

8. Van de Hulst, H.C., Light Scattering by Small Particles, Wiley, New York, 1957.

9. Mie, G., Ann. Phys., 25, p. 377 (1908).

10. Azzam, R.M.A., "Photopolarimetric Measurement of the Mueller Matrix by Fourier Analysis of a Single Detected Signal," Optics Letters, 2, No. 6, 148-150 (1978).

11. Hamm, R.N., MacRae, R.A. and Arakawa, E.T., "Polarization Studies in the Vacuum Ultraviolet," J. Opt. Soc. Am., 55, 1460-1463 (1965).

Appendix A. Mathmatical Model of Mie Scattering Calculations

The following is a fortran program for calculating the surface scattering in the Mie scattering region for islands of molecular contamination. Input for the program is the complex index of refraction for the contaminant and the surface diameter distribution of the islands. The output is the scattering amplitude versus diameter (time) for any scattering angle and for both incident s- and p-polarization states.

```fortran
c
c       Program to calculate the value of scattered light versus
c              angle
c       for spheres of varying sizes
c
        program MIESCAT
c
c       include "c:\lahey22\f771\mie.inc"
        common /norm/ x, pi, spi
        common /polys/ polypi(0:21,100), polytau(0:22,100)
        common /ints/ iprint
c        common /plex/ zj1(50), zj2(50), fact(0:200)
c
        implicit integer*2 (i-n)
        implicit real*8 (o-z)
c        real*8 fact
        complex*16 an(20), bn(20), em, a(0:20), cy, tp1, tp2,
       *w(-1:20), s1(0:100), s2(0:100), tp3, tp4, tp5, tp6
        character aprint
c
        pi=3.141592654d0
        spi=dsqrt(pi)
c
c
        print *, 'You are entering the world of Mie scattering...'
        print *, 'Want to enter the data or use the RUN.DAT file?'
        print *, 'Enter "D" for hand entry of data'
        read(*,*) iprint
        if (iprint.eq.999) then
1       continue
        print *, '...Enter the starting and ending radii?'
        read(*,*)  x1, x2
        print *, '...Enter the complex index of refraction?'
        read(*,*) em
        print *, '...Enter the wavelength'
        read(*,*) wavl
c
        print *, 'You have entered the following values...'
        print *, 'starting radius      = ', x1
        print *, 'ending radius        = ', x2
        print *, 'index of refraction = ', em
        print *, 'wavelength           = ', wavl
        print *, 'Are these values correct (Y/N)?'
        read(*,*) aprint
        if (aprint.eq.'N') then
           goto 1
        endif
c
        else
        open (5,err=800,file='run.dat', status='old')
        read (5, *) wavl
        print *, wavl
        read (5,*) em
        print * , em
```
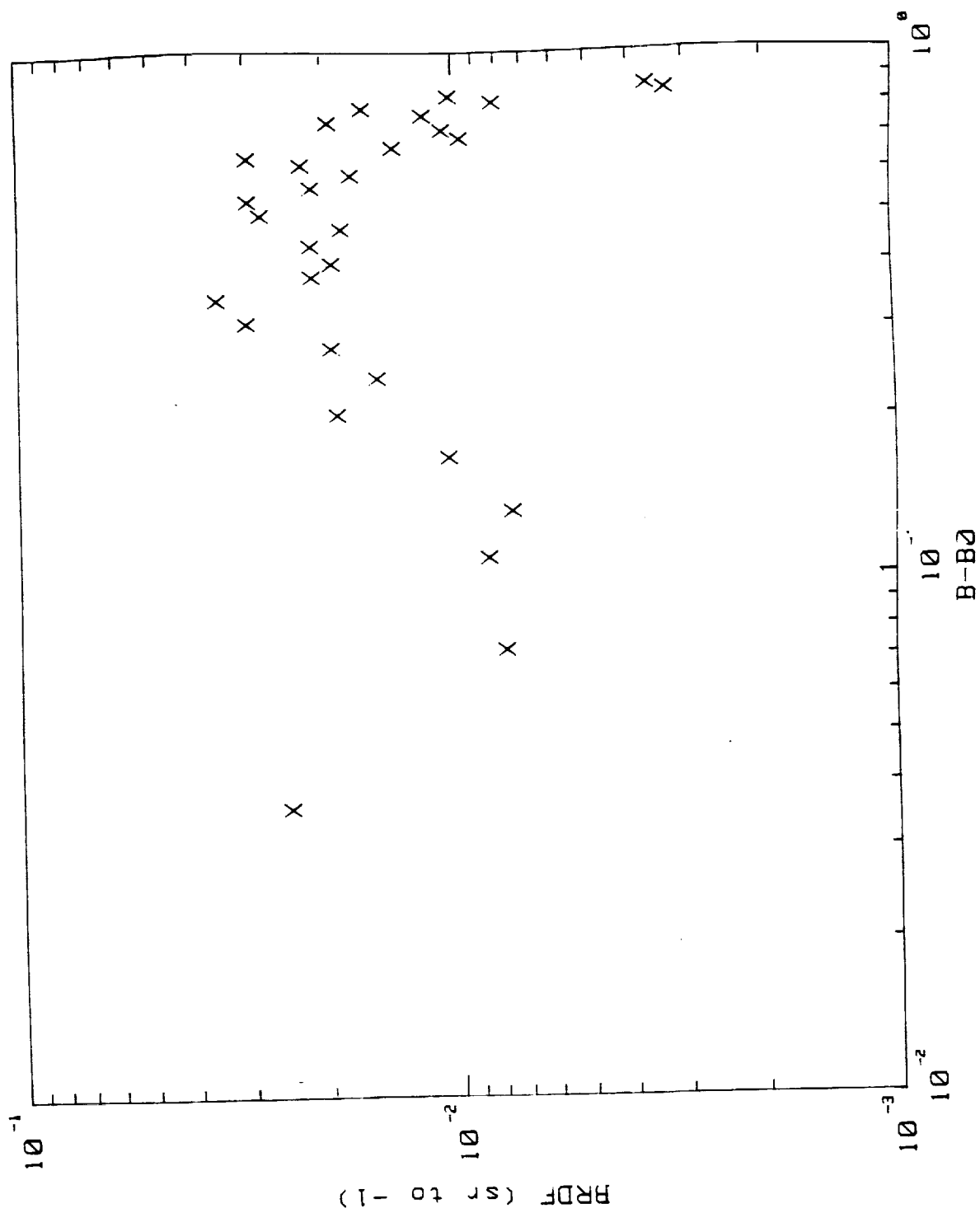
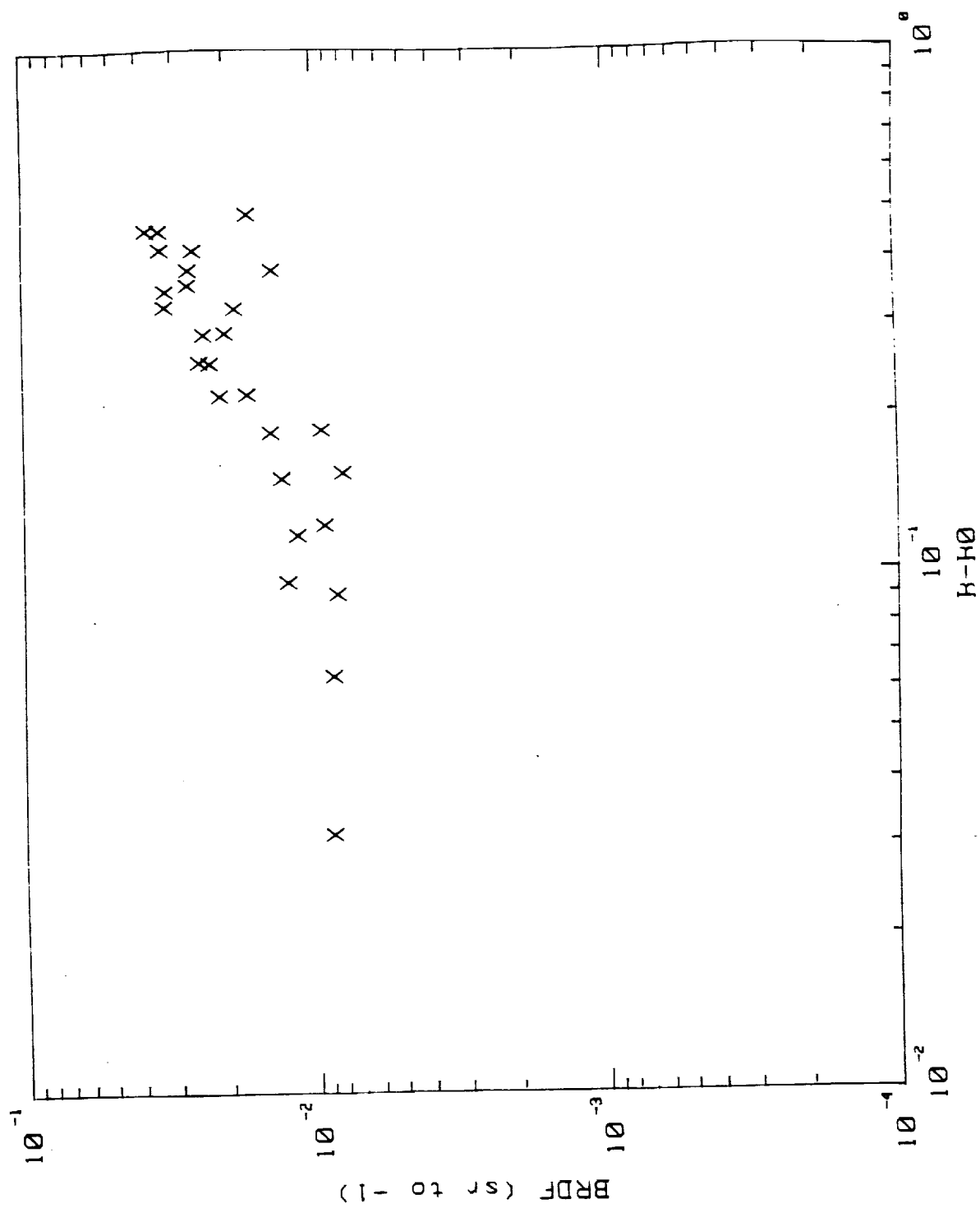Figure 5.21. BRDF of a highly contaminated mirror at normal incidence.

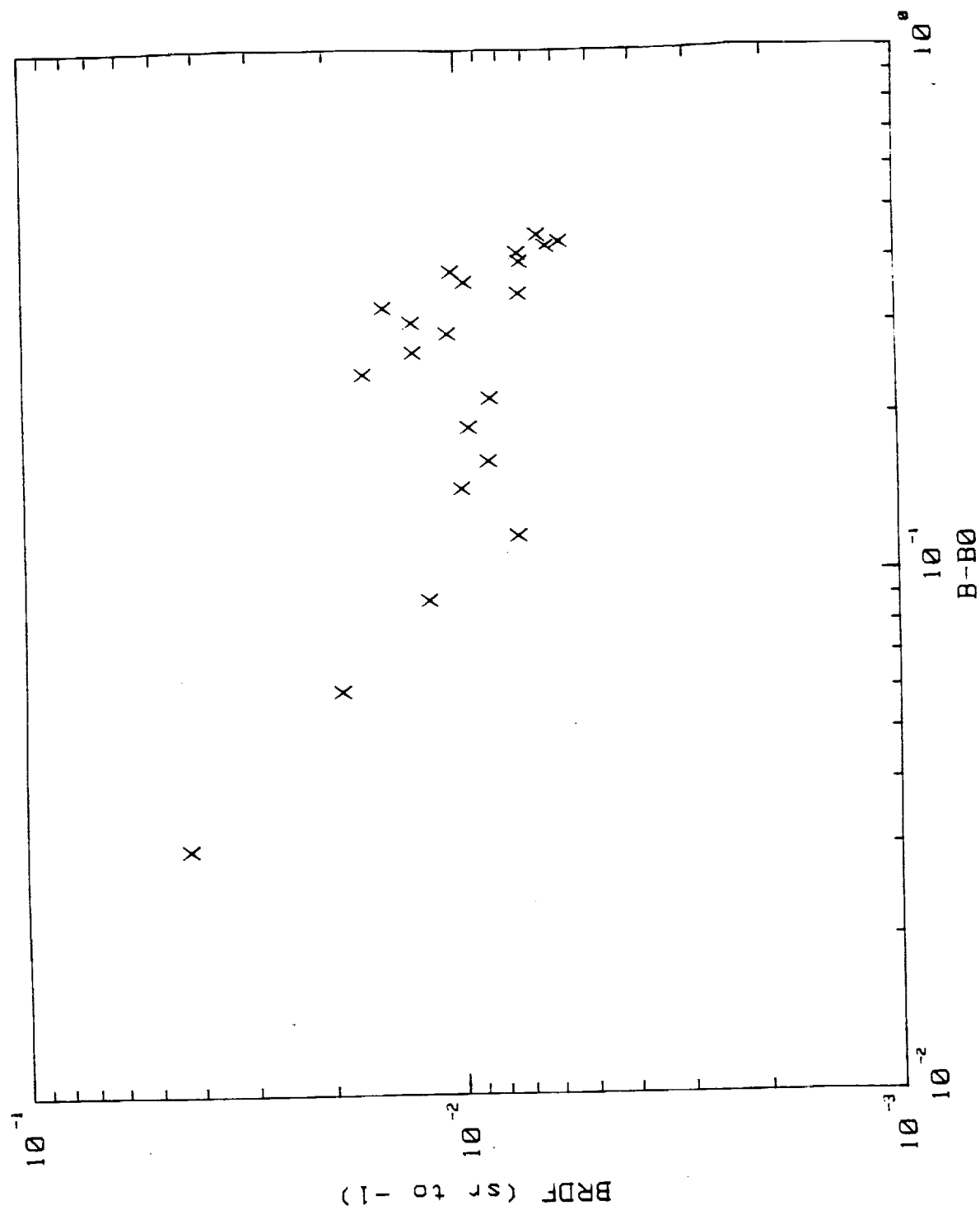Figure 5.22. BRDF in the back scatter direction at 30° incidence.

Figure 5.23. BRDF in the forward scatter direction at 30° incidence.

```fortran
      read (5,*) x1, x2
      print *, x1, x2
c
      endif
c
      print *, ' Enter the angle you wish to observe...(I3 format)'
     read(*,*) mprt
      mm = mprt - (mprt/2)*2
      if (mm.ne.0) then
         mprt = mprt + 1
      endif
      print *, 'The program will be run for the following angle ',
     *          mprt
c
      call angle
c
c  open the output file and write some initial values
c
      open (unit=7, err=800, file='xdata.dat',status='unknown')
      open (unit=8,err=800,file='ydata.dat',status='unknown')
c
      write (7, 18)
 18   format(1x, ' Wavelength       Sphere radius          x
     *    index of refraction')
      write (7, 20) wavl, x1, x2, em
 20   format (1x, 3(e16.4,1x), (e16.4,e16.4))
c
      xdel = (x2-x1)/20.
c
      do 9000 iloop = 1, 21
      r = dfloat(iloop-1)*xdel + x1
      x=2.0 * pi * r / wavl
      write (7, 118)
 118  format(1x, ' Wavelength       Sphere radius          x
     *    index of refraction')
      write (7, 120) wavl, r, x, em
 120  format (1x, 3(e16.4,1x), (e16.4,e16.4))
c
c
c
      p = real(em) * x
      q = dabs(dimag(em) * x)
      cy = cmplx(p,-q)
      psin = dsin(p)
      pcos = dcos(p)
      qsinh = dsinh(q)
      qcosh = dcosh(q)
      temp = psin*psin+qsinh*qsinh
c
      a(0) = cmplx((psin * pcos)/temp, (qsinh * qcosh)/temp)
      n=0
      write (7,6)
 6    format( ' Following is the A(n) ')
      write (7,8) n, a(0)
```

```
      do 10 n = 1,20
         tp3 = cmplx(dfloat(n), 0.) / cy
         a(n) = -tp3 + cmplx(1.,0.)/(tp3 - a(n-1))
      write (7,8)  n,a(n)
  8   format (1x, i3, (e16.4,1x,e16.4))
  10  continue
c
c  Generate half integer order Bessel functions
c
      w(-1) = cmplx(cos(x), -sin(x))
      w(0) = cmplx(sin(x), cos(x))
      write (7,375)
 375  format('Value of the circular functions follow')
      k=-1
      write (7,8) k, w(-1)
      k=0
      write (7,8) k, w(0)
         do 400 k=1,20
         tp3 = cmplx(dfloat(2*k - 1)/x, 0.)
         w(k) = tp3 * w(k-1) - w(k-2)
         write (7,8) k, w(k)
         if (iprint) 400,400,390
 390     print *, k,w(k)
 400  continue
c
      write (7, 485)
 485  format( 'following is the An and Bn coefficients')
      do 500 n = 1, 20
         tp1 = a(n)/em + cmplx(n/x,0.)
         tp3 = (tp1 * real(w(n)) - real(w(n-1)))
         tp4 = (tp1*w(n) - w(n-1))
         an(n) = tp3/tp4
c         print, tp1,tp3,tp4,an(n)
         tp2 = em * a(n) + cmplx(n/x,0.)
         tp5 = (tp2 * real(w(n)) - real(w(n-1)))
         tp6 = (tp2*w(n) - w(n-1))
         bn(n) = tp5/tp6
         write (7,490) n, an(n), bn(n)
 490     format (1x, i3, 2(1x, e16.4,1x,e16.4))
 500  continue
c
c     Now compute the values of S1(theta) and S2(theta)
c
       write (8,910)
 910   format ('Output values for angular fcns S1 and S2')
       do 1000 m = 1, 180/2
         mn = (m-1)*2
         s1(m) = 0.d0
         s2(m) = 0.d0
         do 900 n = 1, 20
           temp1 = dfloat(2*n + 1)/dfloat(n*(n+1))
           tp3 = cmplx(temp1,0.)*(an(n)*polypi(n,m) +        *
     bn(n)*polytau(n,m))
           s1(m) = s1(m) + tp3
```

```
            tp6 = cmplx(temp1,0.)*(bn(n)*polypi(n,m) +
     *          an(n)*polytau(n,m))
            s2(m) = s2(m) + tp6
            print *, n, temp1, tp3, tp6
c            print, an(n), bn(n)
            print *, n,m, polypi(n,m)
 900       continue
            print *,  m , s1(m), s2(m)
         write (8, 950)  mn,s1(m), s2(m)
 950      format (1x, i4, 2(1x,(e16.4, e16.4)))
            if (iloop .eq. 1) then
                write (8, 950)  mn, x,s1(m), s2(m)
         endif
         print *, 'enter a letter, q to quit'
         read(*,*) iprint
         if (iprint .eq. 999) then
            go to 999
         endif
          if (mn .eq. mprt) then
         print *, 'done with x value = ', x
         write (7, 1950)  mn, x,s1(m), s2(m)
         endif
 1950     format (1x, i4, 2x, f8.4, 2(1x,(e16.4, e16.4)))
 1000 continue
c
 9000 continue
c
      goto 999
 800  print *, 'Error opening data file'
 999  continue
c
      close (7)
      end


         subroutine angle
c
c         include c:\lahey22\f77l\mie.inc
         common /norm/ x, pi, spi
         common /polys/ polypi(0:21,100), polytau(0:22,100)
         common /ints/ iprint
c         common /plex/ zj1(50), zj2(50), fact(0:200)
c
         implicit integer*2 (i-n)
         implicit real*8 (o-z)
           dimension p(0:22)
           real*8  conv
c
c          ' Initialize some constants
         conv = pi / 180.d0
         m = 0
c
c          'Pi sub n is polypi(1,n) where 1=poly # and n=angle value
c           ' Load the first element of pi sub n with known values
```

```
          isum = 0
          do 100 n = 1, 20
                  isum = isum + n
                  polypi(n, 1) = dfloat(isum)
                  polytau(n,1) = dfloat(isum)
  100     continue
c            ' Calculate Legendre polynomial versus angle
          m = 1
          do 50 ideg = 2, 178, 2
                  thdeg=dfloat(ideg)
                  m = m + 1
                  thrad = thdeg * conv
                  xc = dcos(thrad)
                  IF (thrad .eq. 0.d0) THEN
                      thrad = .0001d0
                      else
                      y = dsqrt(1.d0 - xc * xc)
                  endif
                  p(0) = 1.d0
                  p(1) = xc

c
c            'Polyaray is the Legendre polynomials for angle m
c
                  polypi(0,m) =   0.d0
                  polytau(0,m) = 0.d0
                  polytau(1,m) = xc
c              do 200 n = 1, 20
                      n1 = n + 1
                      p(n1) = (dfloat(2*n+1)/dfloat(n1)) * xc * p(n)
         *                    - dfloat(n)/dfloat(n1) * p(n-1)
                      polypi(n, m)=(dfloat(n)/(y*y)) * (p(n-1) -
         *                      xc*p(n))
                      if (n.gt.1) then
                      polytau(n,m) = xc*(polypi(n,m)-polypi(n-2,m))
         *                       + polytau(n-2,m)
          *                      -       *
          *                      dfloat(2*n-1)*(y*y)*polypi(n-1,m)
                      endif
  200             continue
   50     continue
  310   return
        END
```

Appendix B. Conference Papers

    I. SPIE Paper. August 1989.

   II. ICES Paper. July 1990.

Measurements of polarization scattering
in the vacuum ultraviolet

Kenneth A. Herren

Center for Applied Optics
The University of Alabama in Huntsville
Huntsville, Al 35899

ABSTRACT

NASA's In-Situ Contamination Effects Facility, Marshall Space Flight Center will be used to measure the polarization scattering from optical surfaces due to outgassed molecular contamination. Measurements will be taken using a non-coherent vacuum ultraviolet (VUV) source at 123.6 nm and a set of three solar blind VUV photomultipliers. An in-plane VUV BRDF experiment is described and details of the on-going program to characterize optical materials exposed to the space environment is reported.

INTRODUCTION

Light incident on any real surface will scatter some portion of the incident energy into all allowed angles relative to the surface normal. In the scalar scattering theory, the intensity of the scattered light will be a function of both the incident angles and scattered angles as well as the surface material and its condition. The accepted parameter for describing this bidirectional reflectance, or angular scattering, is the Bidirectional Reflectance Distribution Function (BRDF). Figure 1 shows the BRDF geometry considered in this paper.

However, to adequately describe the scattering, the vector nature of the light must be included. That is, the scattered light must be written in the following way;

$$\underline{S}'(\theta_0, \phi_0, \Pi_0, \lambda) = [M] * \underline{S}(\theta_s, \phi_s, \Pi_s, \lambda) \tag{1}$$

where $\underline{S}$ is the Stokes vector of the incident light, M is the Mueller matrix of the surface under consideration and $\underline{S}'$ is the Stokes vector of the scattered light. Π is the polarization state and λ is the wavelength. Note that we can also carry the angular dependence of the incident and scattered light in the Stokes vector. (See, for example Bickel, et. al.)[1].

At short wavelengths the scattering process is strongly wavelength dependent due to the relative scale sizes between surface irregularities and the incident wavelength. And since we want to measure M as a function of surface contamination, the total

description of the scattering matrix must also include this time dependence.

The surface Mueller matrix is well behaved when the wavelength is much larger than the characteristic surface irregularity but becomes increasingly more complicated as the wavelength to characteristic irregularity dimension ratio approaches zero (i.e. small wavelengths/rough surface).

Figure 2 shows a mirror that has been contaminated with a molecular contaminant used in this program. As can be seen, the contamination proceeds in a discrete fashion, i.e. islands of contaminant appear rather than a uniform layer or film. During a typical contamination run, a mirror will develop surface irregularities whose diameters approach that of the incident wavelength and, according to Mie theory, there will occur a peak in the scattered intensity when the surface scatterers are approximately equal to the wavelength. We want to take advantage of this to determine the growth rate of the contamination.

Therefore, the thrust of this work is to provide measurements of scattered light in the region where the long wavelength approximations no longer hold and to compare these data with measurements of the scattering functions at long wavelengths.

THEORY

Light incident on an optical surface will be scattered due to the irregular structure of the surface at the microscopic level. These irregularities will cause some of the incident light to be reflected, or scattered, at an angle not predicted by Snell's law applied to the mean surface value. The phenomenon of scattered light can be broken into the following three broad categories based on the surface irregularities causing the scattering[2];

1. Short Wavelength Region
   -Irregularities large relative to the wavelength

2. Intermediate Wavelength Region
   -Isolated irregularities comparable in size to the wavelength

3. Long Wavelength Region
   -Correlated irregularities with heights small compared to the wavelength but covering the entire surface

Note that each of these depend strongly on the incident wavelength and an effect in the first category at a wavelength of 200 nm might well be in the third category at a wavelength of 10 microns.

We need only consider the short and intermediate wavelength regions in this work. The intermediate region is governed by resonant scattering of the type known as Mie scattering. Bennett[2] presents
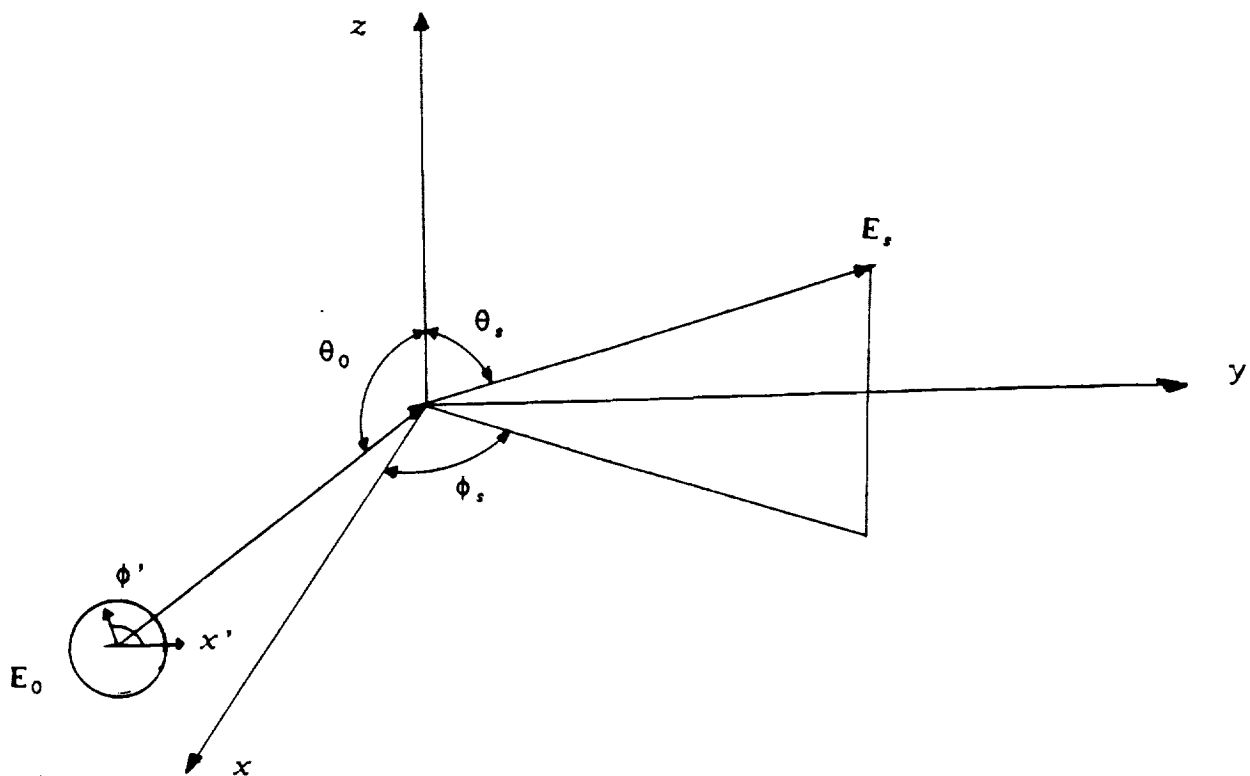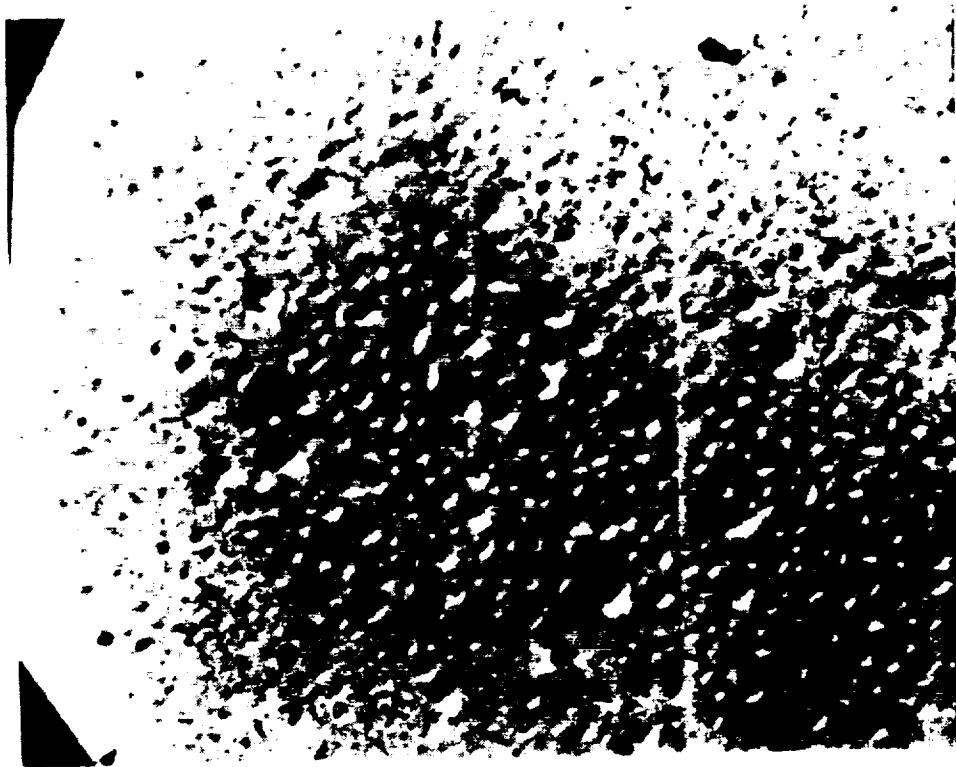
Figure 1. BRDF Geometry

Figure 2. High Magnification Picture of a Contaminated Mirror

data that shows this type of scattering with the resonance at approximately one micron due to dust particles.

The Bidirectional Reflectance Distribution Function (BRDF) is the accepted functional description for scattered light. (See figure 1 for nomenclature.) Light is incident at polar angle θ_0 and azimuthal angle Φ_0 and the scattered light is measured at polar angle θ_s and azimuthal angle Φ_s. Some authors have defined the BRDF with the incident azimuthal angle at zero and the fourth angle, Φ', being the polarization angle measured relative to the plane of incidence.[3,4]

In this case setting Φ' equal to zero gives an incident s-polarization and setting it to $\pi/2$ gives a p-polarization. Any arbitrary incident linear polarization can be described by a combination of these two orthogonal polarization states.

Elson[3] has chosen to expand the angular dependence using the latter case with the incident azimuthal angle, Φ_0, set equal to zero. No loss of generality should occur with this condition. In that paper Elson solves the wave equation $\mathbf{LA} = 0$ using the coordinate transformation below to map the roughness profile into a plane.

$$u_1 = x, \quad u_2 = y, \quad u_3 = z - \zeta(x,y) \tag{2}$$

By insuring that proper boundary conditions are met, the Laplacian can be reduced to one like $L = L^{(0)} + L^{(1)}$ that is correct to first order in $\zeta(x,y)$.

This first order approximation to the scattered light is given below,

$$\frac{1}{P_0}\frac{dP}{d\Omega} = \frac{(\omega/c)^4}{\pi^2} \cdot \cos\theta_0 \cdot \cos^2(\theta\,|\,1-\epsilon\,|^2) \cdot g(\mathbf{k}-\mathbf{k}_0)\left[\frac{|X_\theta|^2}{|q'+q\epsilon|^2} + \frac{|X_\phi|^2}{|q'+q_0|^2}\right]$$

$$X_\theta = \frac{(q'q_0'\cos\phi - kk_0\epsilon)\cos\phi'}{q_0'+q_0\epsilon} + \frac{(\omega/c)q'\sin\phi\sin\phi'}{q_0'+q_0}$$

$$X_\phi = \frac{\omega}{c}\left\{\frac{q_0'\sin\phi\cos\phi'}{q_0'+q_0\epsilon} - \frac{(\omega/c)\cos\phi\sin\phi'}{q_0'+q_0}\right\} \tag{3}$$

where

$$q_i = \frac{\omega}{c}\cos\theta_i \quad ; \quad k_i = \frac{\omega}{c}\sin\theta_i' \quad ; \quad q_i' = \sqrt{\epsilon(\omega/c)^2 - k_i^2}$$

This result can be reduced to the following form.

$$f_r = \frac{1}{P_0}\frac{dP}{d\Omega} = \frac{1}{\pi^2}k^4 F(\theta)W(P)$$

(4)

where   k = 2π/lambda
   $F(\theta)$ is an optical factor dependent on polarization
   W(P)   is the power spectrum of the height distribution
   P   is $k(\beta - \beta_0)$ where β is related to sin(θ)

Note that the first term in F( ) is in the plane of the scattered light and the second term is normal to the plane of scattered light and can therefore be considered to be the p- and s-polarizations of the scattered light, respectively.

Furthermore we can rewrite $F(\theta)$ as

$$F(\theta) = (Q_{ss} + Q_{sp} + Q_{ps} + Q_{pp})$$

(5)

where Q_{ab} is the angular dependence and "a" is the input polarization and "b" is the observation polarization as defined above.

Thus we can write the Q's as follows[5],

$$\frac{Q_{ss}}{|1-\epsilon|^2} = \left| \frac{\cos\phi_s}{(\cos\theta_0 + \sqrt{\epsilon - \sin^2\theta_0})(\cos\theta_s + \sqrt{\epsilon - \sin^2\theta_s})} \right|^2$$

$$\frac{Q_{sp}}{|1-\epsilon|^2} = \left| \frac{(\sqrt{\epsilon - \sin^2\theta_s})(\sin\phi_s)}{(\cos\theta_0 + \sqrt{\epsilon - \sin^2\theta_0})(\epsilon\cos\theta_s + \sqrt{\epsilon - \sin^2\theta_s})} \right|^2$$

(6)

$$\frac{Q_{ps}}{|1-\epsilon|^2} = \left| \frac{\sqrt{\epsilon - \sin^2\theta_0}\sin\phi_s}{(\epsilon\cos\theta_0 + \sqrt{\epsilon - \sin^2\theta_0})(\cos\theta_s + \sqrt{\epsilon - \sin^2\theta_s})} \right|^2$$

$$\frac{Q_{pp}}{|1-\epsilon|^2} = \left| \frac{\sqrt{\epsilon - \sin^2\theta_0}\sqrt{\epsilon - \sin^2\theta_s}\cos\phi_s - \epsilon\sin\theta_0\sin\theta_s}{(\epsilon\cos\theta_0 + \sqrt{\epsilon - \sin^2\theta_0})(\epsilon\cos\theta_s + \sqrt{\epsilon - \sin^2\theta_s})} \right|^2$$

If we limit ourselves to very small scattering angles it can be shown that the Q's will reduce to the following forms,

$$Q_{ss} = \left| \frac{\cos\theta_0 - \sqrt{\epsilon - \sin^2\theta_0}}{\cos\theta_0 + \sqrt{\epsilon - \sin^2\theta_0}} \right|^2 = R_s(\theta_0)$$

(7)

$$Q_{pp} = \left| \frac{\epsilon\cos\theta_0 - \sqrt{\epsilon - \sin^2\theta_0}}{\epsilon\cos\theta_0 + \sqrt{\epsilon - \sin^2\theta_0}} \right|^2 = R_s(\theta_0)$$

$$Q_{sp} = Q_{ps} = 0$$

where R_s and R_p are the Fresnel intensity reflectances for s- and p-polarizations, respectively. Note that these functions explain how light incident at a particular polarization is scattered from the given surface but does not develop the Jones or Mueller matrix of the scatterer.

The above results are not easily derived from the Mueller calculus for the vector scattering process, although those results will follow. It is obvious that the correct form for the scattering from a surface is that given in equation (1) and thus the problem reduces to finding the elements of the Mueller matrix and applying it in each case of a particular incidence angle. The above equations should then be derived from the elements of the scattering matrix.

Unfortunately this is an overwhelmingly difficult problem to solve explicitly and must be attacked by measurement of the individual matrix elements for each set of incidence angles and scattering angles.

By using the technique similar to that developed by Azzam[6] we can take individual transmission measurements and determine nine of the sixteen elements of the scattering matrix. Since we have no method for altering the phase of the incident light we cannot determine the entire matrix.

EQUIPMENT

These measurements will be carried out at the In-Situ Contamination Effects Facility at NASA's Marshall Space Flight Center, Huntsville, Alabama.

The In-Situ Optical Surface Measurement Facility, shown schematically in Figure 3, is an equipment package designed to measure the real time deposition of outgassed molecular constituents from candidate space materials. These measurements are made using VUV light and monitoring the deleterious effects of the material deposition on the surface reflectivities of optical materials while those depositions are in process. This arrangement is used to

simulate the on-orbit effects of contamination and degradation of optical surfaces such as Space Telescope.
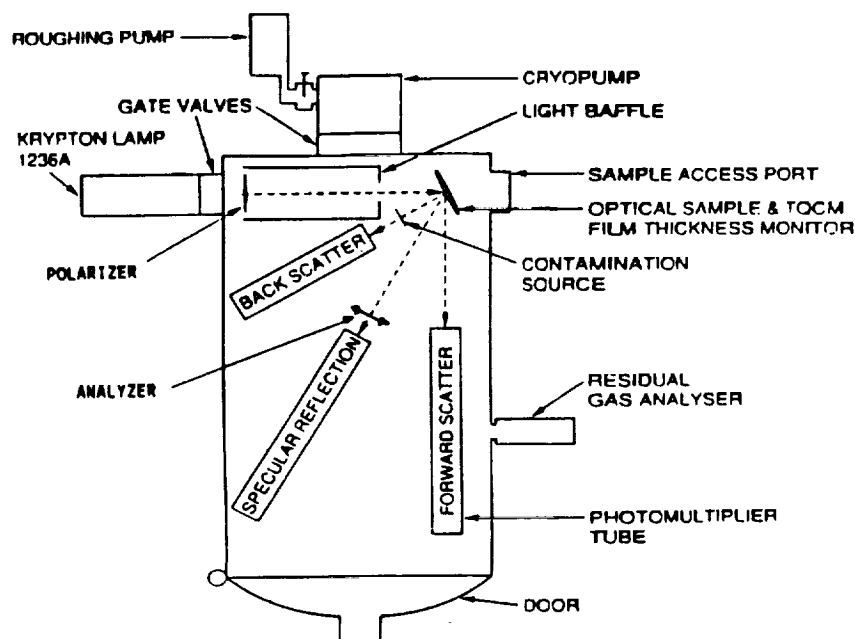

Figure 3. In-Situ Optical Surface Measurement Facility

VUV light is generated using a low pressure RF excited discharge Krypton lamp. The krypton resonance line at 123.6 nm is coupled into the vacuum chamber through a window and filter port. Typical VUV filters have a spectral width of 10 nm and any continuum output in the longer wavelengths are down by five or more orders of magnitude. The physical mount for the source tube and filter housing serve as a limiting aperture of approximately 6 mm, used in collimating the incident light.

After the filter we place the reflection type polarizer followed by the second aperture in the collimating scheme. This work will employ three mirror metal front surface polarizers of the type reported by Hamm et.al.[7] Diattenuation values as high as 0.996 have been reported for these polarizers. These polarizers allow minimum deflection of the optical axis and introduce little problem in alignment of the system.

The collimated light is incident on the sample mirror and specular light and scattered light is collected by the three fixed solar blind photomultiplier tubes (PMT). Placed in front of the PMT's is another polarizer used as an analyzer. These PMT's are arranged so that the specular channel is at 30 degrees angle of reflection to the sample and the forward scatter and back scatter channels are at a scatter angle of 30 degrees.

The contamination source is a simple resistance heater in contact with the outgassing material and is housed in front of and beside the

back scatter PMT. The temperature of the sample is held to within one degree either side of the desired temperature. Mass loss and therefore contamination level is determined by using a temperature controlled quartz crystal microbalance (TQCM). The TQCM is a precision matched pair of 15 Mhz quartz crystals, one being the sensor and the other the reference. The output of the TQCM is the beat frequency between the two crystals. If the sensor is mass loaded by contaminant the resonant frequency changes and the output beat frequency changes. For this 15 Mhz TQCM the mass loading, m, is given by the following.

$$m = 1.56 \times 10^{-9} \ g/cm^3 \ hz \tag{8}$$

In this application the TQCM is located directly above the sample mirror and the housing is temperature controlled to less than one degree.

This set-up approximates a planer BRDF measurement at three positions, i.e. the incident light, surface normal and scattered light are in the same plane. Measurements can then be taken using incident linearly polarized light at any orientation and analyzed at any orientation while contaminant is being deposited.

EXPERIMENT METHOD

Molecular contamination of optical surfaces from outgassed material has been shown to proceed from acclimation centers (see figure 2). The origin of these centers at the surface is not well understood but each grows faster than the surrounding surface area. This implies that the contaminant has a higher sticking ratio for itself than the surface and as a result the surface will appear on the microscopic level to be composed of many small "islands" of accumulated material with plains of relatively clean surface in between. This situation provides the experimenter with many roughly hemispherical scattering centers that are growing with time. This is analogous to the common static situation for scattering of near infrared light from surfaces by dust particles (see Bennett[1]).

By using a fixed wavelength and observing the scattered light as the islands grow, we will observe the typical resonance peak in scattered light predicted by the Mie theory. The form of the scattering can be used to shed some light on the growth rates of the islands and therefore the activation energies of the outgassing phenomena.

CONCLUSIONS

By using established techniques for determining the components of the surface scattering Mueller matrix, we expect to measure this matrix at the vacuum ultraviolet wavelengths. In addition, these measurements will be made in-situ, i.e. while the contaminant is being deposited at the surface.

REFERENCES

1. Bickel, W.S., Hsu, J., Chiao, S., Abromson, D. and Iafelice, V., "The Mueller Matrix-Stokes Vector Representation of Surface Scattering", _Polarization Considerations for Optical Systems_, SPIE Vol. 891, 32-39 (1988)

2. Bennett, H.E., "Scattering Characteristics of Optical Materials", Optical Engineering, 17, 480-488, (1978).

3. Elson, J. M. and Bennett, J. M., "Vector Scattering Theory," Opt. Eng., 18, No.2, p.116 (1979).

4. Elson, J.M., "Light Scattering from Semi-infinite Media for Non-Normal Incidence", Phys. Rev. B, 12, No. 6, p. 2541 (1975).

5. Church, E.L., Jenkinson, H.A. and Zavada, J.M., "Relationship Between Surface Scattering and Microtopographic Features", Opt. Eng., 18, No. 2, p. 125-136 (1979).

6. Azzam, R.M.A., "Photopolarimetric Measurement of the Mueller Matrix by Fourier Analysis of a Single Detected Signal", Optics Letters, 2, No. 6, 148-150 (1978).

7. Hamm, R.N., MacRae, R.A. and Arakawa, E.T., "Polarization Studies in the Vacuum Ultraviolet", J. Opt. Soc. Am., 55, p. 1460-1463 (1965).

SAE Technical Paper Series

901412

In Situ Measurements of Scattering from Contaminated Optics in the Vacuum Ultraviolet

Kenneth A. Herren
University of Alabama in Huntsville
Center for Applied Optics
Huntsville, AL

Roger C. Linton and Ann F. Whitaker
Materials and Processes Laboratory
Marshall Space Flight Center
Huntsville, AL

In Situ Measurements of Scattering from Contaminated Optics in the Vacuum Ultraviolet

Kenneth A. Herren

University of Alabama in Huntsville

Center for Applied Optics

Huntsville, AL

Roger C. Linton and Ann F. Whitaker

Materials and Processes Laboratory

Marshall Space Flight Center

Huntsville, AL

ABSTRACT

NASA's In Situ Contamination Effects Facility, Marshall Space Flight Center has been used to measure the time dependence of the angular reflectance from molecularly contaminated optical surfaces in the Vacuum Ultraviolet (VUV). The light scattering measurements are accomplished in situ on optical surfaces in real time during deposition of molecular contaminants. The measurements are taken using non-coherent vacuum ultraviolet (VUV) sources with the predominant wavelengths being the Krypton resonance lines at 1236 and 1600 Angstroms. Detection of the scattered light is accomplished using a set of three solar blind VUV photomultipliers. An in-plane VUV BRDF experiment is described and details of the on-going program to characterize optical materials exposed to the space environment is reported.

INTRODUCTION

Light incident on any real surface will scatter some portion of the incident energy into all allowed angles relative to the surface normal. In the scalar scattering theory, the intensity of the scattered light will be a function of both the incident angles and scattered angles as well as the surface material and its condition. The accepted parameter for describing this bidirectional reflectance, or angular scattering, is the Bidirectional Reflectance Distribution Function (BRDF)[1]. Figure 1 shows the geometry considered in this paper.

However, to adequately describe the scattering, the vector nature of the light must be included. That is, the functional form of the scattered light should be written in the following way;

$$\underline{S}'(\theta_o,\phi_o,\pi_o,\lambda_o) = [M] * \underline{S}(\theta_s,\phi_s,\pi_s,\lambda_s) \qquad (1)$$

where $\underline{S}$ is the Stokes vector of the incident light, M is the Mueller matrix of the surface under consideration and $\underline{S}'$ is the Stokes vector of the scattered light. Note that we can also carry the angular dependence of the incident and scattered light in the Stokes vector. (See, for example Bickel, et. al.[2]).

At short wavelengths the scattering process is strongly wavelength dependent due to the relative scale sizes between surface irregularities and the incident wavelength. And since we are measuring M as a function of surface contamination, the total description of the scattering matrix must also include this time dependence.

The surface Mueller matrix is well behaved when the wavelength is much larger than the characteristic surface irregularity but becomes increasingly more complicated as the wavelength to characteristic irregularity dimension ratio approaches zero (i.e. small wavelengths/rough surface).

Figure 2 shows a mirror that has been contaminated with a molecular contaminant (Chemglaze Z-306) used in this program. As can be seen, the contamination due to this contaminant proceeds in a discrete fashion, i.e. islands of contaminant appear rather than a
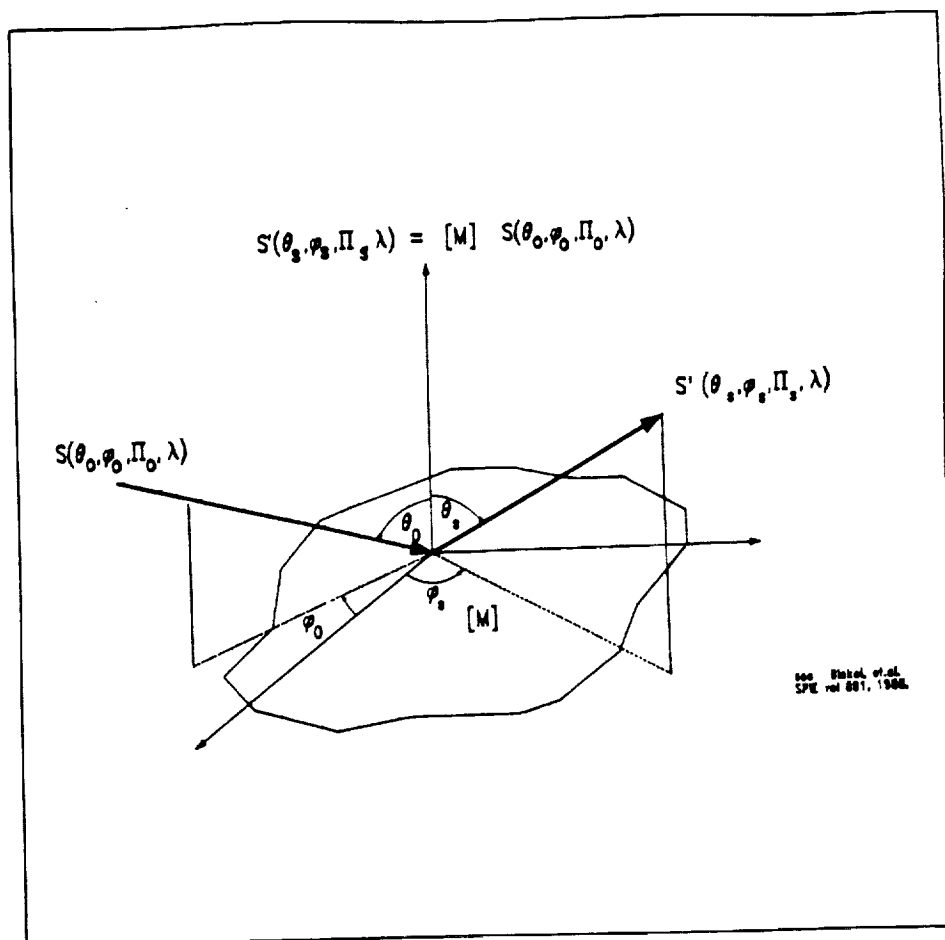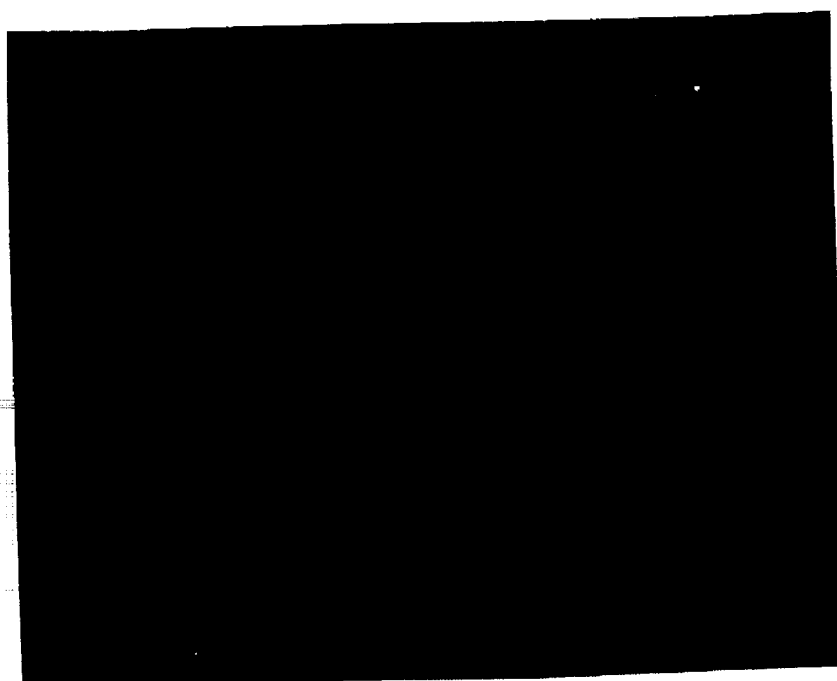
Ahh

$$S'(\theta_s,\varphi_s,\Pi_s,\lambda) = [M] \quad S(\theta_0,\varphi_0,\Pi_0,\lambda)$$

Figure 1. Angular Scattering Geometry

Figure 2. Mirror Contaminated with Chemglaze Z-306

uniform layer or film. During a typical contamination run, a mirror will develop surface irregularities whose diameters approach that of the incident wavelength and, according to Mie theory, there may occur peaks in the scattered intensity when the surface scatterers are approximately equal to the wavelength. We want to take advantage of this to determine the growth rate and optical properties of the contamination.

Therefore, the thrust of this paper is to describe the measurements of scattered light in the region where the long wavelength approximations no longer hold and to compare these data with measurements of the scattering functions in the long wavelength approximation.

THEORY

Light incident on an optical surface will be scattered due to the irregular structure of the surface at the microscopic level. These irregularities will cause some of the incident light to be reflected, or scattered, at an angle not predicted by Snell's law applied to the mean surface value. The phenomenon of surface scattering is commonly divided into broad categories based on the size of the surface irregularities causing the scattering[3]. There are two important regions dealt with in this work. First is the long wavelength region where scattering arises from small imperfections on the surface. Secondly is the intermediate wavelength region where the scattering is caused by imperfections comparable to the wavelength in size.

LONG WAVELENGTH REGION - The Bidirectional Reflectance Distribution Function (BRDF) is the accepted functional description for scattered light. (See figure 1. for nomenclature.) Light is incident at polar angle θ_0 and azimuthal angle Φ_0 and the scattered light is measured at polar angle θ_s and azimuthal angle Φ_s. Some authors have defined the BRDF with the incident azimuthal angle at zero and the fourth angle, Φ', being the polarization angle measured relative to the plane of incidence.[4],[5]

In this case setting Φ' equal to zero gives an incident s-polarization and setting it to $\pi/2$ gives a p-polarization. Any arbitrary incident linear polarization can be described by a combination of these two orthogonal polarization states.

The accepted form for the BRDF is given as follows (for example see Wang and Wolfe[6])

$$f_r = \frac{1}{P_0} \frac{dP}{d\Omega} = (k^4/\lambda^2) F(\theta) W(P) \qquad (2)$$

where

k = $2\pi/\lambda$

$F(\theta)$ optical factor dependent on polarization

$W(P)$ is the power spectrum of the height distribution

P is $k(\beta - \beta_0)$ where β is related to $\sin(\theta)$

We see that the BRDF can be broken into two parts, one that contains only the angular dependence of the scattering and one that contains the surface nonuniformity.

To investigate the mueller matrix traditionally one illuminates with either parallel or perpendicularly polarized light and observes with either a parallel or perpendicular analyzer. This results in four measurements and we can rewrite $F(\theta)$ to accomodate these as follows;

$$F(\theta) = (Q_{ss} + Q_{sp} + Q_{ps} + Q_{pp}) \qquad (3)$$

where the Q_{ab}'s are the angularly dependent measurements and "a" is the input polarization and "b" is the observation polarization as defined above.

We then write the Q's as follows[7],

$$\frac{Q_{ss}}{|1-\epsilon|^2} = \left| \frac{\cos\phi_s}{(\cos\theta_0 + \sqrt{\epsilon - \sin^2\theta_0})(\cos\theta_s + \sqrt{\epsilon - \sin^2\theta_s})} \right|^2$$

$$\frac{Q_{sp}}{|1-\epsilon|^2} = \left| \frac{(\sqrt{\epsilon - \sin^2\theta_s})(\sin\phi_s)}{(\cos\theta_0 + \sqrt{\epsilon - \sin^2\theta_0})(\epsilon\cos\theta_s + \sqrt{\epsilon - \sin^2\theta_s})} \right|^2$$

$$\frac{Q_{ps}}{|1-\epsilon|^2} = \left| \frac{\sqrt{\epsilon - \sin^2\theta_0}\sin\phi_s}{(\epsilon\cos\theta_0 + \sqrt{\epsilon - \sin^2\theta_0})(\cos\theta_s + \sqrt{\epsilon - \sin^2\theta_s})} \right|^2$$

$$\frac{Q_{pp}}{|1-\epsilon|^2} = \left| \frac{\sqrt{\epsilon - \sin^2\theta_0}\sqrt{\epsilon - \sin^2\theta_s}\cos\phi_s - \epsilon\sin\theta_0\sin\theta_s}{(\epsilon\cos\theta_0 + \sqrt{\epsilon - \sin^2\theta_0})(\epsilon\cos\theta_s + \sqrt{\epsilon - \sin^2\theta_s})} \right|^2$$

$$(4)$$

3

If we limit ourselves to very small scattering angles it can be shown that the Q's will reduce to the following forms,

$$Q_{ss} = R_s(\theta)$$

$$Q_{pp} = R_p(\theta) \tag{5}$$

$$Q_{ps} = Q_{sp} = 0$$

where R_s and R_p are the Fresnel intensity reflectances for s- and p-polarizations, respectively. These functions explain how light incident at a particular polarization is scattered from the given surface but does not develop the Jones or Mueller matrix of the scatterer.

As shown by Van de Hulst[8], we require not only parallel and perpendicularly polarized input but also two other independent input polarization states of the incident light, as well as a method for retardation of the states in order to solve for the entire Mueller matrix of the surface.

INTERMEDIATE WAVELENGTH SCATTERING - When the particle size of the scatterer approaches the value of the wavelength of the incident light, the above theory no longer holds and new equations for the scattered light must be developed. We must derive a formal solution from Maxwell's equations. This was first accomplished by Mie in 1908[9], hence the name and has been modified later by many authors. In this paper we will follow the results derived by Van de Hulst[8].

From the geometry shown in figure 1. the incident electric field is given by the following equation;

$$E(x,t) = E_o \exp[-ikz + iwt] \tag{6}$$

and by matching the boundary conditions at the particle and observing the scattered field far from the source, we can write the scattered field as follows;

$$E_\phi = H_\theta = -\frac{i}{kr}e^{-ikr+iwt} \cdot \cos\phi \cdot S_2(\theta) \tag{7}$$

$$-E_\theta = H_\phi = -\frac{i}{kr}e^{-ikr+iwt} \cdot \sin\phi \cdot S_1(\theta)$$

where the argument, $x = kr = 2\pi r/\lambda$ and the amplitude functions S_1 and S_2 are given by the following;

$$S_1(\theta) = \sum_{n=1}^{\infty} \frac{2n+1}{n(n+1)} \{a_n\pi_n(\cos\theta) + b_n\tau_n(\cos\theta)\}$$

$$S_2(\theta) = \sum_{n=1}^{\infty} \frac{2n+1}{n(n+1)} \{b_n\pi_n(\cos\theta) + a_n\tau_n(\cos\theta)\} \tag{8}$$

The coefficients a_n and b_n are determined from the boundary conditions and the angular functions are given below;

$$\pi_n(\cos\theta) = \frac{1}{\sin\theta} P_n^1(\cos\theta)$$

$$\tau_n(\cos\theta) = \frac{d}{d\theta} P_n^1(\cos\theta) \tag{9}$$

Figure 3. shows the results of the previous equations for light incident on spheres with a complex index of refraction, m = 1.1 - 0.0431 i and scattered at zero degrees (forward scatter) and at 30 degrees. Notice that there is a resonance in the scattering amplitude where x = 25. This resonance is typical of the scattering from spheres where the wavelength is approximately equal to the radius of the scatterer.

The above results are not easily derived from the Mueller calculus for the vector scattering process, although those results will follow. It is obvious that the correct form for the scattering from a surface is that given in Eq (1) and thus the problem reduces to finding the elements of the Mueller matrix and applying it in each case of a particular incidence angle.

Unfortunately this is an overwhelmingly difficult problem to solve explicitly and must be attacked by measurement of the individual matrix elements for each set of incidence angles and scattering angles.

By using the technique similar to that developed by Azzam[10] we can take individual transmission measurements and determine nine of the sixteen elements of the scattering matrix. Since we have no method for altering the phase of the incident light we cannot determine the entire matrix.

Frequently the BRDF is cylindrically symmetric and the experimenter can limit himself
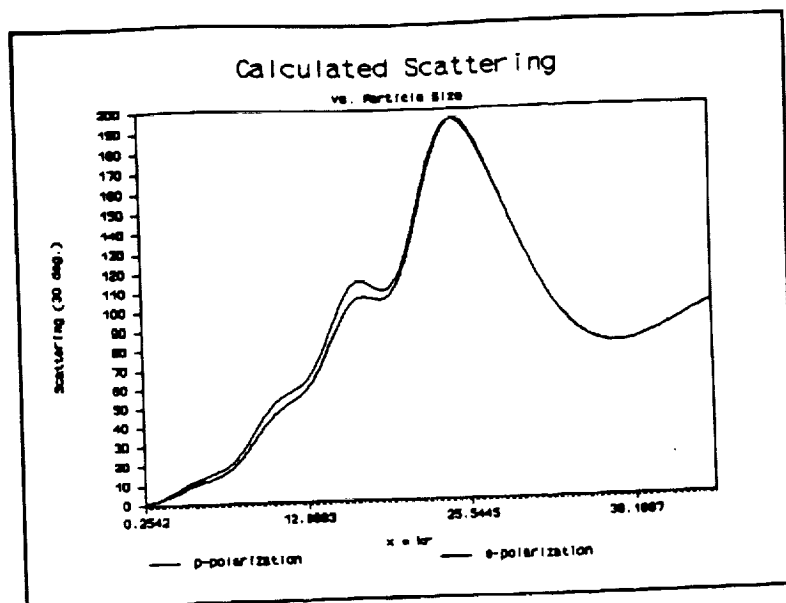
Figure 3. Model Prediction of Time Dependent Scattering From Contaminated Surface in Figure 2.

to scattering in a plane, i.e. when the polar angle of incidence and the polar angle of observation are both limited to $\pi/2$ (known as one-dimensional vector theory). This has been the case for our previous work and all data presented in this paper has been taken in the horizontal plane.

EQUIPMENT

These measurements have been carried out at the In Situ Contamination Effects Facility at NASA's Marshall Space Flight Center, Huntsville, Alabama.

The In Situ Optical Surface Measurement Facility shown schematically in figure 4. is an equipment package designed to measure the real time deposition of outgassed molecular constituents from candidate space materials. These measurements are made using VUV light and observing the deleterious effects of the material deposition on the surface reflectivities of optical materials while the depositions are in process. This arrangement is used to simulate the on-orbit effects of contamination and degradation of optical surfaces such as Space Telescope.

VUV light is generated using a low pressure RF excited discharge Krypton lamp. The krypton resonance line at 123.6 nm is coupled into the vacuum chamber through a window or filter port. Typical VUV filters have a spectral width of 10 nm

and any continuum output in the longer wavelengths are down by five or more orders of magnitude. The physical mount for the source tube and filter housing serve as a limiting aperture of approximately 6 mm, used in collimating the incident light.

After the filter we place the reflection type polarizer followed by the second aperture in the collimating scheme. This work employs three mirror metal front surface polarizers of the type reported by Hamm et.al.[11] Typical diattenuation values of 0.996 have been reported for these polarizers. These polarizers allow minimum deflection of the optical axis and introduce little problem in alignment of the system.

The collimated light is incident on the sample mirror and specular light and scattered light will be collected by the three fixed solar blind photomultiplier tubes (PMT). Placed in front of the PMT's is another polarizer used as an analyzer. These PMT's are arranged so that the specular channel is at 30 degrees angle of reflection, the forward and back scatter channels are at +30 and -45 degrees, respectively, relative to the specular.

In addition to the signal PMT's there is a reference channel PMT at the output of the source. Part of the signal is picked off by the beamsplitter and directed to the reference. This setup allows us to monitor the condition of the source output.
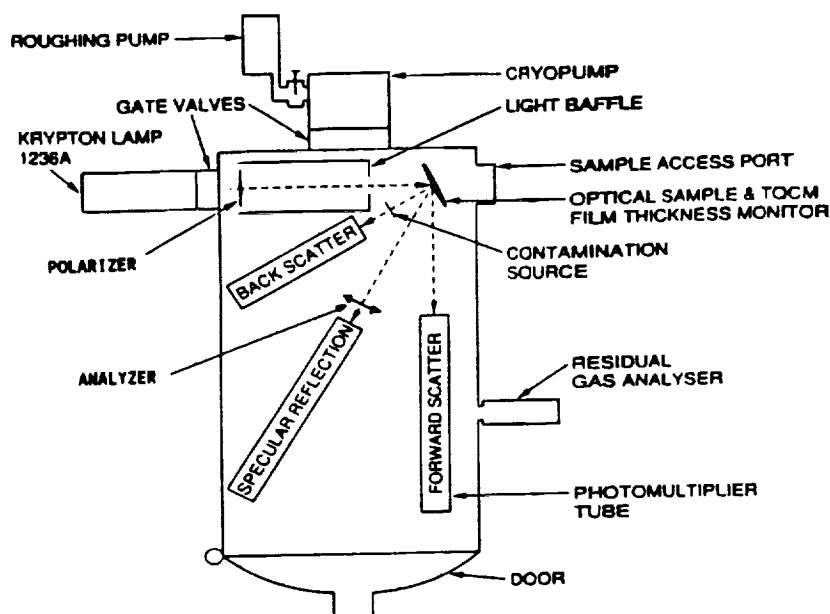
IN-SITU OPTICAL CONTAMINATION TEST FACILITY

Figure 4. Schematic Diagram of the In Situ Optical Surface Measurement Facility

The contamination source is a simple resistance heater in contact with the outgassing material and is housed in front of and beside the back scatter PMT. The temperature of the sample is held to within one degree either side of the desired temperature. Mass loss and therefore contamination level is determined by using a temperature controlled quartz crystal microbalance (TQCM). For our 15 Mhz TQCM the mass loading, m, is given by m = 1.56×10^{-9} g/cm^3 hz. In this application the TQCM is located coplaner above the sample mirror and the housing is temperature controlled and monitored to less than one degree.

This set-up approximates a planer BRDF measurement at three positions, i.e. the incident light, surface normal and scattered light are in the same plane. Measurements can then be taken using incident linearly polarized light at any orientation and analyzed at any orientation while contaminant is being deposited.

In addition there is available a 0.5 meter MacPherson VUV spectrometer for measuring angular scattering in the UV and the VUV. This device uses a mercury vapor lamp as the source and an acrylic light pipe coated with sodium salicylate (a florescent material) as the detector.

The output of the 1/8" florescent spot is directed through the light pipe to a visible photomultiplier. The light pipe is free to rotate about the sample at a distance of 1.5 inches giving a solid angle of roughly 0.007 steradians.

EXPERIMENTAL METHOD

Molecular contamination of optical surfaces from outgassed material has been shown to proceed from acclimation centers (see figure 2). The origin of these centers at the surface is not well understood but each grows faster than the surrounding surface area. This implies that the contaminant has a higher sticking ratio for itself than the surface has for it and as a result the surface will appear on the microscopic level to be composed of many small "islands" of accumulated material with plains of relatively clean surface in between. This situation provides the experimenter with many roughly hemispherical scattering centers that are growing with time. This is analogous to the common static situation for scattering of near infrared light from surfaces by dust particles (see Bennett[5]). By using a fixed wavelength and observing the scattered light as the islands grow,

we will observe the typical resonance peak in scattered light predicted by the Mie theory.

This sort of scattering situation suggests using the Mie Theory to explain the angular scattering; and the form of the scattering can be used to shed some light on the growth rates of the islands and therefore the activation energies of the outgassing phenomena.

RESULTS

Figure 5.a shows a typical optical surface before contamination. These mirrors are one inch quartz flats with a 1000 angstrom coating of aluminum and a final 250 angstrom overcoat of magnesium fluoride which provides a high reflection coating at 1200 angstroms. Close inspection shows some imperfections in the MgF coating as well as the Al reflective coat.

Figure 2 shows a mirror contaminated by Chemglaze Polyurethane Z-306. This mirror was exposed to the contaminant at elevated temperatures up to 160 degrees centigrade for approximately four hours. The Z-306 paint had previously been baked at 60 degrees for two days.

Figure 5.b shows a mirror contaminated with Silastic E. The material was cured at 100 degrees centigrade for four hours before this 90 minute run at 125 degrees. Note how the form of the contamination is in roughly circular islands similar to those formed by Z-306 but are much more sharply peaked than the hemispherical islands of the Z-306. However, the scattered light is very different in that the scatter channels don't show the resonance scattering that occurs with the Z-306 contamination. Figure 6.a shows the results of the BRDF measurements done on the 0.5 meter VUV spectrometer at about 2300 angstroms. The mirror K-1 is heavily contaminated with Z-306 and mirror 47-89 is the Silastic E. The data shows the increased scatter at large angles from Z-306 over that from the Silastic E. Also notice that since our detector has such a large solid angle we are measuring the beam shape at small angles relative to specular. For comparison figure 6.b shows the measured BRDF at a wavelength of 6328 angstroms for mirror K-1. This mirror was highly contaminated with Z-306

Figure 7. shows the relevant data on the mirror shown in figure 2. Notice that there is the resonance peak in the scattered light as predicted by the Mie theory (see figure 4). We calculate from this curve that the index of refraction of the surface contaminant is approximately given by m = (1.1 -

0.04 i). It should be pointed out that the numbers that are derived from this model are relatively soft. The model can accommodate a plus or minus ten percent change in the real part and factors of two to three in the imaginary part of the index of refraction and still give good fit to the experimental data. This derives from the complexity of the model and the lack of knowledge of the size distribution of scatterers on the surface. We also see that the specular reflectivity drops fairly quickly after contamination starts but reaches a steady state value with no further significant change.
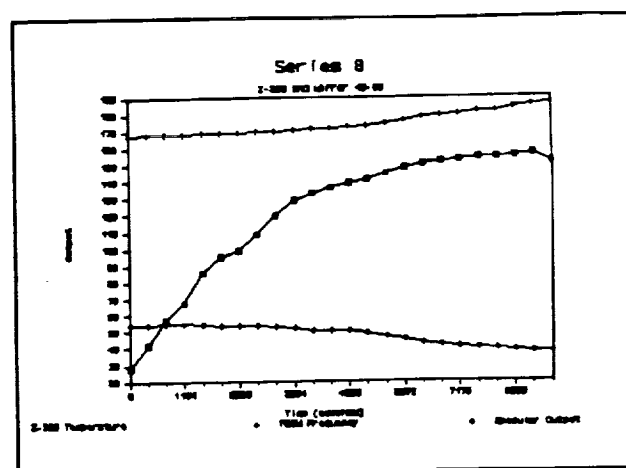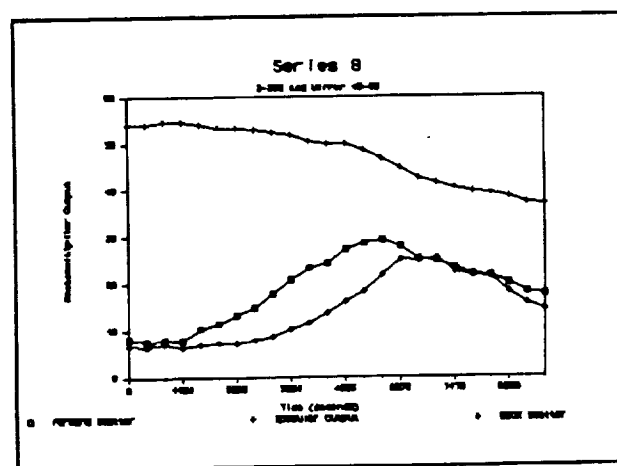

Figure 7.a. Data from Run #3_89

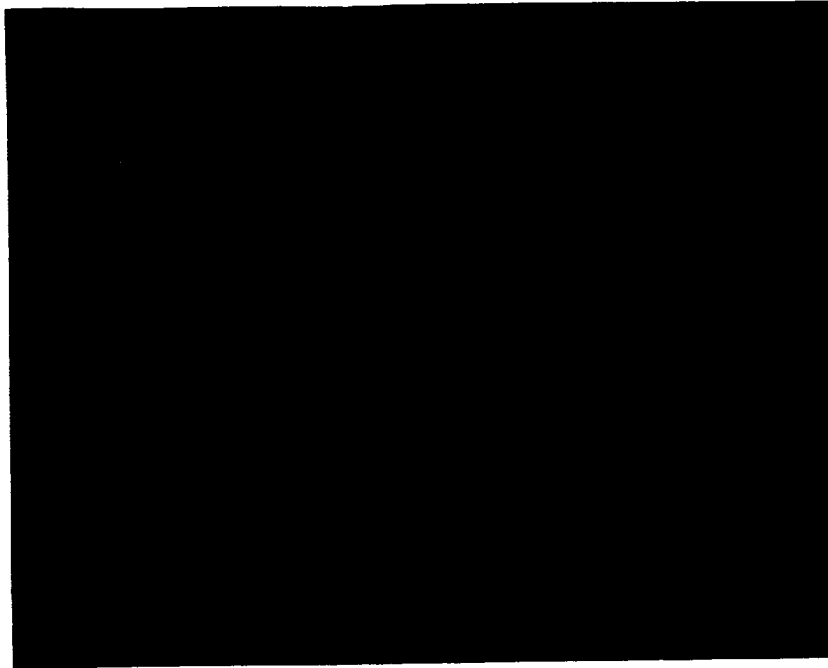Figure 7.b. PMT Outputs for Mirror #3_89

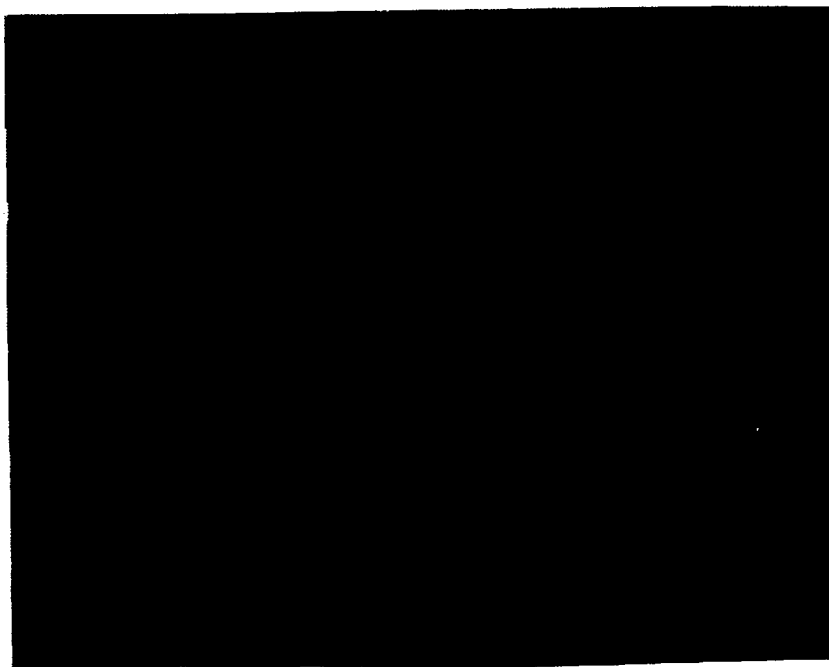Figure 5.a. Clean Uncontaminated Mirror
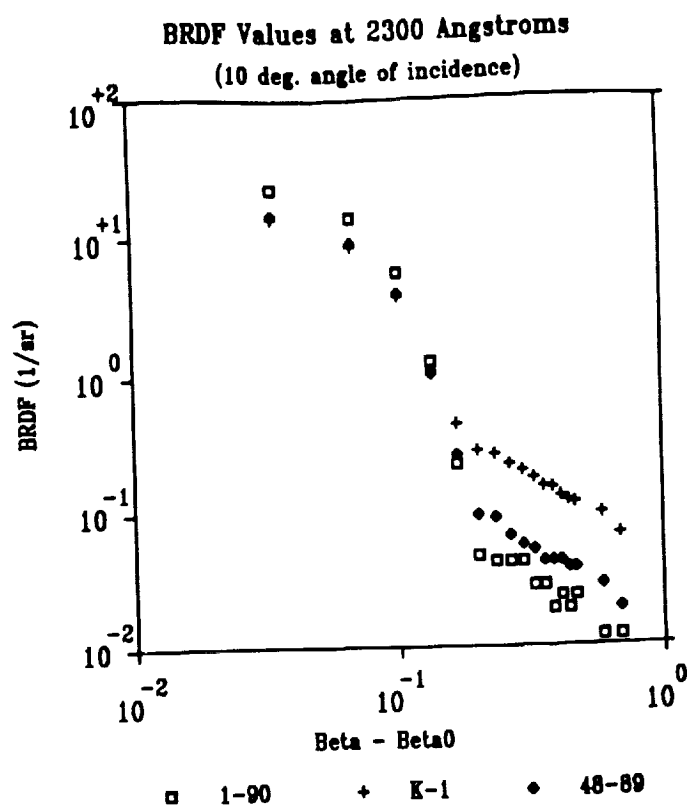

Figure 5.b. Mirror Contaminated with Silastic E.

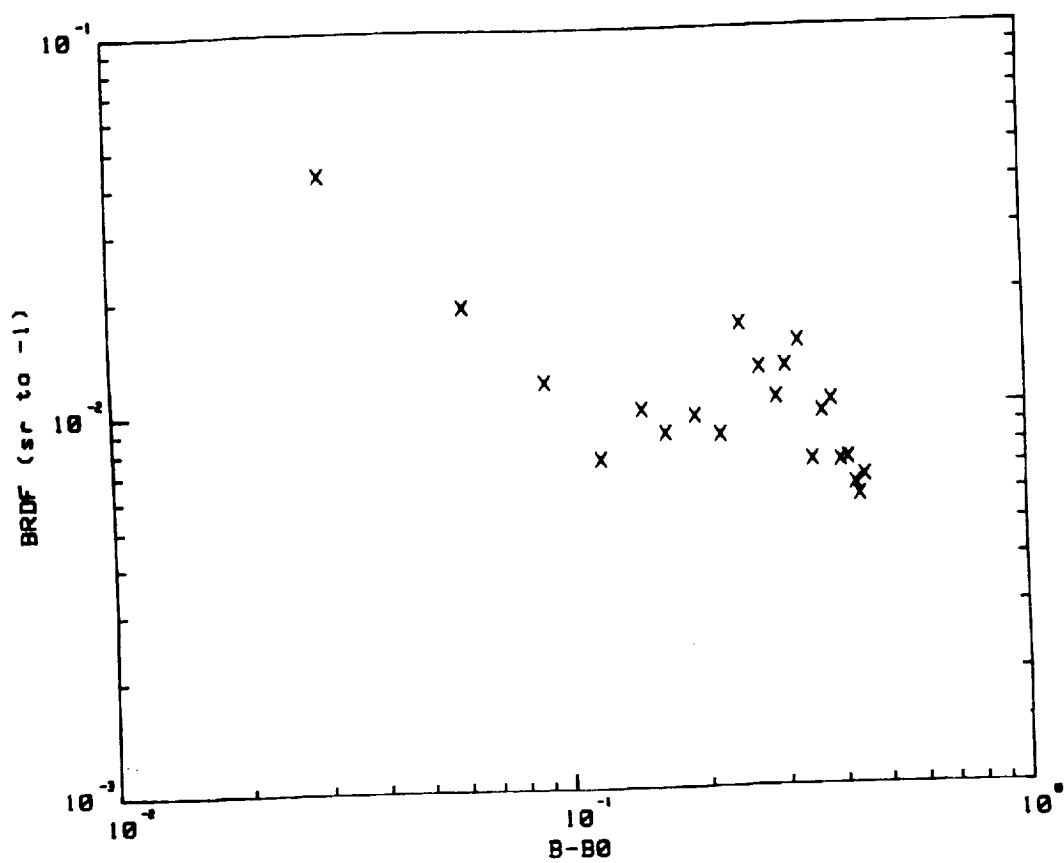Figure 6.a. BRDF Values for Several Mirrors in the Ultraviolet

Figure 6.b. BRDF for Mirror Highly Contaminated with Z-306 Taken in the Visible

10
CONCLUSIONS

Measurements of the contamination of optical surfaces show that in some cases the material grows in separate distinct islands of contamination rather than in a uniform thin film. This can produce an increase in scattered light due to Mie type resonance scattering which can, because of the angular distribution of the scattering, impact the design of optical systems. We see that the current tests for acceptable levels of optical contamination must include not only loss of surface reflectance but also the distribution of any scattered light. In addition we have seen that by measuring the scattering in situ we can determine the effectiveness of a potential contaminant in a short time.

REFERENCES

1. Nicodemus, F.E., "Reflectance Nomenclature and Directional Reflectance and Emissivity," Appl. Opt. 9, 1474 (1970).

2. Bickel, W.S., Hsu, J., Chiao, S., Abromson, D. and Iafelice, V., "The Mueller Matrix-Stokes Vector Representation of Surface Scattering," Polarization Considerations for Optical Systems, SPIE Vol. 891, 32-39 (1988).

3. Bennett, H.E., "Scattering Characteristics of Optical Materials," Opt. Eng., 17, 480-488 (1978).

4. Elson, J.M. and Bennett, J.M., "Vector Scattering Theory," Opt. Eng., 18, No. 2, p. 116 (1979).

5. Elson, J.M., "Light Scattering from Semi-infinite Media for Non-normal Incidence," Phys Rev B, 12, No. 6, p. 2541 (1975).

6. Wang, Y. and Wolfe, W.L., "Scattering from Microrough Surfaces: Comparison of Theory and Experiment," J. Opt. Soc. Am., Vol. 73, No. 11, p. 1596, (Nov. 1983).

7. Church, E.L., Jenkinson, H.A. and Zavada, J.M., "Relationship between Surface Scattering and Microtopographic Features," Opt. Eng. 18, No. 2, p. 125 (1979).

8. Van de Hulst, H.C., Light Scattering by Small Particles, Wiley, New York, 1957.

9. Mie, G., Ann. Phys., 25, p. 377 (1908).

10. Azzam, R.M.A., "Photopolarimetric Measurement of the Mueller Matrix by Fourier Analysis of a Single Detected Signal," Optics Letters, 2, No. 6, 148-150 (1978).

11. Hamm, R.N., MacRae, R.A. and Arakawa, E.T., "Polarization Studies in the Vacuum Ultraviolet," J. Opt. Soc. Am., 55, 1460-1463 (1965).